ILEANA FERNANDA MÁRQUEZ

THE EFFECT OF LATERAL INTERACTIONS:
A biophysical characterization of *E. coli* FtsZ lateral mutants

Instituto de Materiales Nicolás Cabrera
Facultad de Ciencias
Universidad Autónoma de Madrid

THE EFFECT OF LATERAL INTERACTIONS:

A biophysical characterization of *E. coli* FtsZ lateral mutants

Memoria para optar al grado de Doctor en Biofísica
presentada por ILEANA FERNANDA MÁRQUEZ
dirigida por MARISELA VÉLEZ TIRADO

Mayo 2014

a María Eva,
a Luis,
por tanto amor incondicional y
enseñarme a no dejar de luchar.

A mi familia.

AGRADECIMIENTOS

Quisiera comenzar este apartado dedicado a los agradecimientos mencionando en primer lugar a mi directora de tesis, Marisela Vélez. Sin ella me hubiera sido imposible haber llegado hasta aquí.

Marisela, te agradezco la oportunidad que me has dado al aceptarme en tu grupo. Gracias por el apoyo que siempre he recibido, los ánimos constantes cuando la vida y los experimentos se complicaban, y por creer siempre en mis capacidades incluso cuando yo dudaba de ellas. Quiero agradecerte también por el todo el tiempo que me has dedicado tanto para enseñarme todo lo que he aprendido así como para ayudarme a reconvertime dentro de la ciencia. A tu lado la transición fue muy fácil.

A Octavio Monasterio, y por extensión a los integrantes de su laboratorio, por darnos las proteínas mutantes de FtsZ que sin ellas hubiera sido imposible realizar este trabajo. A Germán Rivas y toda la gente que forma su laboratorio, en especial a Mercedes Jiménez, por brindarme ayuda incondicionalmente siempre que lo he necesitado. A Jesús Mingorance y en particular a Estefanía Salvarelli por proporcionarnos las proteínas purificadas de FtsZ nativa y ZipA, y el tiempo dedicado a enseñarme las técnicas necesarias para su caracterización. A Miguel Vicente quiero agradecer el uso de su laboratorio y el tiempo que su gente ha dedicado para ayudarme sin nada a cambio. En particular quiero agradecer a Anabel porque a pesar de tener una agenda apretada nunca me negaste un minuto de tu tiempo siempre que lo necesité.

A mis compañeros de laboratorio les agradezco todo: los cafés, las charlas, las risas, las broncas, todo lo que me enseñaron, la critica constructiva, la destructiva también, y por hacer que todos estos años de tesis valieran la pena vivirlos. Pablo, por ser el primer compañero que tuve en el laboratorio, y por ser con el que mas tiempo he compartido en él, te merecés el premio a la paciencia, gracias por compartir todo tu conocimiento conmigo, tu amistad, tus consejos y prestarme un hombro donde apoyarme. David, gracias por el ánimo que siempre me has dado, por llenar el laboratorio de energía, y por enseñarme dónde están las moléculas. Mario, gracias por aguantarme en mi época mas difícil, y por darte cuenta que poner un check-point charlie iba a ayudar muchísimo a paliar esos momentos. Y por último, Álvaro (Alvarito), muchas gracias por hacerme recordar lo que es tener esas ganas tremendas de aprender, el por qué nos dedicamos a hacer ciencia, y por las horas y horas de música y charlas compartida viendo pasar nuestros días en una línea de AFM.

El tiempo que dediqué a completar esta tesis también me ayudó no solo a hacerme de amigos sino a conocer gente valiosa y divertida. A Judith gracias por ese primer año de tesis en el cual tuve que aprender a trabajar en equipo, hiciste que fuera muy fácil; gracias por ser tan divertida y excelente persona. Lara, quiero agradecerte por acompañarme a dar esos primeros pasos en la caracterización bioquímica, sin tu ayuda me hubiera sido imposible aprender tantas cosas al mismo tiempo; y muchas gracias por darme tu amistad. Cristi, con vos gané una gran amiga; gracias por toda la ayuda en temas de laboratorio; gracias por hacer que mi día a día terminara siempre con un balance positivo y por darme tanto cariño. A Óscar por enseñarme que ser alegre y divertido no va en contra del trabajo, todo lo contrario, lo hace mucho mas llevadero. A Marchin, Alicia y Moira, muchas gracias por tanta calidez junta y hacerme sentir que nos conocemos desde siempre. Y a todas las demás personas que no nombro una a una pero que han embellecido estos años de formación en el ámbito personal.

Quiero agradecer también a mi familia, a mi primera mamá Rosa, a mi segunda mamá Betty, y a mi papá Ruben por estar siempre a mi lado, por sentirse orgullosos de la persona en la que me he convertido y hacérmelo saber. A mis hermanos Dani, Popi, Yoryi y Matías por hacer que las distancias en kilómetros dejaran de existir y que los años no pasen entre nosotros.

A mi hermosa Maria Eva: hacés que mi vida florezca todos los días. Es gracias a vos que siempre he encontrado la fuerza y motivación para seguir avanzando y superar todos los obstáculos. Gracias por facilitarme el camino para conseguir este objetivo en mi vida.

A Luis, por todo, sin tu apoyo y comprensión no hubiera terminado esta tesis. Gracias por enseñarme a luchar sin parar, y que todo lo que me propongo puedo conseguirlo. Gracias por caminar a mi lado en esta parte final haciéndome sentir que siempre estabas a mi alcance.

Hubiera podido tal vez asombrarte

con extraños cuentos inverosímiles;

pero he preferido relatar llanamente los hechos,

en el modo y estilo mas sencillos,

porque mi designio principal era instruirte,

no deleitarte.

Los viajes de Gulliver

– Jonathan Swift –

Si hubiéramos sabido lo que estábamos haciendo,

no se llamaría investigación,

¿no?

– Albert Einstein –

I could, perhaps, like others,

have attonished thee with strange improbable tales;

but I rather chose to relate plain matter of fact,

in the simplest manner and style;

because my principal design was to inform,

and not to amuse thee.

Gulliver´s travels

– Jonathan Swift –

If we knew what it was we were doing,

it would not be called research,

would it?

– Albert Einstein –

RESÚMEN

La bacteria *Escherichia coli* (*E. coli*) es uno de los organismos que se utiliza para estudiar la división celular bacteriana dada su fácil reproducción y crecimiento en laboratorios. Esta bacteria, del tipo Gram-negativa, ha sido investigada exhaustivamente en los últimos veinte años intentando entender los mecanismos de su división celular. Muchas de las bacterias Gram-negativas son patógenas por lo que desarrollar nuevos fármacos capaces de controlar su proliferación es importante para curar infecciones.

Gracias al meticuloso estudio realizado por varios grupos de investigación, se han identificado las proteínas y genes involucrados en la división celular de *E. coli*. Un complejo macromolecular constituido por al menos 10 proteínas esenciales, y otras 15 proteínas accesorias, es el responsable de dividir la bacteria. Este complejo de proteínas altamente dinámico, llamado divisoma, debe ensamblarse en el sitio donde se producirá la división de la célula bacteriana.

La división se inicia con la formación del proto-anillo. Este anillo lo constituyen polímeros de la proteína FtsZ (el anillo Z) y dos proteínas asociadas a la membrana celular interna: FtsA que interacciona a través de una hélice anfipática, y ZipA que se encuentra integrada a través de una única hélice transmembrana. Dado que FtsZ se halla soluble en el citoplasma bacteriano, los polímeros necesitan interaccionar al menos con FtsA o ZipA para ser anclados a la membrana interna a través de su interacción con el carboxi-terminal de FtsZ. También se han identificado otras proteínas accesorias, aunque no esenciales, que se localizan en el sitio de división y contribuyen a la estabilización del anillo Z antes de iniciarse la constricción de ambas paredes celulares, interna y externa.

FtsZ es una proteína capaz de polimerizar uniendo dos monómeros por medio de la incorporación de una molécula de nuclótido GTP. Inmediatamente después de la unión de GTP se produce la hidrólisis del nucleótido en GDP que se intercambia nuevamente por otro GTP manteniendo la unión entre monómeros estable. Esta actividad GTPasa sumada al rápido intercambio de monómeros dentro de un polímero hace que FtsZ muestre *in vitro* un alto polimorfismo y dinamismo bajo distintas condiciones de polimerización. Mediante técnicas de microscopía, tales como microscopía electrónica o microscopía de fuerzas atómicas, se han observado filamentos simples, dobles, curvos, rectos, circulares, en forma de espiral y planchas de polímeros asociados lateralmente, así como superestructuras del tipo cintas y toroides.

Dado que FtsZ exhibe *in vitro* este extenso polimorfismo, las preguntas inmediatas que surgen son *¿cómo se encuentran dispuestos estos polímeros dentro del anillo Z?* y *¿cómo es el mecanismo de generación de fuerza necesaria para la constricción de la célula bacteriana?*

Para responder a estas preguntas se han realizado diversos estudios tanto *in vivo* como *in vitro*, y se han propuesto diferentes modelos de organización de los polímeros de FtsZ y de posibles mecanismos generadores de fuerza.

Experimentos *in vivo* han mostrado que mutaciones en ciertos amino ácidos de FtsZ alteran la funcionalidad de la proteína inhibiendo la división de *E. coli*. Sorprendentemente, todas las mutaciones de FtsZ dirigidas a las zonas de contacto lateral entre polímeros han impedido que la bacteria se divida indicando así la importancia de las interacciones laterales para su división.

A partir de datos experimentales *in vitro* se han propuesto diferentes modelos matemáticos de mecanismos posibles para que los filamentos de FtsZ sean contráctiles. Estos modelos se basan en cambios en la curvatura de la unión entre monómeros debido a la hidrólisis del nucleótido, interacciones laterales o restricciones en la torsión natural del filamento según su anclaje a la membrana.

A pesar del extenso trabajo *in vitro* y del avance de la microscopía de alta resolución *in vivo*, no se ha llegado a un consenso sobre la disposición de los polímeros de FtsZ dentro del anillo de división así como del mecanismo molecular generador de la fuerza constrictiva.

Se han propuesto como aspectos relevantes para la constricción a la curvatura y a las interacciones laterales de los filamentos de FtsZ. En esta tesis nos proponemos explorar *in vitro* el comportamiento de dos mutantes laterales no funcionales de FtsZ descritos previamente por Shin et al. [Shin et al., 2013], y compararlo con el de la proteína nativa mediante un sistema reconstituido en superficies *in vitro*. Queremos identificar qué características del comportamiento *in vitro* de estos dos mutantes puede asociarse a su no funcionalidad *in vivo*.

Para caracterizar el efecto de estas mutaciones disponemos de dos técnicas biofísicas de caracterización en superficie: Microscopía de fuerzas atómicas (AFM) y Microbalanza de cuarzo (QCM). Mediante AFM estudiaremos cómo estas mutaciones laterales de FtsZ afectan la forma y dinamismo de los polímeros en mica, así como la formación de agregados en mica y en bicapas lipídicas ancladas, cuando estos filamentos están unidos a través de ZipA. Con QCM cuantificaremos la interacción de FtsZ y ZipA en bicapas lipídicas ancladas a superficies planas para compararla con las medidas disponibles en solución.

SUMMARY

Escherichia coli (E. coli) bacterium is one of the organisms used to study bacterial cell division given its easy grow and proliferation in laboratories. This Gram-negative bacterium has been studied extensively during the last two decades aiming to understand the mechanisms of its cell division. Many Gram-negative bacteria are pathogens and to develop new compounds to control their proliferation is important to cure infections.

From the meticulous research made by several groups, the proteins and genes involved in *E. coli* cell division have been identified. A macromolecular complex is the responsible for dividing the bacterial cell, composed by at least 10 essential proteins and other 15 accessory proteins. This highly dynamic protein complex, the divisome, must assemble at the cell division site.

The bacterial cell division starts with the formation of a proto-ring. This ring is constituted by polymers of the protein FtsZ (the Z-ring) and two membrane associated proteins: FtsA that interacts through an amphipathic helix, and ZipA a bitopic protein integrated into the membrane with a single transmembrane helix. FtsZ is a cytoplasmic protein, therefore, its polymers need to interact with at least FtsA or ZipA to be anchored to the bacterium inner membrane through their interaction with the C-terminus of FtsZ. Other proteins, although not essential, have been identified to localize at the division site that contribute to stabilize the Z-ring before the constriction of both inner and outer cellular walls begins.

FtsZ is a protein able to polymerize by binding two monomers incorporating a molecule of nucleotide GTP. Immediately after the binding of a GTP, the nucleotide is hydrolyzed into GDP and it is interchanged by another GTP molecule stabilizing the bond between monomers. This GTPase activity in addition to a fast exchange of monomers within a polymer makes FtsZ displays a high polymorphism and dynamism *in vitro*. By means of electron microscopy and atomic force microscopy techniques it has been observed FtsZ single filaments, double, curved, straight, circular, spiral and sheets where polymers are associated laterally, as well as superstructures like ribbons and toroids.

Given this extensive FtsZ *in vitro* polymorphism the immediate questions that arise are *how are these polymers arranged within the Z-ring?* and *how is the force generating mechanism needed for the constriction of the bacterial cell?*

To answer these questions several studies have been made *in vitro*, and different models have been proposed for the organization of the FtsZ polymers and possible force generator mechanisms.

In vivo experiments have shown that mutations on certain amino acids of FtsZ alter its functionality preventing *E. coli* bacterium from dividing. Surprisingly, all site-directed mutations to the lateral contact zones between polymers are non-functional indicating the importance of these lateral interactions for bacterial cell division.

From *in vitro* experiments, there have been proposed several mathematical models for the mechanisms in order to have contractile FtsZ polymers. These models are based on changes in curvature induced by the nucleotide hydrolysis, lateral interactions or restrictions on the filament natural torsion depending on its anchoring to the membrane.

In spite of the extensive work *in vitro* and the advance of the high resolution microscopy techniques, there have been no consensus about the arrangement of the FtsZ polymers within the division ring nor the molecular mechanism able to generate the constrictive force.

Both lateral interactions and curvature of the FtsZ filaments have been proposed as relevant for constriction. On this thesis we want to explore *in vitro* the behavior of two non-functional FtsZ lateral mutants early described by Shin *et al.* [Shin et al., 2013] and compare them with that of the native protein by means of a reconstituted systems on surfaces. We want to identify which characteristics *in vitro* for these two mutants can be associated to their non functionality *in vivo*.

To characterize the effect of these mutations we will use two biophysical techniques on surfaces: Atomic force microscopy (AFM) and Quartz Crystal Microbalance (QCM). With AFM we will study how these mutations affect the shape and dynamism of the polymers on mica, and the formation of bundles on mica and supported lipid bilayers when these polymers are anchored through ZipA. With QCM we will quantify the interaction between FtsZ and ZipA on planar lipid bilayers comparing them to the reported values in solution.

CONTENTS

LIST OF FIGURES

LIST OF TABLES

ACRONYMS

GTP guanosine 5′-triphosphate

GMPCPP guanosine 5′-[(α, β)-methyleno]triphosphate

PC phosphatidylcholine

PE phosphatidylethanolamine

PG phosphatidylglycerol

EPC L-α-Phophatidylcholine, Egg chicken extract

DOPC 1,2-dioleoyl-sn-glycero-3-phosphocholine

DOGS-NTA 1,2-dioleoyl-sn-glycero-3-[(N-(5-amino-1-carboxypentyl)-iminodiacetic acid)succinyl]

EcPl *E. coli* polar lipid extract

SLB Supported Lipid Bilayer

MLVs multilamelar vesicles

SUVs small unilamelar vesicles

LUVs large unilamelar vesicles

GUVs giant unilamelar vesicles

STM Scanning tunneling Microscope

AFM Atomic force microscopy

SPM Scanning probe microscopy

TSM Thickness shear mode

QCM Quartz crystal microbalance

FRAP Fluorescence recovery after photobleaching

SAM Self-Assembled Monolayer

Part I

INTRODUCTION

This introduction will summarize what is known about the bacterial cell division process, the machinery involved and its protein components.
I first present an introduction to Gram-negative bacteria and a description of the essential structures for bacteria survival. Then, I describe two essential proteins involved in bacterial cytoskeleton: the cytoplasmic protein FtsZ, responsible in part of generating the force needed for cell division, and ZipA, the FtsZ filaments anchor membrane protein; and how they interact to form polymers and aggregates. Then I address some mathematical models proposed to explain where the constriction force comes from and how protein mutations are a helpful tool to reveal nonfunctional division machinery. Lastly, I present the objectives of the thesis.

1

GRAM NEGATIVE BACTERIA

Bacteria and archaea are the two mayor domains of prokaryote organisms. The mayor characteristic of prokaryotes is that they lack of internal membrane system, contrary to eukaryotes which present several degrees of internal cell organization or organelles.

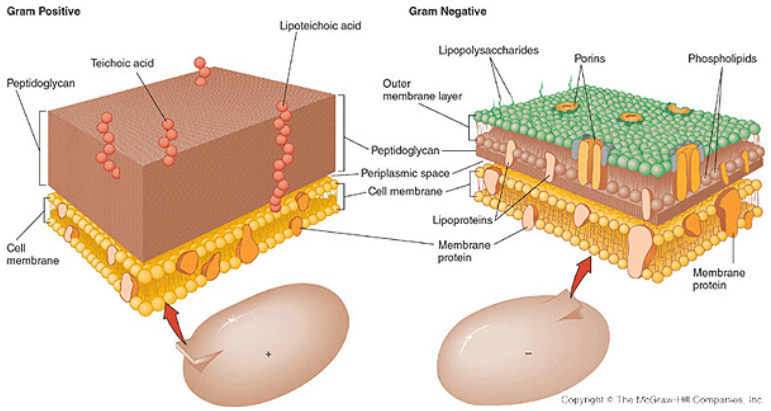

Figure 1: Cartoon for Gram-positive and Gram-negative bacteria cell walls.

Besides their differences in cellular morphologies, mostly spherical or rod-like shaped, bacteria divide in two types: Gram-positive or Gram-negative. The name is given by a largely used staining test to differentiate bacteria. This method developed by Hans Christian Gram distinguishes bacteria by the properties of their cell walls and its peptidoglycan (Figure 1). Gram-positive bacteria are surrounded by a single lipid membrane and a thick wall with many layers of peptidoglycan responsible for retaining the Gram-stain. On the contrary, Gram-negative bacteria have a thin cell wall consisting of a few layers of peptidoglycan surrounded by a second lipid membrane. This outer membrane, containing a unique component, lipopolysaccharide, protects the bacteria from several antibiotics and provokes an immune response in human body.

There is about ten times as many bacterial cells as there are human cells in the body, most of them are harmless and some are even beneficial. Nevertheless, several bacteria are pathogenic and cause serious infectious diseases.

1.1 ESCHERICHIA COLI

Most bacteria are Gram-negative, thus by studying the essential cell functions might help to elucidate ways to control proliferation and viability, and to develop novel compounds to cure infections.

Escherichia coli (*E. coli*) is a Gram-negative bacterium commonly found in the lower intestine of warm blooded organisms. This particular bacterium has been intensively investigated over the years given its easy and inexpensive growth in a laboratory becoming the dominant and model organism to study bacterium cell division.

Figure 2: AFM image of an *E. coli* bacterium. Adapted from http://www.icmm.csic.es/spmage/ spmagegallery07.php.

1.1.1 *Cell division*

Divisome: assembly of all proteins required for cell division

Cell division implies the formation of a highly dynamical macromolecular complex constituted by at least ten essential proteins, and about fifteen more accessory proteins recruited to the division site [Egan and Waldemar, 2013, Natale et al., 2013]. The divisome must assemble in a multistage process at midcell to form a division ring giving as a result two cell poles [Vicente and Rico, 2006], where all cell envelope layers must remodel during division.

Bacteria multiplication must go under cycles of cell growth and division, in which all its components must be synthesized and distributed between daughter cells. There are two components that each daughter cell inherits directly from their mother: the chromosome and the cell wall peptidoglycan sacculus. Therefore, both compo-

nents need an efficient machinery to be replicated and distributed to the daughter cells.

1.1.2 *The division Ring*

E. coli cell division proteins and genes have been defined over several decades of work by means of classical and molecular genetics and the fluorescent protein accessibility. The current picture is that the proteins are recruited based on their topological properties and not according to a linear time sequence [Vicente and Rico, 2006].

The main features of *E. coli* bacteria cell division have been extensively reviewed [Errington et al., 2003, Margolin, 2009, de Boer, 2010, Natale et al., 2013, Egan and Waldemar, 2013, den Blaauwen, 2013, Cava et al., 2013]. To divide, the bacterium needs to:

- select the division site;
- form the cytoplasmic apparatus, the early assembly of the so called proto-ring;
- form a periplasmic ring;
- constrict and close the septum.

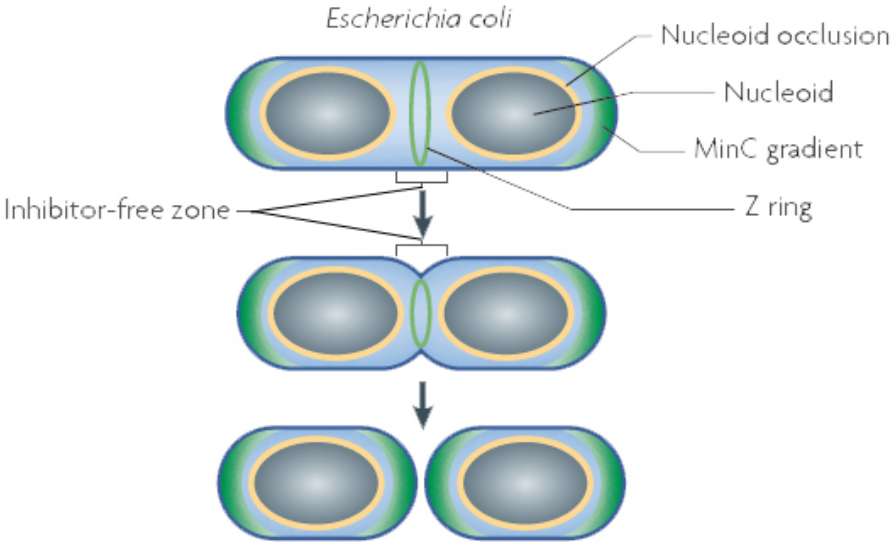

Figure 3: *E. coli* bacterium cell division cartoon. Adapted from Adams and Errington [2009]

Most bacteria divide at midcell, and they identify this site through the coordinated activity of different cytoskeleton complexes participating in cell elongation and division.

FtsZ: filamentous temperature sensitive protein Z displaying GTPase activity

The division of *E. coli* bacterium initiates by the polymerization of the tubulin homolog FtsZ in a ring-like structure and other essential proteins at midcell. FtsZ polymerizes in a GTP-dependent manner organized in a head-to-tail association of the monomers, the *Z-ring*, and it must be stabilized at midcell until cell division is almost complete. This raises two questions: how does FtsZ finds the middle of the cell, and how is it stabilized at the inner face of the cytoplasmic membrane.

The polymerization of FtsZ must be inhibited at all places in the cytosol until the cell is ready to divide. There are two negative regulators of FtsZ assembly to ensure the septum is localized at the right place (Figure 4): i) nucleoid occlusion and ii) the Min system.

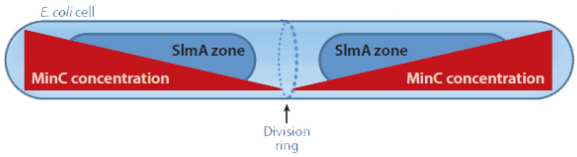

Figure 4: FtsZ inhibitors, MinC and SlmA, ensure division ring assembles at the center of the bacterium. Adapted from Young [2010].

Cell division is not finished until complete replication and segregation of the chromosomes is done. In *E. coli* bacterium SlmA proteins, binding to specific DNA sequences, inhibit FtsZ assembly until the appearance of a nucleoid-free zone by enhancing FtsZ GTPase activity and promoting its disassembly. The second regulatory mechanism, the Min system, consisting of MinC/MinD/MinE proteins restricts the formation of the Z-ring at the center of the cell. Abolition of this system leads division at the poles with chromosome free minicells. Association of MinC and MinD, a membrane bound ATP-ase protein, negatively regulates Z-ring assembly. At the same time, MinE inhibits MinCD complex by inducing its dissociation. The complex fluctuates in a pole-to-pole manner generating a gradient of protein [Loose et al., 2008]. When the bacterium reaches a certain length, the maximum of FtsZ inhibitor is concentrated at both poles, allowing FtsZ assembly at midcell. At least these two mechanisms ensure the correct localization of the division machinery.

ZipA: FtsZ interacting protein A, is a bitopic protein of the cytoplasmic membrane with and amino-terminal helix integrated into the membrane

FtsZ, the most critical component of the divisome, does not attach directly to the bacterial inner membrane, instead it is stabilized by using a carboxy-terminal tail interacting at least with one membrane anchor protein. The proto-ring, formed by the interaction of FtsZ and two membrane-associated proteins FtsA and ZipA, assembles in an early stage on the cytoplasmic membrane followed by a late assembly of a periplasmic ring. The early recruitment of FtsA and ZipA

depends on the localization of FtsZ at midcell. At the same time, attachment of FtsZ to the membrane occurs solely in the presence of FtsA or ZipA. Other associated proteins (ZapA, ZapB, ZapC, ZapD and FtsEX), although not essential for cell division, assembly early at the division site ensuring stabilization of Z-ring and stimulating FtsZ polymer bundling before cell constriction. This way, proto-ring formation might stimulate constriction through synthesis of peptidoglycan [reviewed in Rico et al., 2013, and references therein].

FtsA: cytoplasmic ATP binding protein of the actin family with a short amphipathic carboxy-terminal helix important to its association to the membrane

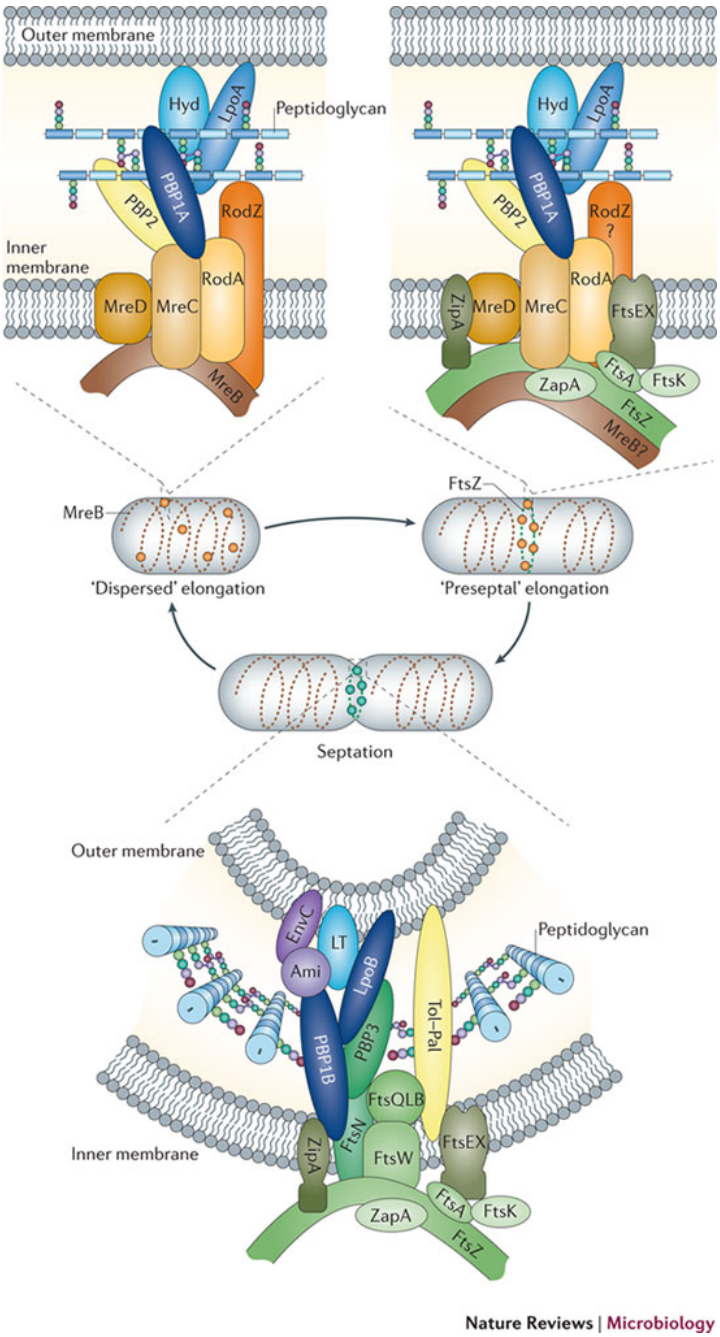

Figure 5: Proteins involved in the division and elongation machinery in *E. coli*. Adapted from Typas et al. [2012].

At a late stage during division, a connection must be set between the cytoplasmic division ring and the proteins that form the periplasmic ring (FtsK, FtsQ, FtsB and FtsL, FtsN) and peptidoglycan machinery (PBPs, penicillin-binding proteins). They assemble the Z ring almost simultaneously and in an independent manner, being FtsN a protein that interacts with both early and late cell division proteins.

Cytoskeleton proteins interact with membrane embedded proteins which at the same time interact and control proteins that are on the outer membrane that synthesize and remodel peptidoglycan (MreB and lipoproteins LpoA and LpoB). MreB is an actin-like protein found in non spherical shaped bacteria, and by directing uniformly the synthesis of peptidoglycan along cell ensures their rod-like morphology [Young, 2010, Popp and Robinson, 2010].

When the cell grows the synthesis of peptidoglycan is also regulated by the LpoA and LpoB proteins. These proteins belong to the outer membrane of the cell and they reach the periplasmic zone, between inner cell and peptidoglycan layer, by holes in the now stretched peptidoglycan activating its synthesis to maintain peptidoglycan surface density and thickness [Egan and Waldemar, 2013].

At septation site a remodeling of outer cell membrane and peptidoglycan must take place. The combined activities of peptidoglycan synthesis (by means of hydrolases and amidases responsible for hydrolyzing and removing old peptidoglycan material) and the Tol-Pal system (a complex of several cytoplasmic and periplasmic proteins that colocalize at midcell) facilitate constriction of the outer membrane and final division of the cell.

2

FTSZ CELL DIVISION PROTEIN

The first step in bacteria cytokinesis is the localization and polymerization of the protein FtsZ, a self activating GTPase homolog to tubulin [Mukherjee and Lutkenhaus, 1994]. FtsZ assembles into a highly dynamic ring-like structure, the Z-ring, close to the cytoplasmic membrane at midcell and serves as scaffold for recruitment of other division proteins. Conserved among several bacteria, FtsZ is also present in some eukaryote organelles like chloroplasts and mitochondria [Osteryoung and Nunnari, 2003, TerBush et al., 2013].

2.1 FTSZ STRUCTURE

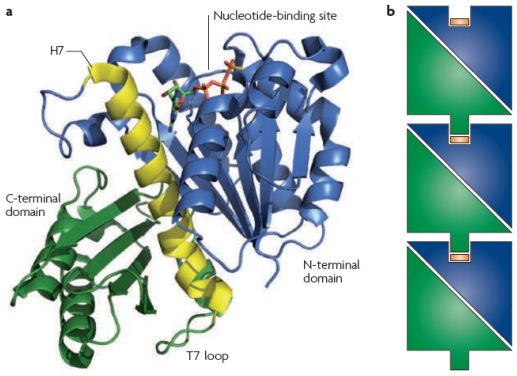

Figure 6: FtsZ (a) monomer bound to GTP and (b) polymerization. Adapted from Adams and Errington [2009].

FtsZ is a $\sim$ 40kDa protein composed by two globular domains separated by a central helix H7. The amino-terminal has the nucleotide binding site and the carboxy-terminal domain the catalytic loop T7 [Löwe and Amos, 1998, Oliva et al., 2004, Adams and Errington, 2009]. The unstructured C-terminal tail is the binding place for several other divisome proteins, which is not visible in its crystal structure. In the presence of GTP, FtsZ polymerizes by the association of subunits in a head-to-tail fashion. The synergic tail, T7, inserts into the nucleotide site of the following subunit placing the catalytic residue near the γ-phosphate allowing then nucleotide hydrolysis. Hence, FtsZ GTPase activity depends on polymerization. Likewise, FtsZ polymerization strongly depends on GTP binding but not on hydrolysis, since GTP

induces FtsZ-FtsZ interactions, giving as a result a polymer that is mostly GTP-bound [Mingorance et al., 2001, Oliva et al., 2004].

2.2 POLYMERS AND AGGREGATES

FtsZ strong GTPase activity is depending on the ionic strength, magnesium and protein concentration. It has been shown *in vitro* that potassium ions (K^+) are needed for polymerization, one mol of K^+ is taken up per mol of FtsZ added to the growing polymer [Tadros et al., 2006]. K^+ participates in the longitudinal interaction between FtsZ monomers and activates GTPase activity at neutral pH [Mendieta et al., 2009]. Moreover, even at low pH there is a direct relation between the concentration of $K^+$and GTPase activity. In the absence K^+, divalent cation Mg^{2+} induces FtsZ oligomerization in the presence of GDP but prevents it with GTP [Tadros et al., 2006]. Increasing Mg^{2+} concentration leads to a stabilization of the polymers by reducing their GTPase activity. All in all, both K^+ and Mg^{2+} are essential for GTP-FtsZ polymerization at physiological neutral pH 7.5 [Mukherjee and Lutkenhaus, 1999, Rivas et al., 2000, Mingorance et al., 2001].

Polymerization does not close the GTP binding site; there is an open gap large enough to be accessible by the nucleotide. Then, the binding site is at equilibrium where bound nucleotide is able to exchange with free nucleotide pool [Mingorance et al., 2001, Oliva et al., 2004].

There is a protein critical concentration ($\sim 1\,\mu$M) above which FtsZ subunits supports polymerization [Mukherjee and Lutkenhaus, 1998, Sossong et al., 1999, Mukherjee and Lutkenhaus, 1999]. These polymers are very dynamic, and they depolymerize as GTP is exhausted [Mateos-Gil et al., 2012b]. All these results suggest that GTP hydrolysis might be responsible for polymer dynamics.

Besides FtsZ dynamic behavior, polymerization *in vitro* displays a rich polymorphism. From single straight protofilaments, rings, spirals, sheets to bundles are observed under different assembly conditions. Polycations like DEAE dextran induce FtsZ to assembly into sheets of about 15 parallel and highly organized protofilaments, with either GDP or GTP [Erickson et al., 1996, Lu et al., 1998]. On positively charged lipid monolayers, FtsZ assembled not only into sheets but also long filaments and minirings ($23-25\,$nm diameter) [Erickson et al., 1996]. It has also been shown that lateral interactions can be enhanced by the divalent cation Ca^{2+} at high concentrations [Löwe and Amos, 1999]. Also, in buffers promoting GTPase activity, long single stranded and curved filaments were found [Chen et al., 2005, Mingorance et al., 2005, González et al., 2005] and sometimes paired [Lu et al., 1998, Romberg et al., 2001, Chen and Erickson, 2005].

In vitro, FtsZ polymers assemble mainly as single filaments, under crowded conditions and below the critical concentration. Above

the critical concentration of crowding agents filaments arrange into rings of about 200 nm diameter [Popp et al., 2009]. While at higher crowding agent concentration, the formation of suprastructures of one subunit-thick ribbon ($\sim$ 25 single protofilaments) [González et al., 2003] and toroids [Popp et al., 2009] were also observed.

Beuria *et al.* [Beuria et al., 2006] studied bundling of FtsZ protofilaments under different pH and ionic strengths. They showed that protofilament bundling decreased while increasing pH (from 6.0 to 7.9), and also that it could be inhibited by increasing the ionic strength. These results suggest that basic intracellular pH could play as bundling destabilizing agent, and that electrostatic interactions among protofilaments are important to regulate assembly of the Z-ring *in vivo*.

Surprisingly, during *E. coli* cell cycle and under different growth conditions, FtsZ concentration remains constant [Rueda et al., 2003]. Therefore, division must be regulated by the divisome assembly at the future division place in these bacteria.

As was previously stated, there are two major components of the *E. coli* Z-ring besides FtsZ: FtsA and ZipA, both proteins are associated with the inner membrane stabilizing the FtsZ ring close to it.

2.2.1 *Structure of ZipA*

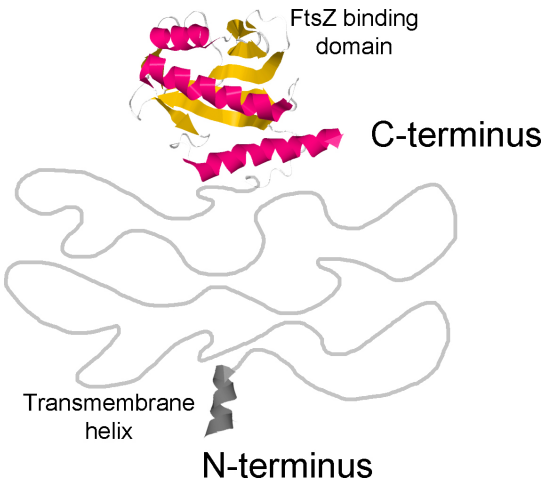

Figure 7: Cartoon model of ZipA. PDB entry 1F7W.

ZipA is a transmembrane protein found in *E. coli* cytoplasmic membrane as monomer or homodimer [Skoog and Daley, 2012]. It is an essential protein in *E. coli* cell division that interacts directly with FtsZ *in vivo* and *in vitro* [Hale and de Boer, 1997]. Their association is needed for cell constriction, and a disruption of FtsZ-ZipA interaction disrupts cell division [Hale and de Boer, 1999].

Composed by a polypeptide of 328 amino acids, ZipA is a bitopic protein, with a N-terminal spanning the cytoplasmic membrane once and the rest of the protein is residing in the cytoplasm (Figure 7). The protein, with a 36.4 kDa molecular weight, contains a hydrophobic N-terminal domain (aa 1-25) inserted in the membrane as a single anchor, followed immediately by a highly basic domain (aa 26-85) with a net charge +8. Within the cytoplasmic part of ZipA, there is a region (aa 86-188) rich in proline and glutamine residues (P/Q domain) forming a linker between the membrane and the C-terminal globular domain (aa 189-328) [Hale and de Boer, 1997].

2.2.2 *Interaction of ZipA with FtsZ*

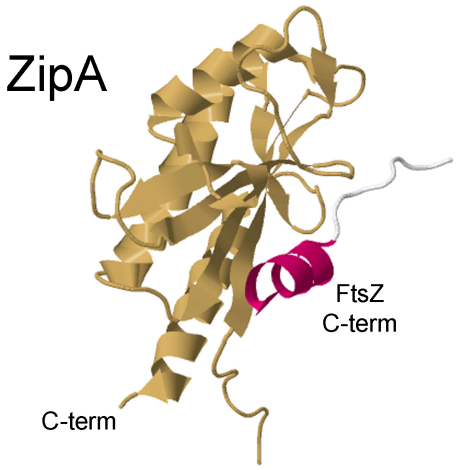

Figure 8: ZipA globular domain and its interaction with FtsZ C-terminal peptide. PDB entry 1F47 [Mosyak et al., 2000].

Interaction of ZipA and FtsZ is done through their C-terminus. A small peptide of FtsZ located at its C-terminus and a significant larger C-terminus domain of ZipA are both required for the specific interaction between these two proteins [Hale et al., 2000]. An X-ray crystal structure of the C-terminal FtsZ-binding domain of ZipA identified a hydrophobic cleave to be the responsible for the complex formation between the two proteins [Mosyak et al., 2000, Kuchibhatla et al., 2011].

Several experiments have been made *in vitro* to determine the affinity for the FtsZ-ZipA complex formation. In solution studies [Martos et al., 2010] have shown a moderate affinity (micromolar range) for the binding of a ZipA soluble form, sZipA, to FtsZ (GDP) by means of sedimentation equilibrium and of gradient-static light scattering

techniques. Hernández-Rocamora *et al.* [Hernández-Rocamora et al., 2012b] have measured a moderate affinity of the full-length ZipA incorporated into *E. coli* phospholipids nanodiscs (Nd-ZipA) for FtsZ-GTP polymers, and they reported it to be similar as for FtsZ-GDP oligomers.

Kuchibhatla *et al.* [Kuchibhatla et al., 2011] have shown that ZipA is distributed uniformly along the length of FtsZ filaments and induces the formation of large protein structures resulting in thick bundles of FtsZ polymers. Surprisingly, full-length ZipA reconstituted into nanodiscs [Hernández-Rocamora et al., 2012a] binds FtsZ polymers without inducing filament bundling.

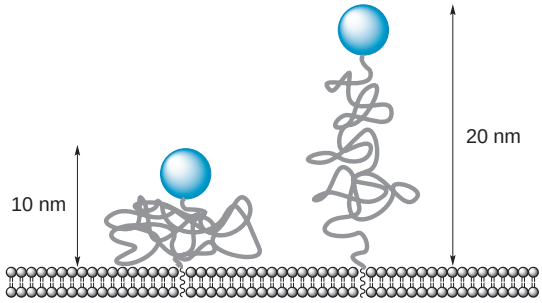

Figure 9: Schematic conformation of ZipA [López-Montero et al., 2013a].

While the flexible C-terminal peptide of FtsZ is the feature needed for ZipA to bind to it, the unstructured P/Q domain of ZipA might give a much longer flexible tether (Figure 9), mediating this way the reorganization of the rest of FtsZ structure for a functional interaction [Erickson, 2001, Ohashi et al., 2002, Mateos-Gil et al., 2012a, López-Montero et al., 2013a]. Mateos-Gil *et al.* [Mateos-Gil et al., 2012a] have shown that charged *E. coli* lipid membranes affect the kinetics and shape of the formed FtsZ aggregates. Other *in vitro* experiments also have shown that the presence of FtsZ induces softening and fluidization of the membrane when ZipA is reconstituted into a membrane (*E. coli* lipids) either into GUVs or Langmuir monolayers suggesting a mechanical role for FtsZ polymers on the bacterial inner membrane as force generators [López-Montero et al., 2012, 2013b]. All these results indicate that the presence of a lipid surface might be relevant for the reorganization of the FtsZ filaments and their later bundling.

E. coli inner membrane is composed predominantly by phosphatidylethanolamine (PE), phosphatidylglycerol (PG) and cardiolipin (CA) phospholipids. There is no phosphatidylcholine (PC), phosphatidylinositol (PI) or sphingomyelin (SM). *In vivo* studies demonstrated that the absence of PG phospholipid in the inner *E. coli* membrane prevents cells from growing [Raetz and Dowhan, 1990]. PE is uniformly distributed over the whole *E. coli* cell membrane while CA is polar

and septal localized [Nishibori et al., 2005], and that the septal localization of CA rich domains depends on FtsZ, as observed also by López-Montero *et al.* [López-Montero et al., 2012].

All the extensive work mentioned indicate ZipA does not only anchor FtsZ polymers to the cytoplasmic face of the membrane, but also enhances stability to the Z-ring. The distribution of phospholipids in bacterial cell membranes indicate a possible relevance of the lipid domains to specific cellular processes as cell division [Matsumoto et al., 2006].

3

EVIDENCE OF THE IMPORTANCE OF LATERAL INTERACTIONS

Different approaches have been developed to understand the force generating mechanism in *E. coli* through FtsZ: mutational studies and theoretical models among others [Mingorance et al., 2010].

3.1 MUTATION AS A MEAN OF STUDYING THE Z-RING

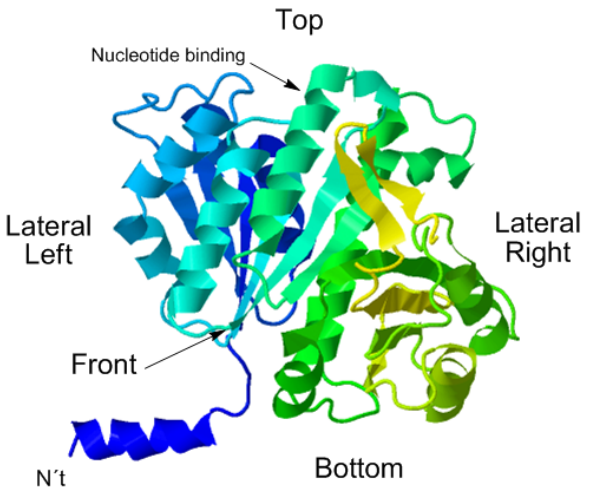

Figure 10: FtsZ protein faces as described by Lu *et al.* [Lu et al., 2001]. PDB entry 1FSZ.

An interesting approach to identify regions of FtsZ protein relevant for force generation has been site-directed mutations. Some mutations affected cell viability, cell morphology and location of the Z-ring *in vivo*; and some altered GTPase activity, protein (FtsZ mutants) polymerization and bundling *in vitro* [Phoenix and Drapeau, 1988, Addinall et al., 1996, 1997, Yu and Margolin, 2000, Lu et al., 2001, Koppelman et al., 2004, Addinall et al., 2005, Chen and Erickson, 2011].

Lu *et al.* [Lu et al., 2001] mutated FtsZ mapping all faces (front, back, lateral, and GTP region) of the protein (Figure 10). Their results showed that a high FtsZ GTPase activity is not essential for *in vivo* function of the Z-ring. Mutations on the front and back side of FtsZ are all benign and surprisingly, all lateral mutation failed to complement the bacteria.

3.1.1 *Lateral mutants*

Lateral association between FtsZ protofilaments seems to be important for cell division. Changes within a lateral motif of FtsZ of other bacteria like *Bacillus subtillis* (i. e. H9 and H10 helix) also cause to inhibit bundling jeopardizing this way cell division [Monahan et al., 2009].

Jaiswal *et al.* mutated the 93 amino acid changing its charge and replacing it with an arginine aa (positive to negative charge) giving as a result an enhanced bundling and stability of the FtsZ protofilaments [Jaiswal et al., 2010]. Arginine amino acid appears to be an abundant residue at protein-protein interfaces, giving therefore a combined stabilizing effect to this particular FtsZ mutant. FtsZE93R suppressed Z-ring dynamism inhibiting cell division, suggesting assembly (and disassembly) dynamics is tightly regulated within the cell.

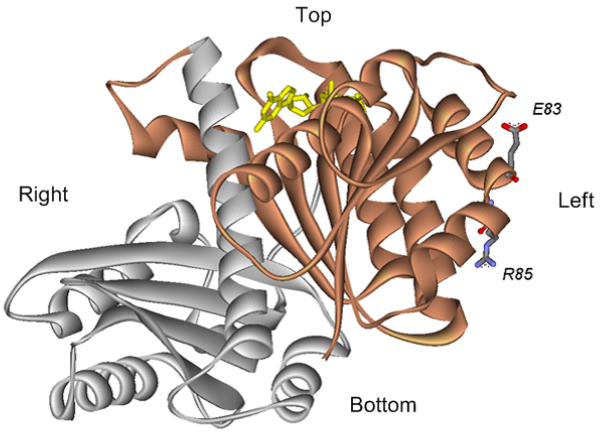

Figure 11: FtsZ structure model displaying the location of the lateral residues E83 and R85. Adapted from Shin et al. [2013].

Two interesting mutations located at the lateral side of FtsZ have also been studied [Shin et al., 2013]. Mutations on two highly conserved amino acids, glutamic acid on aa 83 and arginine on aa 85,

shown to be relevant for Z-ring formation (Figure 11). Both single-site mutations were made by a change in the charge of the corresponding residue by a neutral amino acid. Interestingly, both mutants changed cell viability and localization of the Z-ring *in vivo*, being the FtsZR85Q the most damaging one. From their experiments *in vitro* it can be seen how important these two mutations on FtsZ are: they affected the GTP-ase activity and impaired the lateral association of the filaments. Surprisingly, FtsZR85Q could not bundle even in the presence of ZipA or Ca^{2+} *in vitro*.

3.2 MODELING FTSZ POLYMERS

From available polymerization data *in vitro* some mechanisms have been proposed based on theoretical calculations for the Z-ring formation and how it can generate the force needed for constriction in bacteria [Lu et al., 2000, Osawa et al., 2008, 2009, Osawa and Erickson, 2011, Mateos-Gil et al., 2012a]. GTP hydrolysis promotes its disassembly being this the driving motor for the highly dynamic nature of FtsZ polymers observed *in vivo* and *in vitro*. Some models are based on curvature induced by GTP binding and hydrolysis [Díaz et al., 2001, Allard and Cytrynbaum, 2009, Turner et al., 2012, Hsin et al., 2012, Cytrynbaum et al., 2012, Li et al., 2013]. In these models a change in curvature of the FtsZ polymer is the responsible for constrictive force generation (Figure 12).

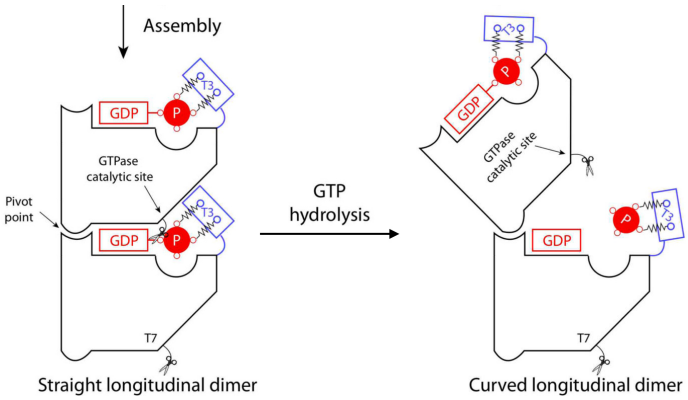

Figure 12: GTP hydrolysis responsible for the change in FtsZ polymer curvature. Adapted from Li et al. [2013].

Mathematical models have been proposed for the dynamic behavior of FtsZ polymers, where the force can be generated independently of nucleotide hydrolysis. These models are based on condensation of the FtsZ filaments (Figure 13). They address the formation of the Z-ring on cylindrical surfaces, the formation of FtsZ polymer structures that involve cross-liking and bundling, annealing of broken

polymers, and condensation by means of lateral interactions [Hörger et al., 2008b, Lan et al., 2008, Hörger et al., 2008a, Páez et al., 2009b, Lan et al., 2009, Páez et al., 2009a].

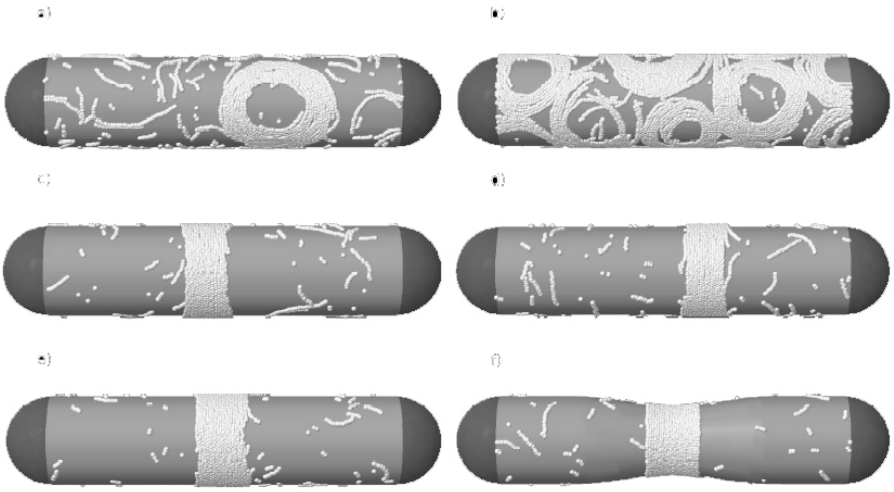

Figure 13: Snapshots of FtsZ polymers Monte Carlo simulations on a cylindrical surface. (a-b) Simulation parameters taken from AFM images extrapolated on a cylinder. f) Simulation obtained by decreasing the bonding surface energy and addition of a central deformation on the cylinder inducing constriction. Adapted from Páez et al. [2009a].

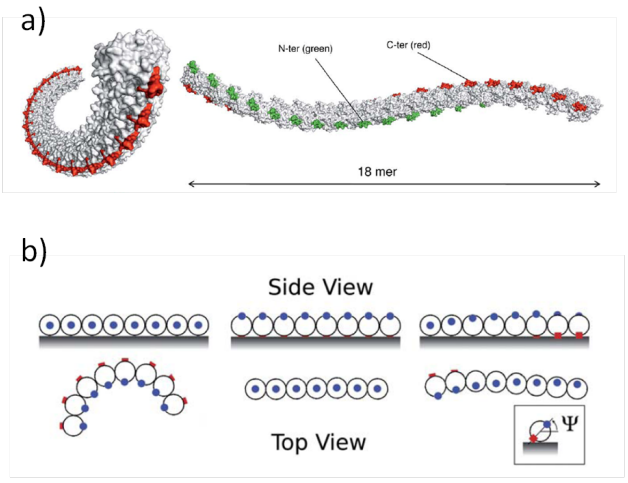

Figure 14: Torsion model. (a) Structural model for FtsZ polymer in solution, where red and green residues correspond to C-ter and N-ter ends respectively. (b) Orientation of FtsZ filaments on surfaces, where red and blue dots indicate the position of the C-ter and N-ter ends respectively. Adapted from González de Prado Salas et al. [2014].

González de Prado Salas *et al.* [González de Prado Salas et al., 2014] have lately proposed a theoretical model in which an FtsZ polymer shows a curvature and a twist (Figure 14), and that the presence of the torsion can explain the shape distribution observed by atomic force microscopy (AFM). This model stresses that FtsZ polymers can modulate the force applied to the cell membrane with a combination of filament curvature, torsion, and strength and orientation of its attachment to the surface.

It is worth noting that filament condensation model is not mutually exclusive with the curvature based ones, because in condensation models the GTPase activity is needed for polymer remodeling and FtsZ subunit turnover. Therefore, both lateral interactions and curvature of the FtsZ filaments are proposed to be responsible of generating in part the constriction force in the bacterium.

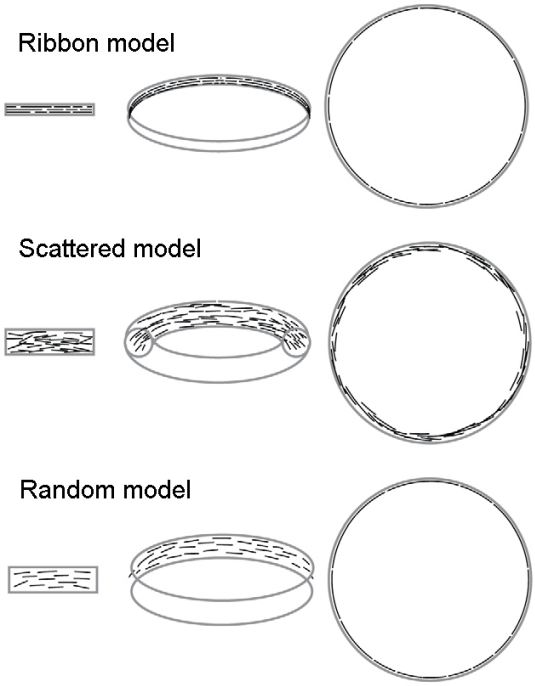

Figure 15: Schematic arrangement of protofilaments for the different proposed models inside the Z-ring. Adapted from Fu et al. [2010].

Filaments arrangement within the Z-ring is still under controversy (Figure 15). There are two models proposed: scattered and ribbon [Erickson et al., 2010, Mingorance et al., 2010]. Scattered model proposes an arrangement of short FtsZ filaments spanning the width of the Z-ring scattered randomly in longitudinal and radial directions, and they are stabilized by the other proteins present in the Z-ring

(ZipA, FtsA and Zap's proteins) and by points where lateral interactions take place [Si et al., 2013].

In the ribbon model filaments are ordered one next to each other, and they might or might not connect head-to-tail to form longer filaments. In this model, lateral interactions are the main component to stabilize a large bundle of filaments that surround the bacteria [Lan et al., 2009, Mingorance et al., 2010].

Fu *et al.* [Fu et al., 2010] propose yet another model, the random model, where protofilaments arrange randomly in a narrow band. The protofilaments in this model are separated by large spaces without the need of any lateral interactions.

It is still not clear how protofilaments are organized within the Z-ring. Single molecule approaches with enhanced resolution like Photoactivated Localization Microscopy (PALM) or 3D Structured Illumination Microscopy (3D-SIM) are not able to elucidate how these FtsZ filaments are arranged *in vivo* [Si et al., 2013, Piro et al., 2013, Buss et al., 2013]. Further advances in microscopy imaging *in vivo* along with reconstitution *in vitro* might help to resolve this dilemma.

4

OBJETIVES

Substantial progress has been made in understanding the function and structure of the Z-ring *in vivo* and *in vitro* during the last decade, but some information is still lacking. Arrangement of the FtsZ polymers within the Z-ring and the molecular basis of the force generation is still under controversy. Both filament curvature and lateral interactions, known to be required for cell division, have been proposed as relevant for constriction.

In this thesis we will explore the behavior of two non functional FtsZ lateral mutants described by Shin *et al.* [Shin et al., 2013]. Our purpose is to compare the mutants behavior *in vitro* on surfaces with that of the native protein.

We will describe how these lateral mutations affect:

- filament curvature and distribution on mica surface.
- FtsZ interaction with ZipA anchored to a surface.
- filament bundling on mica and on lipid bilayer surfaces of different compositions, when anchored through ZipA.

To provide a biophysical characterization of these two FtsZ lateral mutants we will use two surfaces techniques: Atomic force microscopy (AFM) and Quartz crystal microbalance (QCM). With AFM we will address FtsZ polymer shape and dynamism, and with QCM we will quantify their interaction with ZipA.

Part II

MATERIALS AND METHODS

A description of all materials used for the completion of this thesis are detailed below, as well as an introduction to the methodologies employed. I include also a step by step for sample preparation under each methodology described.

5

MATERIALS

5.1 REAGENTS

All reagents needed to prepare solutions such as $Tris - HCl$ (Trizma® hydrochloride), $NaCl$, $CaCl_2$, KCl, $MgCl_2$, KOH and $NaOH$ were acquired at Sigma-Aldrich, as well as guanosine 5′-triphosphate (GTP) sodium salt. The GTP nucleotide analog GpCpp, guanosine 5′-[(α, β)-methyleno]triphosphate (GMPCPP) sodium salt, was purchased at Jena Bioscience. All solutions to regulate pH and all buffer solutions were prepared with distilled and deionized water Milli-Q (Millipore®) and were filtered through a 0.2 μm cellulose membrane filter immediately before use.

5.2 PROTEIN PURIFICATION

E. coli FtsZ wild type (FtsZwt) was purified following the calcium-induced precipitation method as described by Rivas *et al.* [Rivas et al., 2000]. We will use a soluble ZipA protein (sZipA) constructed by eliminating its hydrophobic N-terminal domain completely (aa 1-25) and replacing those amino acids by a six histidines tail (6 His-tag) as described by Martos *et al.* [Martos et al., 2010]. Both FtsZwt and sZipA were purified by Estefanía Salvarelli at Jesús Mingorance laboratory (Hospital Universitario La Paz, Madrid, Spain).

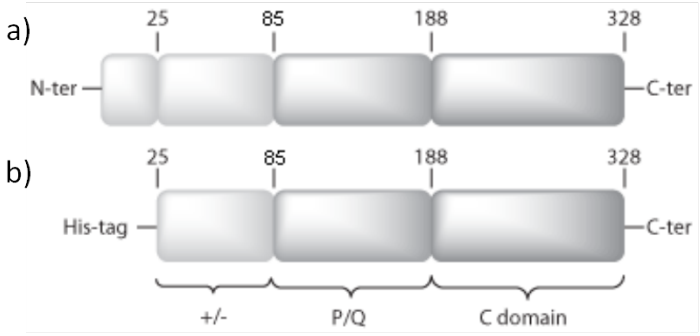

Figure 16: Domain structures os (a) ZipA and (b) sZipA . Adapted from Hale and de Boer [1997].

E. coli FtsZ mutants FtsZE83Q and FtsZR85Q were purified at Octavio Monasterio laboratory (Universidad de Chile, Santiago, Chile)

following a ammonium sulfate precipitation method as described by Shin *et al.* [Shin et al., 2013].

5.3 LIPIDS

The phospholipids used through this thesis are:

- L-α-Phophatidylcholine, Egg chicken extract (EPC),
- 1,2-dioleoyl-sn-glycero-3-phosphocholine (DOPC),
- 1,2-dioleoyl-sn-glycero-3-[(N-(5-amino-1-carboxypentyl)- iminodiacetic acid)succinyl] (DOGS-NTA) nickel salt,
- *E. coli* polar lipid extract (EcPl): PE, PG and CA.

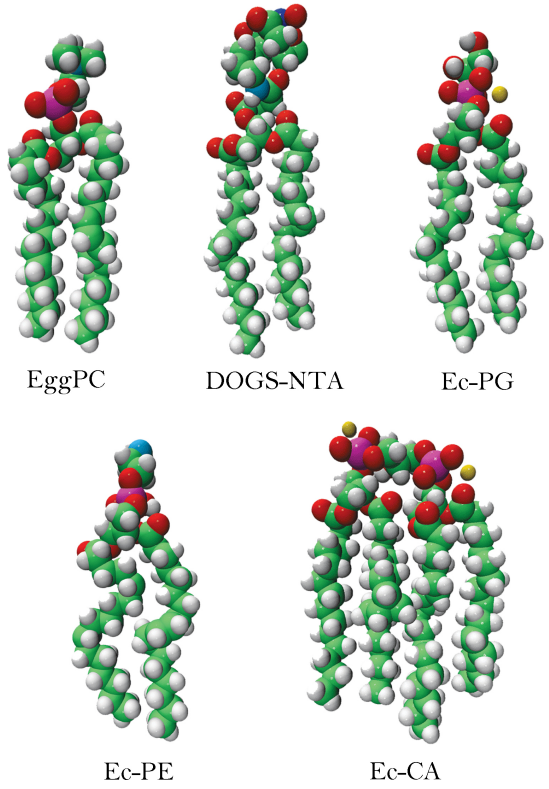

Figure 17: Phospholipids cartoon structures. Adapted from http://avantilipids.com/

All lipids were purchased at Avanti Polar Lipids Inc. in powder form. They were solubilized in a mixture of chloroform:methanol (1:1, v/v) and stored at -20°C.

The lipophilic tracer DiI (C18) was purchased at Invitrogen^{TM}, this fluorescent tracer was used to label the phospholipid bilayer membranes to measure lipid diffusion by Fluorescence recovery after photobleaching (FRAP).

5.4 SUBSTRATES

High quality Ruby muscovite mica (V1) needed for atomic force microscopy experiments was purchased at Aname. Ruby muscovite mica can be cleaved into thin films exposing a uniform mica surface upon splitting.

Substrates for Quartz Crystal Microbalance experiments were purchased at Q-sense with a fundamental resonance frequency of 5 MHz. We used high quality sensors of 14 mm diameter coated with either a uniform 50 nm layer of Silicon dioxide (SiO_2) or a 100 nm layer of Gold (Au).

6 METHODS

6.1 SUPPORTED LIPID BILAYER

A Supported Lipid Bilayer (SLB) is one of the components that forms the reconstituted system studied in this thesis. Here I describe how an SLB is obtained from a liposome solution.

6.1.1 *Liposome preparation*

Amphipathic lipids or phospholipids are one class of lipids that are more abundant in cell membranes [Rawn, 1983]. Phospholipid structure consists of a hydrophilic, water soluble head and hydrophobic hydrocarbon tails of variable length. It is most common to find hydrocarbon chains with an even number of carbon atoms, from 4 to 26 and they can be saturated or unsaturated. The degree of unsaturations, number of double bonds, present on the hydrocarbon chains affects the properties of membranes such as fluidity. The head polar groups can be phosphatidylcholine (PC), phosphatidylserine (PS), phosphatidylethanolamine (PE), phosphatidylglycerol (PG) and phosphatidylinositol (PI).

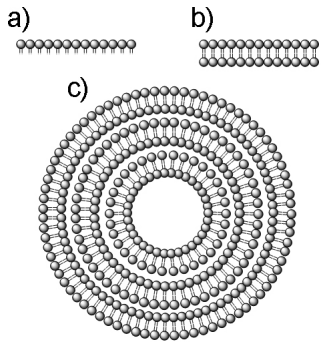

Figure 18: Schematic self-assembled lipid aggregates. (a) Monolayer. (b) Bilayer. (c) Multilamelar vesicle.

Due to the amphiphilic nature of phospholipids they spontaneously form aggregates by self-assembly (Figure 18). This process requires that many lipid molecules act together. In these lipid aggregates the polar heads are hydrated, and therefore exposed to the aqueous solvent while their hydrophobic carbonated chains are tugged away

from it. The simplest aggregate is a lipid monolayer; and two monolayers constitute a so called lipid bilayer with the hydrophobic chains pointing toward the center of the sheet. The hydrophobic effect provides the driving force for the formation of lipid bilayers. Because open ends in aqueous solutions are not energetically stable, lipid bilayers have to arrange themselves into two molecules thick closed structures called vesicles or liposomes. If dehydrated phospholipids are exposed to an aqueous solution they will spontanoeusly form multilamelar vesicles (MLVs), with several bilayers arranged concentrically separated by the aqueous solution [Hoff et al., 1995, Mouritsen, 2004].

Different methods like sonication or extrusion through a porous membrane are able to break those initial vesicles into single layer liposomes [Huang, 1969, Jr. et al., 1980, Woodle and Papahadjopoulos, 1989]. Unilamelar liposomes are the simplest vesicles, and they are extensively used as model for a cell membrane or drug delivery carriers to target cells. Depending on the diameter they can be classified as small unilamelar vesicles (SUVs) ($20 - 100\,\text{nm}$), large unilamelar vesicles (LUVs) ($0.1 - 1\,\mu\,\text{m}$), or giant unilamelar vesicles (GUVs) (several tens of micrometers). Large unilamelar vesicles were used in this thesis.

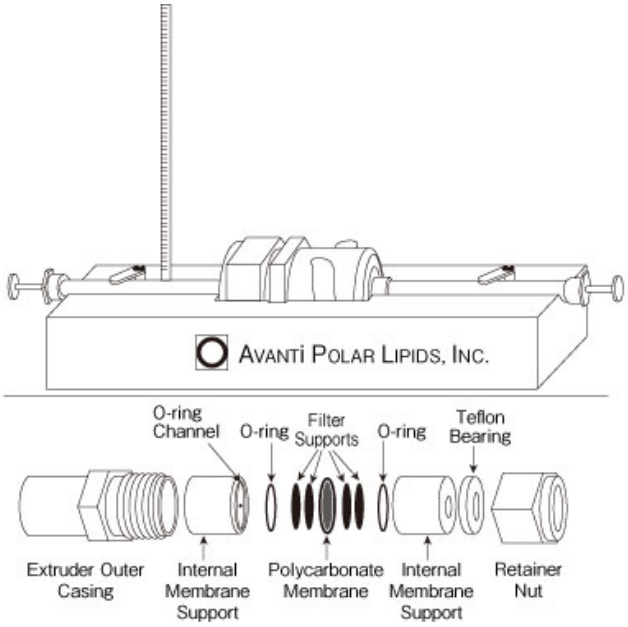

Figure 19: Avanti mini extruder diagram.

We chose the extrusion method to prepare LUVs, which can be summarized as follows: (i) a lipid mixture is put into a round bottomed flask and gently dried under a Nitrogen stream by 30 min until a thin layer of lipids forms in the bottom. (ii) Then a certain volume

of buffer solution (buffer A: $Tris - HCl$ 10 mM, pH 7.5, $NaCl$ 200 mM) is added to obtain the desired concentration of liposomes, usually 250 μL to have liposomes at 4 $^{mg}/_{mL}$ final concentration. (iii) The resuspended liposomes, now MLVs, are gently vortexed by 30 min until having an homogeneous mixture. (iv) Finally, the liposomes are run though an extruder (Avanti Mini extruder, Figure 19) with a know diameter porous membrane 31 times to form LUVs. Once formed, LUVs are immediately stored in airtight containers at 4°C up to a week.

6.1.2 *SLB formation*

Supported lipid bilayers form as for the adsorption of LUVs on a solid support [Helm et al., 1989, Sackmann, 1996, Richter et al., 2006].

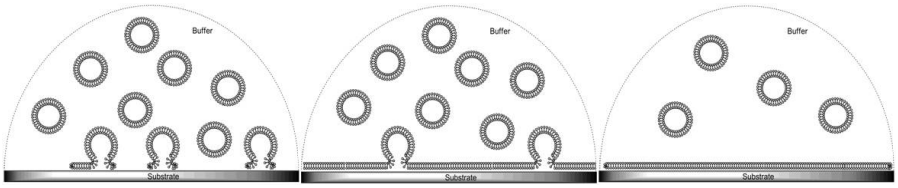

Figure 20: Schematic liposomes adsorption and SLB formation on a planar substrate.

Figure 20 shows a schematic SLB formation on a planar substrate. Substrates have to be clean and hydrophilic previous to the liposome incubation. Liposomes reach the surface and spontaneously spread, leaving a single bilayer where a few hydration molecules are in between the substrate and the bottom of the bilayer, and its upper face is exposed to the solution.

In the experiments done during the completion of this thesis we prepared supported lipid bilayers with a mixture of lipids. The composition was chosen given the net charge of the polar head of the phospholipids [Richter et al., 2006].

EPC and DOPC have a neutral (zwitterionic) polar head group and bilayers with either lipid composition made for a none charged bilayer. Both neutral phospholipids were used indistinguishably: their difference relies in the synthetic nature of DOPC in which all its hydrocarbonated tails are the same length (18 carbon atoms).

The EcPl is a natural extract of all polar lipids present in the inner membrane of the *E. coli* bacterium containing a 67% PE, 23.2% PG and 9.8% CA. Bilayers formed with this mixture have a negative net charge under the range of pH used in this work.

Neutral PC and *E. coli* polar lipid bilayers contain a molar percentage of DOGS-NTA (10% and 20% respectively). This particular

phospholipid has a nickel-chelating head group which is used to immobilize proteins containing a short sequence of histidine residues (a His-tag). In this thesis DOGS-NTA was used to correctly orient sZipA to the bilayer and the amount of this lipid was chosen to ensure a monolayer of protein bound to the bilayer.

6.2 ATOMIC FORCE MICROSCOPY

Atomic force microscopy (AFM) belongs to a larger group of proximal probe microscopy techniques known as Scanning probe microscopy (SPM). These techniques opened new possibilities to research surfaces because of their higher scanning resolution than electronic and optical microscopy. The Scanning tunneling Microscope (STM), the AFM predecessor, was developed by Gerd Binning and Heinrich Rohrer in the early 1980s, which allowed imaging of conducting and semiconducting materials. With the development of the STM it became possible to image single atoms on a flat surface by bringing a conductor (or semiconductor) tip near a conducting (or semiconducting) surface where electrons are able to tunnel from the tip to the surface or vice-versa. The great impact of this technique, able to resolve surface structures in a three dimensional space with a spacial resolution below the Angstrom, owed Binning and Roher a Nobel Prize in 1986. AFM was developed by G. Binning, C. F. Quate and C. Gerber in 1986 extending the STM technique [Binnig et al., 1986], when arose the need to study the structure of conducting surfaces and nonconductive materials. AFM registers the interaction force between a tip and a surface instead of electron current as in STM (Figure 21a).

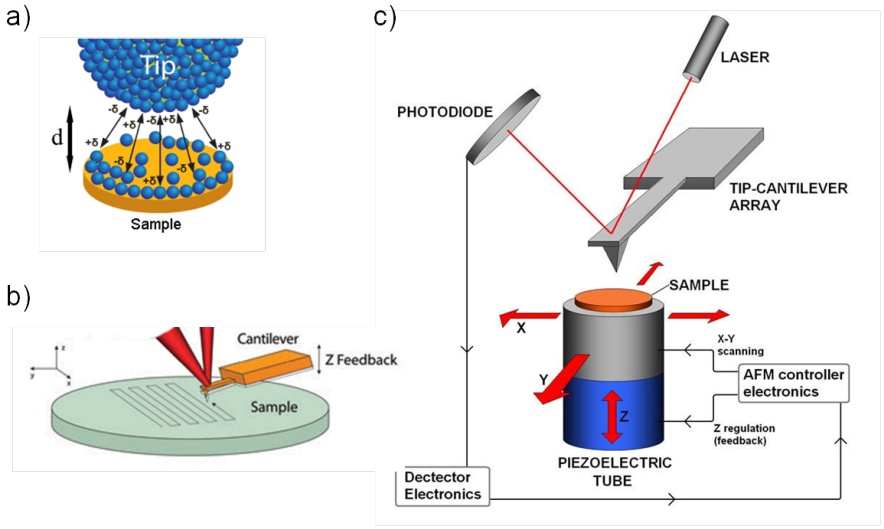

Figure 21: Atomic Force Microscopy. (a) Probe-sample interaction. (b) Raster scan. (c) Schematic AFM general components.

In the AFM a very sharp tip (the probe) at the free end of a cantilever spring with a radius of a few nanometers, is used to raster scan a surface (the sample) [Butt et al., 2005] (Figure 21b). The raster scanning is made by the expansion and contraction of a piezoceramic tube controlled by a computer system with subnanometer accuracy.

An optical system is used to monitor the deflection of the cantilever, and a topographic image of the sample is obtained plotting this deflection versus the position on the sample, sometimes with atomic resolution. To record the height of the sample a feedback loop maintains a constant deflection between the tip and the sample, by calculating the voltage needed for the piezoelectric to expand or contract accordingly (Figure 21c).

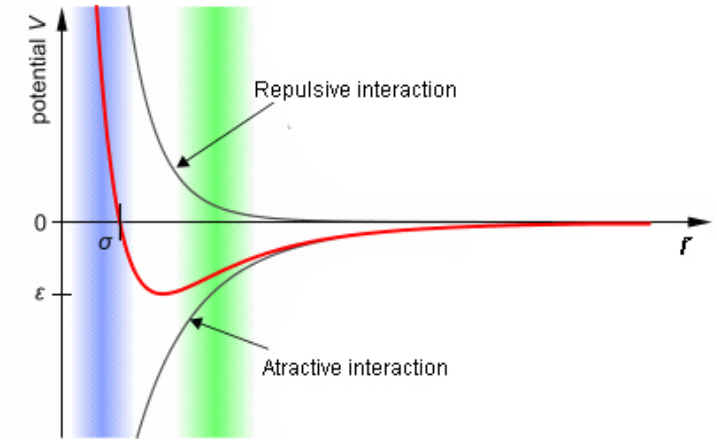

Figure 22: Lennard Jones potential.

The interaction between the probe and the sample can be described by a Lennard-Jones potential (Figure 22), which describes the interaction between two neutral atoms or molecules separated by a distance r:

$$V_{LJ}(r) = 4\epsilon \left[\left(\frac{\sigma}{r}\right)^{12} - \left(\frac{\sigma}{r}\right)^{6} \right] \tag{1}$$

where ϵ is the depth of the potential well and σ is the distance at which the potential is zero. This potential is the contribution of two terms: i) a short-range repulsive term due to the overlapping of electron orbitals $\left(\propto r^{-12}\right)$, and ii) a long-range attractive term due to the Van der Waals force $\left(\propto r^{-6}\right)$.

Van der Waals force, in which the operation of the AFM is based on, includes the interaction between atoms, molecules, surfaces and other intermolecular forces except for covalent and ionic bonding. Another force, the capillary force, contributes also to the probe-sample interaction while using the AFM in air. This force arises from the thin layer of liquid which forms a meniscus between the surfaces of the probe and the sample.

The interaction force between the probe and the sample is given by the derivative of the potential, $V(r)$, with respect to the separation distance r:

$$F(r) = -\frac{\partial V(r)}{\partial r} \tag{2}$$

Figure 23 represents a typical cantilever deflection *vs.* piezo height curve in a complete cycle of approaching and retracting of the probe from the sample. On the right side the piezo is completely retracted and there is no contact between the tip and the sample. There is a distance where the tip contacts the sample and a deflection in the cantilever is registered. Once the completion of the given extension of the piezo, the probe is retracted and the deflection of the cantilever decreases. At the distance where the tip entered into contact with the surface, the probe is still attached to the sample due to adhesion forces, and this is registered as a negative deflection of the cantilever. Finally, the tip snaps off the surface and the deflection of the cantilever is zero while it retracts to the initial position of the piezo.

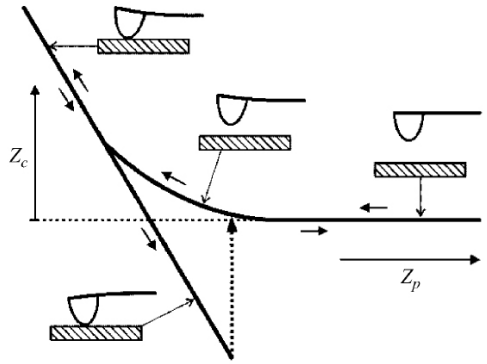

Figure 23: Schematic cantilever deflection *vs.* piezo height curve (Z_c *vs.* Z_p) in a complete cycle. Adapted from Butt et al. [2005].

The cantilever is the key element in the functioning of the AFM and their mechanical properties are responsible for its proper performance. The mechanical properties of the cantilevers are those of a elastic spring described by the Hook´s law, where the force needed to extend the spring a distance x can be written as

$$F(x) = -k \cdot x \tag{3}$$

where k is the spring constant. The sensibility of the measurement is defined by the spring constant k and the resonance frequency ν,

which both can be calculated from the properties of the material and the dimensions of the cantilever. For a rectangular geometry of the cantilever, the spring constant is

$$k = \frac{Evt^3}{4L^3} \tag{4}$$

where E is the Young´s modulus, t is the thickness and L is the length of the cantilever. A good cantilever is the one with high sensibility (a low ratio t/L) able to have a large deflection at small force, this can be achieved by making cantilevers long and thin. Commercial cantilevers are usually made of silicon or silicon nitride and they can be manufactured to have large sensibility and small dimensions (Figure 24a).

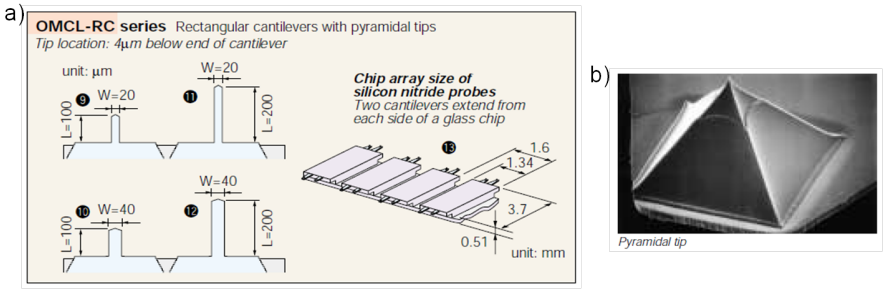

Figure 24: Gold deposited silicon nitride cantilevers. (a) Cantilever arrangement and dimensions. (b) Scanning electron microscopy image of a pyramidal tip. Adapted from http://probe.olympus-global.com/

The cantilever tip can be fabricated with a pyramidal or conic geometry made of silicon or silicon nitride with a typical $15 - 30\,\text{nm}$ radius (Figure 24b). These tips can also be functionalized by different coatings or chemically modified, or prepared by special procedures for particular uses.

The top face of the cantilever is often coated with a layer of gold to increase reflection of the laser beam. The deflection of the cantilever is measured using an optical technique, in which a laser beam focused onto the end of the cantilever, on its golden coated face, reflects and is monitored by a photodiode detector (Figure 25). When the cantilever is bent the reflected laser beam moves accordingly, this change in the spot position onto the detector is recorded to calculate the force between the tip and the sample. The spot size and shape of the laser beam onto the photo-detector influences also the sensibility of the measurement.

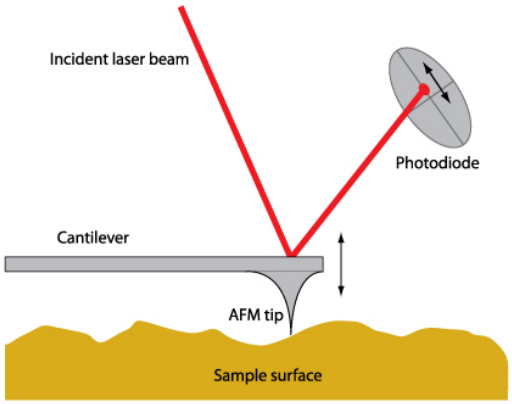

Figure 25: Schematic AFM photo-detection mechanism.

There are three operation modes for the AFM: i) *contact mode*, ii) *dynamic mode* and iii) *intermittent contact mode*.

The *contact mode* is the simplest operation mode where the normal force registered is kept constant. A feedback control is used to account for any topographical changes of the scanned sample to have a constant deflection of the cantilever. The vertical position of the sample is then adjusted by the expansion or contraction of the piezoelectric tube. Lateral forces are present while scanning in this mode and are registered as a lateral torsion of the cantilever. These lateral forces can be much larger than the normal forces applied to the sample and therefore are much destructive when scanning soft samples such as biological.

The *dynamic mode* operates in the non-contact region of the interaction potential. A second piezoelectric piece is needed to put the cantilever under resonance to keep a resonance amplitude constant or a resonance frequency constant. Any change in topography generates a change in the resonance amplitude or frequency.

The *intermittent contact or jumping mode* is characterized by a cycle of approximation and retraction of the piezoelectric tube in each pixel forming the raster scan. The sample is approached to the tip a given jump distance, *jump off*, while the deflection of the cantilever is registered. The vertical position of the sample is adjusted until the deflection reaches a given value determined by the user, *setpoint*, respect to the initial value when the tip is retracted from the sample. This position of the piezo is registered as the height at the corresponding pixel and a topographic image can be constructed from it. Then the piezo retracts and moves to the next scanning point. This operating mode is the preferred with soft samples since it minimizes the lateral forces and the interaction time between tip and sample, where both effects can contribute to sample damaging [de Pablo et al., 1998, Moreno-Herrero et al., 2004].

6.2.1 *AFM imaging in liquid*

AFM allows scanning samples in air, vacuum, different gases, or liquids, becoming an important technique to study biological systems under physiological conditions. It is also an important technique to follow dynamic biological processes taking place in real time, and conformational changes of proteins and their interactions with other proteins [Engel and Muller, 2000, Müller et al., 2002, Müller and Engel, 2002, Kodera et al., 2003, González et al., 2005, Mateos-Gil et al., 2012a,b].

The interaction forces between tip and sample are different than for air measurements, and can be explained by the DLVO theory (named after Derjaguin, Landau, Verwey and Overbeek) [Israelachvili, 2011]. In this theory the interaction of two particles is assumed to be the contribution of two terms: the Van der Waals attraction and the electrostatic double-layer repulsion. The main contribution is the electrostatic Debye double-layer force, due to the counterion layer surrounding the surface of tip and sample. This electrostatic force can be modulated optimizing the salt concentration and pH of the aqueous solution. There are other interactions between tip and sample important in liquid, such as solvation, hydration repulsion, hydrophobic attraction, steric, or even adhesion forces due to the formation of chemical bonds.

The AFM in biology is used to provide a topographic image of a surface and also to study the force between probe and sample at different separations between them. This application is know as force spectroscopy, which have been giving new insights in the study of interactions within and between molecules, as well as ligand-receptor interactions [Carrión-Vázquez et al., 1999, Rief et al., 1997, Clausen-Schaumann et al., 2000, Hinterdorfer and Dufrene, 2006, Valbuena et al., 2012].

In this thesis a commercial AFM from Nanotec Electrónica (Madrid, Spain) was used provided with a laser of 632 nm wave length (red laser beam); commercial rectangular cantilevers RC800PSA from Olympus with 800 nm thickness and spring constants $0.05 - 0.76\,\mathrm{N/m}$; and the jumping operating mode was the preferred. Images were taken applying a force < 100 pN.

To study biological samples under physiological conditions a special chamber is needed where the probe and the sample are both immersed in liquid. The chip containing the cantilever is firmly attached to the upper part of the chamber which is enclosed by a transparent sapphire window. The sample located on the bottom completes the liquid chamber in an open configuration (Figure 26a).

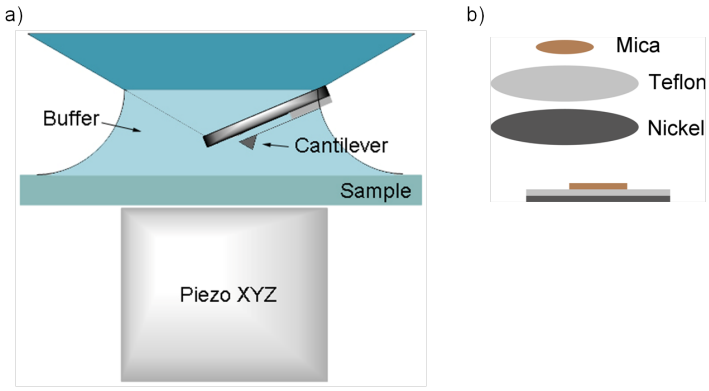

Figure 26: AFM imaging in liquid. (a) Liquid chamber. (b) Sample holder.

The most convenient geometry for an AFM sample holder is a planar surface. The planar sample holder for our specific AFM is made by a stack of three layers (Figure 26b). From top to bottom: a $1/8$ inch diameter disk of mica where the sample will be adsorbed, a $1/2$ inch diameter disk of Teflon, and a $1/2$ inch disk cut from a nickel sheet to ensure a firm attachment to the magnet present on the piezoelectric tube. The AFM used on this thesis has the piezoelectric tube under the sample, hence the Teflon surface is needed to provide an hydrophobic surface able to contain the liquid drop within the mica surface, avoiding this way any spills on the piezoelectric piece.

6.2.2 *Sample preparation*

Adsorption of the proteins on mica.

The sample preparation for the adsorption and polymerization of FtsZ on mica is summarized as follows (represented in Figure 27):

1. Protein equilibration. FtsZ protein was diluted in buffer solution (buffer BPZ: $Tris - HCl$ 50 mM, pH 7.5, KCl 500 mM and $MgCl_2$ 5 mM) to 12.5 μM final concentration and equilibrated at room temperature by 10 minutes.

2. FtsZ adsorption. A 40 μL volume of FtsZ solution was incubated on freshly cleaved mica for 1 minute in the presence of 1 mM GTP. After incubation time, the protein was extensively rinsed with buffer BPZ with 1 mM GTP previous to imaging.

The sample preparation for FtsZ-sZipA interaction on mica is summarized as follows (Figure 28):

1. Protein equilibration. FtsZ and sZipA proteins were diluted together in BPZ to 3 μM and 12.5 μM final concentration respectively, and were equilibrated at room temperature by 10 minutes.

2. Proteins adsorption. A 40 μL volume of FtsZ-sZipA solution was incubated on freshly cleaved mica for 1 minute in the presence of 1 mM GTP. After incubation time, the proteins were extensively rinsed with buffer BPZ with 1 mM GTP previous to imaging.

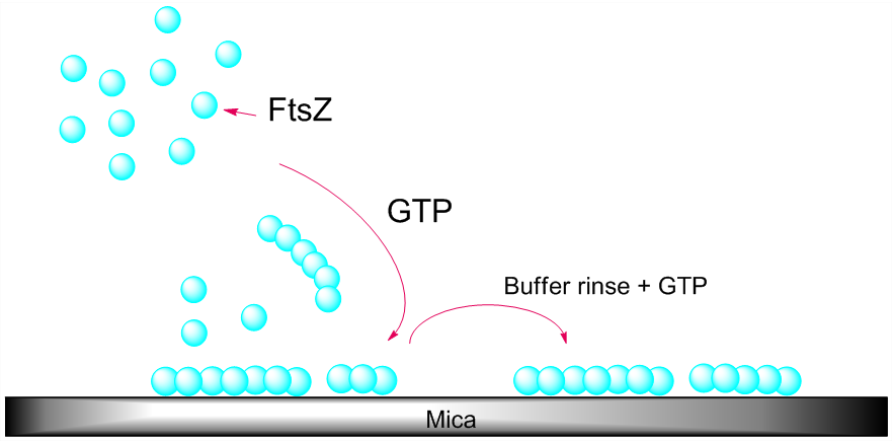

Figure 27: Schematic FtsZ adsorption and polymerization on mica.

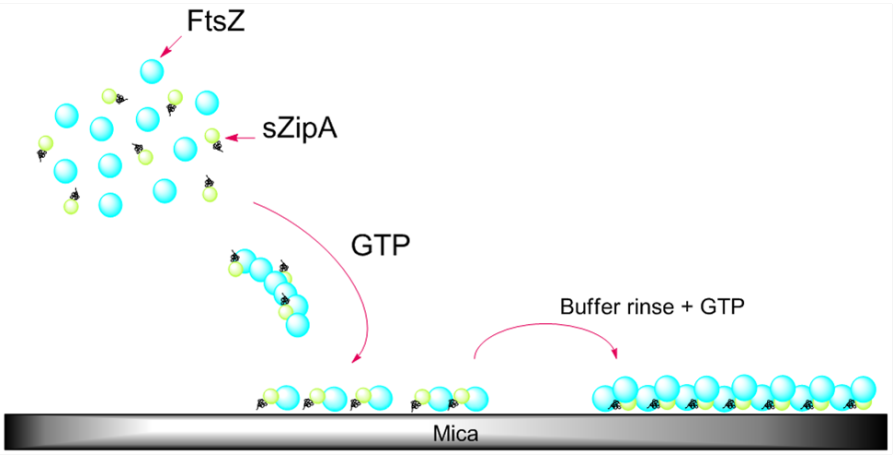

Figure 28: Schematic FtsZ-sZipA adsorption and polymerization on mica.

Adsorption of the proteins on a lipid bilayer.

The sample preparation is summarized in the following steps, and schematically represented in Figure 29:

1. SLB formation. A 40 μL liposomes volume in buffer A at 0.1 $^{mg}/_{mL}$ was incubated on freshly cleaved mica for 1 hour at room temperature. If EcPl lipids were used, a 2 mM $CaCl_2$ was added

to the buffer. Freshly cleaved mica exposes a negative surface charge density, for this reason negatively charged liposomes need a divalent cation to bridge the negative charges to form a SLB. The sample was extensively washed with buffer previously to imaging.

2. Recharge of the chelating lipid DOGS-NTA. When the SLB was completely characterized we proceeded to recharge the chelating lipid DOGS-NTA with the addition of 5 mM $MgCl_2$ to buffer A for 10 min prior to the adsorption of sZipA. This additional step will guarantee all nickel chelating lipid head groups are active to bind a His-tagged protein.

3. sZipA and FtsZ adsorption. sZipA and FtsZ were diluted at 2.5 μ M and 12.5 μ M final concentration respectively in buffer BPZ, and incubated 1 hour at room temperature. After the incubation time, the proteins were washed extensively with buffer previous to imaging.

4. Nucleotide addition. The final step was the addition of the nucleotide, 1 mM GTP was added to the sample and was kept until the completion of the experiment.

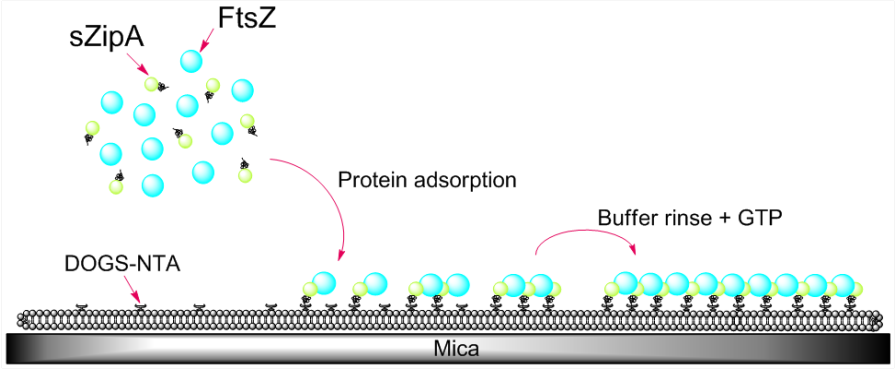

Figure 29: Schematic FtsZ-sZipA adsorption on a supported lipid bilayer on mica.

6.3 QUARTZ CRYSTAL MICROBALANCE

A biosensor is a devise that provides quantitative information using a biological recognition element (e.g. bioreceptors, antibodies, DNA, proteins, enzymes or cells) in direct contact with a transduction element that converts the binding elements into measurable electrical signals [Cooper and Singleton, 2007, Becker and Cooper, 2011]. Acoustic biosensors, based on the propagation of an acoustic wave, have been developed for label-free detection of molecular interactions, molecular recognition and their associated phenomena. They provide a unique method to observe *in situ* and monitor in real time soft matter processes (mass, viscoelasticity, density, etc) since the parameters that describe a propagating wave are dependent on the properties of the propagating material [Thompson and Hayward, 1997, Janshoff et al., 2000].

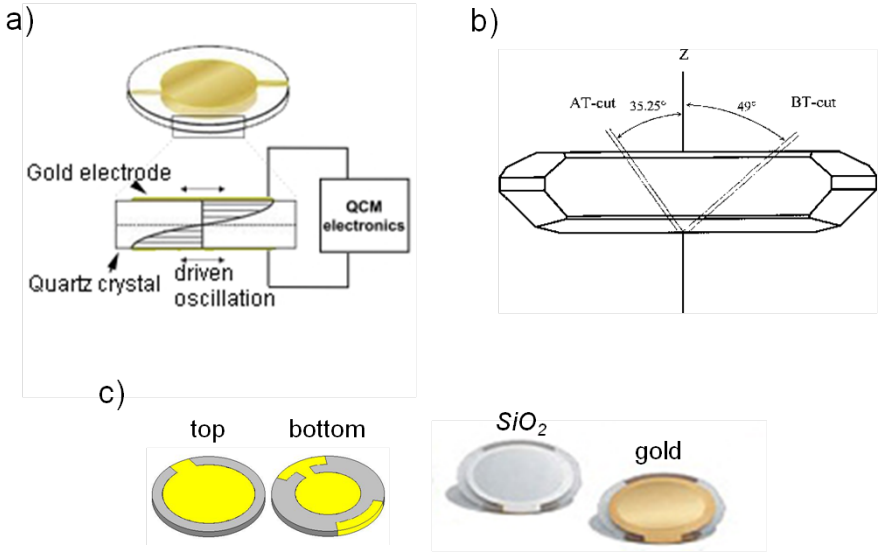

Figure 30: Quartz Crystal Microbalance. (a) Operating principle. (b) Quartz crystal AT-cut. (c) Substrate: top, bottom and surface coatings (SiO_2, Au).

Thickness shear mode (TSM) or Quartz crystal microbalance (QCM) is an acoustic wave resonator in which the piezoelectric properties of quartz are employed (Figure 30). The advantage of a piezoelectric transducer is that it can promote the propagation of a transverse acoustic wave across the bulk of certain crystalline materials, such as quartz, by coupling its mechanical and electrical responses (Figure 30a).

The piezoelectric piece in QCM is an AT-cut thin quartz disk (Figure 30b), cut from a quartz mineral at 35.25° orientation with respect

to its optical axis, sandwiched between two gold electrodes (Figure 30c). An applied electric field will generate a shear, tangential deformation of the crystal, this deformation moves both surfaces in opposite directions.

A standing wave occurs during a phenomenon known as resonance due to the interference of two waves of equal amplitude, frequency and wavelength traveling in opposite directions. The stationary wave propagates in the perpendicular plane to the surfaces, transversal wave, with wavelengths that are multiple factors of double the thickness of the crystal. By solving the wave equation, the resonance frequency can be expressed as:

$$f_n = \frac{n \times v}{2d_Q} \tag{5}$$

where n is the order of the overtone ($n = 1, 3, 5 \ldots$) and v is the acoustic wave velocity; the resonance frequency of an AT-cut quartz crystal will increases with decreasing the crystal thickness d_Q. The acoustic standing wave velocity is dependent on the crystal structure parameters

$$v = \sqrt{\frac{E}{\rho}} \tag{6}$$

where ρ is the density and E is the Young modulus.

The acoustic transducer became interesting to physicists and chemists when Sauerbrey [Sauerbrey, 1959] showed there is a linear relationship between the mass adsorbed to the surface and the resonant frequency. The Sauerbrey expression is derived assuming the film layer deposited at the surface of the crystal follows its vibration, this way the crystal behaves as if it were thicker which leads to a decrease of its resonance frequency:

$$\Delta d_Q = -n \frac{v}{2f_n^2} \Delta f_n \tag{7}$$

since $f_n = nf_0$ (where f_0 is the fundamental frequency of the resonator) and $d_Q = m/\rho$. Replacing this in Equation (7):

$$\Delta f_n = -\frac{2nf_0^2}{Av\rho} \times \Delta m \tag{8}$$

which can be rewritten as:

$$\frac{\Delta m}{A} = -\frac{v\rho}{2f_0^2} \times \frac{\Delta f_n}{n} = -C\frac{\Delta f_n}{n} \tag{9}$$

Equation (9), known as Sauerbrey equation, relates the change in mass Δm per unit area of an ideal thin layer attached to the resonant surface with the decrease in resonance frequency Δf. The sensitivity constant C depends on the fundamental frequency (f_0) and the properties of the quartz crystal (v and ρ):

$$C = \frac{v\rho}{2f_0^2} \tag{10}$$

taking that the quartz density is $\rho = 2650\, Kg/m^3$, the acoustic velocity in the quartz is $v = 3340\, m/s$ and the fundamental frequency is $f_0 = 5\, MHz$ (for the crystal used in this thesis), all yields a value for the sensitivity constant of $C = 18.1\, ng/Hz \cdot cm^2$. Is important to note that this model is valid only when there is a thin (less than 10% of the crystal mass), rigid (no energy dissipation) and uniform (evenly distributed) deposited layer.

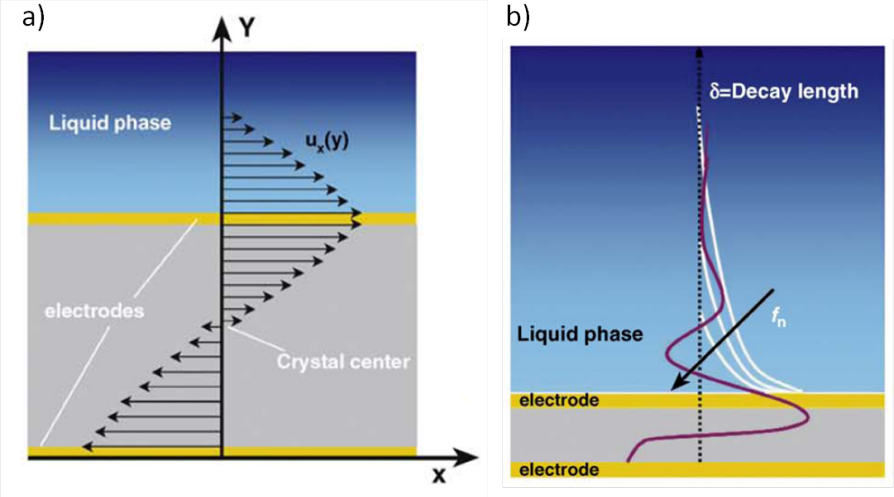

Figure 31: QCM operating in liquid. (a) Acoustic wave propagates into the liquid phase. (b) Decay (penetration) length of the propagating wave. Adapted from Ferreira et al. [2009].

When the resonator operates in liquid the viscoelastic properties of the adsorbed layer is significantly different as those of the sensor. The presence of a semi-finite liquid layer needs to be accounted for because there is an energy loss to the fluid through a viscous coupling. The velocity profile of the fluid subject to a shear deformation is of a laminar flow parallel to the surface described by the Navier-Strokes one-dimensional equation (Figure 31a). The effect of this coupling to the resonance frequency was modeled by Kanazawa and Gordon [Kanazawa and Gordon, 1985] assuming that the fluid in the vicinity

of the surface moves at the same velocity as the surface. They found a relationship between the product of the density and viscosity of the fluid to the frequency shift of the shear resonating wave:

$$\Delta f_n = -\frac{f_0^{3/2}\sqrt{n}}{\pi^{1/2}\rho v}\sqrt{\rho_L \eta_L} \tag{11}$$

where ρ_L and η_L are the density and viscosity of the fluid respectively. This solution predicts a damping in the shear wave with a characteristic length δ dependent on the resonance frequency

$$\delta_n = \sqrt{\frac{2\eta_L}{\omega_n \rho_L}} \tag{12}$$

where $\omega_n = 2\pi f_n$ is the angular frequency, hence Equation (12) can be expressed as

$$\delta_n = \frac{1}{\sqrt{n}}\sqrt{\frac{\eta_L}{\pi f_0 \rho_L}} \tag{13}$$

that is, the penetration length of the acoustic wave propagates a larger distance in fluids with higher (η_L/ρ_L) ratios. Because of the decay length dependency on the frequency

$$\delta_n \propto \frac{1}{\sqrt{n}} \tag{14}$$

recording the overtones will give information about the different layers at different distances from the sensor. For the different overtones, the penetration length is: $\sim$ 252 nm, $\sim$ 146 nm, $\sim$ 113 nm, $\sim$ 95 nm, $\sim$ 84 nm and $\sim$ 76 nm for $N = 1, 3, 5, 7, 9$ and 11 respectively (Figure 31b). On this thesis we measured the loading of the sensor at the 7^{th} overtone.

When operating the QCM in liquid, the change in frequency will be due to the loading mass deposited at the surface of the resonator and to the presence of the semi-fine liquid. Therefore making it difficult to distinguish which one is making the contribution to the resonance frequency.

Martin et. al [Martin et al., 1991] have derived a model in which both contributions are taken into account by adding Equation (9) and (11), Sauerbrey and Kanazawa models:

$$\Delta f = \Delta f_m + \Delta f_L \tag{15}$$

Equation (15) also shows that the overall change in resonance frequency is sensible to changes in the viscosity of aqueous solution

and the loaded sample as well as variations of viscosity due to temperature. Therefore, acquired data have to be carefully treated and interpreted. Besides this disadvantage, QCM has been used with extended success because the resonant frequency of the sensor can be monitored continuously, and because upon injection of a sample, the variation in the resonance frequency can be obtained by comparison with a reference. The mass adsorbed to the resonator surface can be decoupled of the liquid loading by simply subtracting a baseline.

Impedance analysis of the QCM allows a full description of the acoustic load because several factors influence the resonance frequency of the resonator. Mason *et al.* [Mason and Bateman, 1966] developed a model that relates the mechanical oscillation of a resonator with an electrical circuit, and provides the basis for the theoretical description of a composite system.

QCM resonance can be modeled by a damped oscillatory motion. The piezoelectric resonator can be characterized by its mechanical impedance $Z = |Z| \times e^{i\Theta}$ in which the real part represents the loss in mechanical energy while the imaginary part is defined by the mechanical energy storage at the surface. The magnitude of the mechanical impedance ($|Z|$) measures the signal attenuation and the phase (Θ) the lag between the applied field and the resulting displacement.

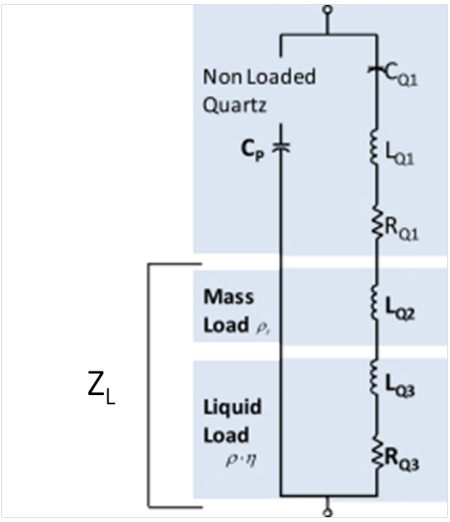

Figure 32: Equivalent lumped circuit: BVD model circuit.

Mason model near resonance can be transformed into an equivalent lumped element model circuit, known as Butterworth–van-Dyke (BVD) circuit. BVD circuit combines a parallel and series resonance circuit (Figure 32). The series part of the circuit is described by the

electrical impedance Z_e which comprises a resistor R, an inductor L and a capacitor C:

$$Z_e = R + i\omega \left(L - \frac{1}{\omega^2 C} \right) \tag{16}$$

where ω is the angular frequency of the voltage applied to the resonator ($\omega = 2\pi f$). The electrode on both sides of the crystal provide an additional parallel capacitance element C_0 to the model circuit. The resistance R includes information about intrinsic viscosities of the quartz and is the term that accounts for the acoustic energy dissipation.

Operating the QCM in liquid leads to a decrease in the resonance frequency, which is associated to a decrease and a widening of the resonance peak. The resonance peak is given by the admittance

$$Y = \frac{1}{|Z_e|} = \frac{1}{\sqrt{R^2 + \left(\omega L - \frac{1}{\omega C}\right)^2}} \tag{17}$$

The quality factor Q is the ratio between the resonance peak and its width at half maximum w, which depends inversely on the width of the resonance peak:

$$Q = \frac{f}{w} \tag{18}$$

Q is defined as the energy stored in the circuit divided by the dissipated energy in one complete cycle at resonance:

$$Q = 2\pi \frac{E_{stored}}{E_{dissipated}} \tag{19}$$

For a series resonant circuit, the dissipation factor D can be calculated as the inverse of the quality factor Q:

$$D = \frac{1}{Q} = R\sqrt{\frac{C}{L}} \tag{20}$$

which gives a quantitative measurement of the energy dissipated in the system.

When Nomura and Okuhara [Nomura and Okuhara, 1982] developed the operation of the QCM circuits in liquids, applications to biological samples became possible. Theoretical models are needed to account for all the observed frequency shifts to explain different types of sample loading, like thick films, viscous liquids, elastic solids and viscoelastic bodies. The impedance of the loaded sensor can be

expressed as an additional element in series in the BVD circuit Z_L representing the load (Figure 32). Multilayers consisting of different kind of loaded layers can be described therefore as linear combination of the impedances of each one.

The impedance approach can provide useful information about the material-specific parameters of the immobilized layers, i.e. film thickness, elastic modulus and viscosity. The ratio $\Delta D/\Delta f$, know as acoustic ratio, have been used to infer about the rigidity of a layer adsorbed to the surface or its water content as it is related to the intrinsic viscosity [Tsortos et al., 2008a,b].

QCM has been used in the analysis of biological systems of diverse nature, from life science research to diagnostic assay development, biomaterials and food safety. It has been proved to be a useful tool for the detection of processes involving small molecular weight ligands, protein adsorption to surfaces, homeostasis, nucleic acids, carbohydrates, protein-protein interactions, viruses, bacteria, cells, lipidic and polymeric interfaces [Cooper and Singleton, 2007, Becker and Cooper, 2011, Speight and Cooper, 2012].

6.3.1 *Sample preparation*

In this thesis a QCM with dissipation monitoring resonator QCM-Z500 from KSV (Finland) was used. The internal temperature was controlled through a peltier, whereas for the external temperature a thermoblock was used in order to avoid any signal drift due to temperature changes. The sample was loaded into the closed chamber (Figure 33) by a channel distributor at a constant flow of 50 $\mu L/min$.

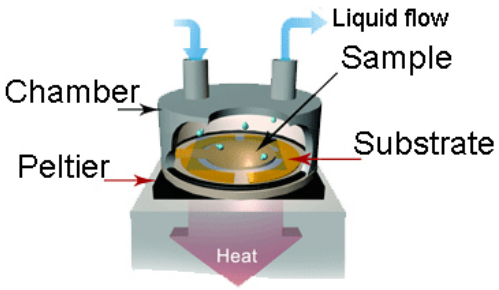

Figure 33: Schematic QCM closed chamber

Previous to adsorption of the sample, substrates have to be properly cleaned and activated.

6.3.1.1 *SiO_2 substrates*

SiO_2 substrates were suitable when neutral phospholipids were used. Substrate were cleaned with a SDS 2% (w/v) solution for 15 minutes, then washed with distilled water Milli-Q and dried under a stream of nitrogen. Following, the surface was activated by exposing it to UV light cleaner for 45 min to 1 hour. The exposition to the UV light cleans the SiO_2 by eliminating organic contaminants and oxidizing the silicon surface rendering it hydrophilic. Immediately after UV cleaning, the substrate was mounted in the QCM chamber.

6.3.1.2 *Au substrates*

Au substrates were used on the experiments involving *E. coli* polar lipids. The substrate was cleaned with a piranha solution (hydrogen peroxide:sulfuric acid, 1:3) for 3 minutes, followed by an extensive wash with distilled water Milli-Q and dried under a nitrogen stream. Then it was submerged into a solution 0.2 mM 3-mercaptopropionic acid (deionized water:ethanol, 1:1) and left 18 h until a self-assembled monolayer (SAM) was formed. The sensor was rinsed with distilled water Milli-Q and dried under a nitrogen stream prior to mounting the sensor in the chamber.

6.3.1.3 *Sample preparation*

We began with a SLB formation, followed by the anchoring of sZipA to the bilayer to a final adsorption of FtsZ (wild type or lateral mutants) to sZipA (Figure 34). Because QCM measurements follow the deposition of the material as time evolves, incubation times were dependent on type and concentration of the sample. However the sample preparation steps can be summarized as follows:

1. Acquisition of a baseline. The chamber was loaded with buffer, which was kept at a constant flow for about 15 minutes to ensure a baseline.

2. Liposome injection. A liposome solution diluted at 0.1 $\mathrm{mg/mL}$ was injected (for about 15 minutes) until a SLB was obtained, followed by a rinse with the same buffer for 10 minutes, operating this way we can account the change in frequency only due to the mass adsorbed to the sensor.

3. Recharge of DOGS-NTA lipid and rinse. Buffer with 5 mM $NiCl_2$ was injected by 10 minutes to recharge the chelating lipid DOGS-NTA followed by a rinse with buffer BPZ prior to the adsorption of the proteins.

4. sZipA injection. sZipA anchoring to the bilayer was registered. After its adsorption, all free protein was rinsed with buffer BPZ for about 15 minutes.

5. FtsZ injection. The last layer of protein was made by the adsorption of FtsZ to sZipA, by injecting it either at a fixed concentration or at different concentrations when a titration experiment took place. As with the previous layer, the free protein was rinsed with buffer BPZ.

6. Control rinsing. To prove specificity of sZipA binding to the chelating lipid DOGS-NTA, a solution of 200 mM imidazole was injected by 10 minutes. Imidazole will compete for the binding site of the Histidines present in sZipA to the chelating lipid group. The experiment finished with a final exchange of the liquid with buffer.

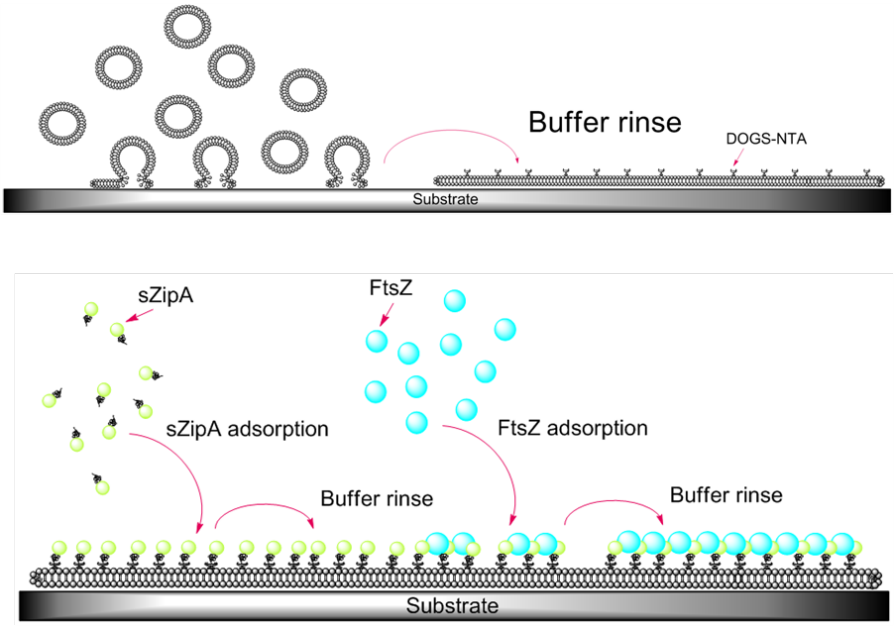

Figure 34: Schematic QCM sample preparation.

6.4 QUANTITATIVE ANALYSIS FOR QCM EXPERIMENTAL DATA

Binding between a receptor and a ligand is an interaction involved in many biological processes. In particular for this thesis a quantitative analysis for QCM experimental data of the formation of FtsZ-sZipA complex was performed.

6.4.1 *The Langmuir isotherm*

A single-site binding model describes the interaction of a ligand and a receptor [Haynie, 2001, Connors, 1987]. At the equilibrium, the binding follows mass action:

$$R + L \Leftrightarrow R \bullet L \tag{21}$$

where R is the receptor, L the free unbound ligand, and $R \bullet L$ is the receptor-ligand complex. The association constant is defined as:

$$K_a = \frac{[R \bullet L]}{([R]\,[L])} \tag{22}$$

and the dissociation constant is $K_d = K_a^{-1}$.

The Langmuir adsorption isotherm states the average number of moles of ligand per mole of receptor is given by

$$\phi = \frac{[R \bullet L]}{[R]_T} = \frac{[L]}{(K_d + [L])} \tag{23}$$

where ϕ is the fraction of occupied sites (or fractional saturation), $[R]_T$ the total concentration of receptor, and $[L]$ the concentration of free ligand. When $\phi = 1/2$, $K_d = [L]$, that is, the dissociation constant measures the concentration of free ligand at which half the binding sites are occupied. Langmuir isotherm derivations assume that there are a fixed number of localized sites present on the surface, and that the dissociation constant K_d is independent of coverage ϕ.

6.4.2 *Empirical Hill function*

To quantify the protein-protein interaction, i.e., between a ligand and a receptor, we used the empirical Hill function [Chang, 2005] for the fractional saturation:

$$\phi(C) = \phi_{max} \frac{(C/C_{1/2})^n}{1 + (C/C_{1/2})^n} \tag{24}$$

where ϕ_{max} is the fractional saturation at the maximum ligand concentration C. $C_{1/2}$ is the ligand concentration at which the fractional saturation is half its maximum, i. e., $\phi = {}^1/_2\phi_{max}$. The number n, know as Hill coefficient, is a parameter that indicates cooperativity: the higher the n is, the higher the cooperativity. If $n = 1$, the interaction process is non cooperative; if $n < 1$ there is a negative cooperativity of the association, that is, the binding of a new ligand is hindered by the ligands previously bound to the receptor; and if $n > 1$ the interaction displays a positive cooperativity in which the binding of a new ligand is favored by the previously bound ligands to the receptor. Equation 24 is an empirical approach to cooperativity; it says nothing about the mechanism involved.

We have used this approach to quantify the interaction of FtsZ to sZipA bound to a lipid bilayer.

6.5 FLUORESCENCE MICROSCOPY

Fluorescence microscopy uses fluorescence to study properties of organic or inorganic substances (Figure 35). Fluorescence occurs when energy is absorbed by the atom which becomes excited, the electron jumps to a higher quantum state and relaxes to its ground state by emitting a photon of light.

The technique of fluorescence microscopy has become an essential tool in biology science. The application of a fluorochrome has made it possible to identify cells and sub-microscopic cellular components. With the use of multiple fluorescence labeling it becomes possible to identify several target molecules at the same time.

Photobleaching is a process in which fluorophores irreversibly lose their ability to fluoresce as they are illuminated because of their interaction with molecular oxygen before emission. Photobleaching is exploited in a technique known as Fluorescence recovery after photobleaching (FRAP). This optical technique makes it possible to quantify the two dimensional lateral diffusion of a molecular thin film containing labeled probes. This method is very useful in biological studies involving cell membrane diffusion and protein binding.

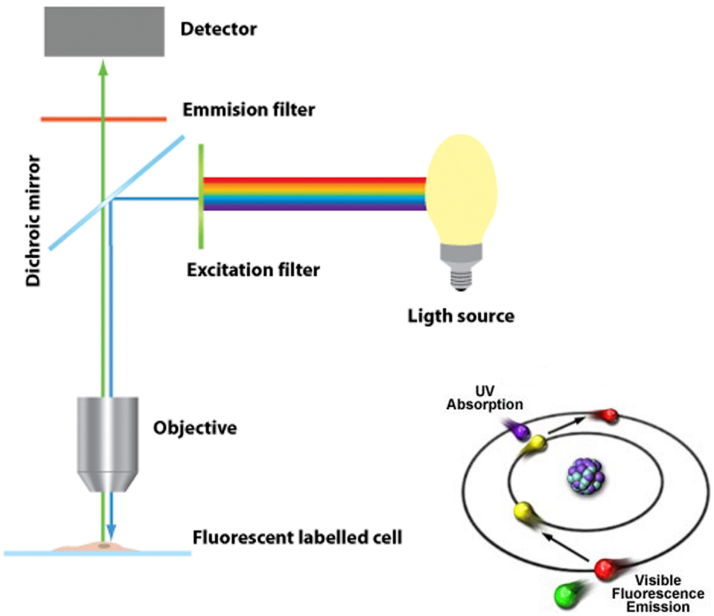

Figure 35: Diagram of fluorescence microscopy.

6.5.1 *FRAP measurements and sample preparation*

On this thesis FRAP experiments were performed using a E600FN Nikon microscope provided with a D-FL EPI-fluorescence attachment.

We used a lipophilic tracer DiI C18 (549 nm, 565 nm excitation and emission wavelengths respectively) for fluorescence measurements of a bilayer adding a 1% molar ratio of the fluorophore to the lipid mixture. The *E. coli* lipid bilayers were formed on *Au*-coated QCM substrate treated with a 3-mercaptopropionic acid and on mica.

A circular area with a radius of 37 μm was photobleached by 8 minutes using the full lamp power. We measured the intensity of the photobleached area and a reference area in all images to normalize the photobleaching measurements. The normalized photobleached area intensity at a time t was calculated using

$$I(t) = I_{pt}(t) + (I_{ref}(0) - I_{ref}(t)) \tag{25}$$

where $I_{pt}(t)$ is the intensity of the photobleached area at a time t, $I_{ref}(0)$ is the intensity of the reference area immediately after photobleaching, and $I_{ref}(t)$is the intensity of the reference area at a time t. To calculate the diffusion coefficient for the phospholipids the following equation was used [Soumpasis, 1983]:

$$D = \frac{0.224r^2}{\tau_{1/2}} \tag{26}$$

where r is the radius of the photobleached area and $\tau_{1/2}$ the half-life recovery time. The values for the fluorescence recovery measurements were fit with an exponential function obtaining this way the half-life recovery time.

Part III

RESULTS AND DISCUSSION

7 RESULTS

Expressions of both FtsZ lateral mutants *in vivo* prevent the *E. coli* bacteria from dividing. In this work we want to understand how these mutations affect *in vitro* polymerization of FtsZ: their interactions with ZipA, their surface reorganization capacity, and the lipid composition effect on these two behaviors.

To address these questions we have used two different surface techniques: QCM with dissipation monitoring and AFM. We have used a biomimetic system for a simplified bacteria division machinery *in vitro* composed by: a lipid bilayer, the bitopic membrane protein ZipA and the GTPase protein FtsZ.

7.1 QUARTZ CRYSTAL MICROBALANCE

QCM-D is a technique able to monitor in real time changes in mass and viscosity of the loaded solid support. This feature makes this technique suitable to follow the formation of the lipid bilayer on the sensor substrate, the subsequent anchoring of ZipA, and the binding of FtsZ, wild type and lateral mutants, to ZipA. This technique will allow quantifying the binding between the different layers and following their absorption kinetics. All data presented in this work were measured at the 35 MHz overtone (the 7^{th} overtone).

7.1.1 *Bilayer formation and oriented sZipA binding*

Adsorption kinetics of neutral and *E. coli* polar lipid liposomes and SLB formation onto the substrate. A lipid bilayer is the first layer on our reconstituted system to be adsorbed to the sensor surface. The two lipid platforms where to anchor ZipA and bind FtsZ will be composed by EPC (neutral) and *E. coli* polar (negatively charged) lipids.

Figure 36a shows the change in resonant frequency and dissipation due to an increase in the loading mass. A negative frequency change indicates the addition of mass. The Sauerbrey equation (Equation 9, Chapter 6.3) relates the change in resonant frequency with the amount of mass adsorbed.

Fusion of neutral liposomes (EPC/DOGS-NTA lipid mixture) on silicon oxide substrates (Figure 36a) needs the presence of a divalent cation, we used $NiCl_2$. Liposome deposition and fusion follows a two step mechanism [Richter et al., 2003, Richter and Brisson, 2004, Dodd et al., 2008, Cho et al., 2010]: i) irreversible vesicles adsorp-

tion, and after a critical vesicle concentration is reached ii) vesicle fusion. The curves exhibit a maximum mass uptake and dissipation due to the total loading coupled to the sensor surface; that is, lipid mass plus the water inside the vesicles. A subsequent increase in frequency change, decrease in mass, follows after a critical coverage of liposomes is reached on the surface. This change is due to the loss of trapped water inside the liposomes released by their spontaneous rupture. Dissipation values decrease after SLB formation indicating the adsorbed layer becomes more rigid. We completed the characterization of the bilayer with a buffer rinse.

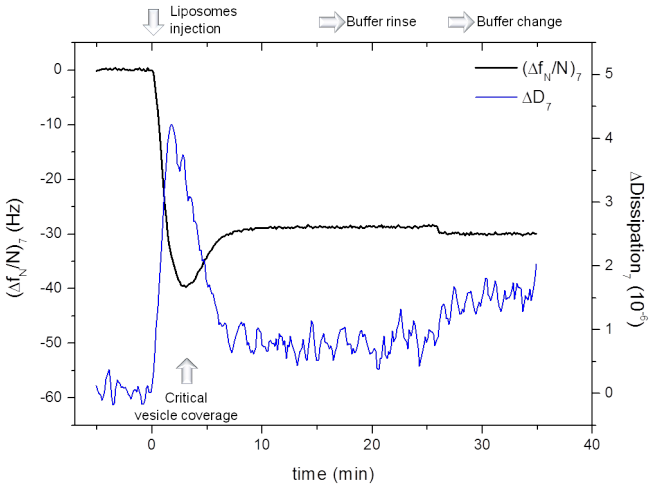

(a) SLB formation on SiO_2 substrate for EPC liposomes.

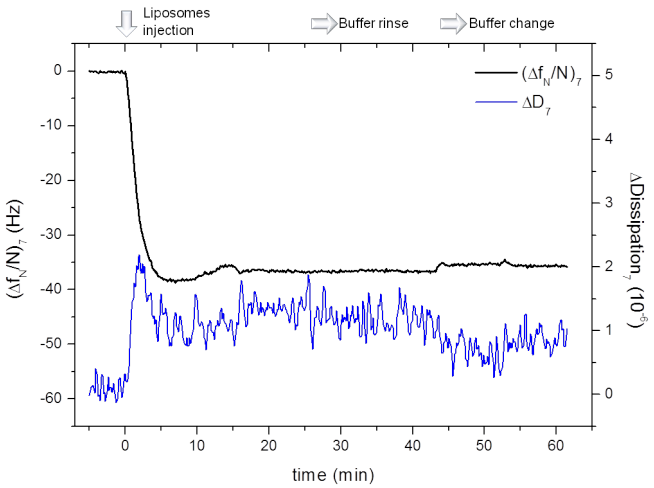

(b) SLB formation on *Au* substrate for *E. coli* polar lipid liposomes.

Figure 36: Simultaneous measurement of frequency change (solid black line) and dissipation (solid blue line) for SLB formation (a) on SiO_2 substrate for EPC liposomes, and (b) on *Au* substrate for *E. coli* polar lipid liposomes.

The average of all experiments indicate a resonance frequency change of -28.6 ± 0.3 Hz, which corresponds to a mass increase per unit area of $520 \pm 5\,^{ng}/_{cm^2}$, and a dissipation value $< 0.5 \times 10^{-6}$.

To form a bilayer from negatively charged vesicles (*E. coli* polar / DOGS-NTA lipid mixture) chemically modified Au substrates with a 3-mercaptopropionic acid self-assembled monolayer (SAM) are needed as described in the Appendix (A). Figure 36b shows the resonant frequency change and dissipation for the SLB formation.

The formation of an EcPl bilayer needs the addition of Ca^{2+} to the buffer solution, instead of $NiCl_2$ used for EPC liposomes. It starts with a slow adsorption of liposomes to the surface. The critical concentration is about the same amount of mass loaded to the sensor as for neutral liposomes on SiO_2, but their spontaneous rupture occurs almost immediately after, as can be appreciated by the maximum peak in the dissipation curve. Averaging all experiments, the resonant frequency change for an *E. coli* polar lipid bilayer is -36.5 ± 2.0 Hz (a loaded mass per unit area of $660 \pm 36\,^{ng}/_{cm^2}$) and a dissipation $< 1.25 \times 10^{-6}$.

The values for mass deposition we measured lie within expected for a complete SLB. For EPC small liposomes adsorption on SiO_2, the reported change in frequency is 26 Hz (which corresponds to a mass increase of $468\,^{ng}/_{cm^2}$) and a dissipation $< 0.2 \times 10^{-6}$ [Keller and Kasemo, 1998]. The differences between our measured values and the previously reported ones can be explained by several factors like lipid composition, ionic strength of the buffer solution, and hydration degree of the adsorbed bilayer [Cho et al., 2010].

sZipA anchoring on EPC lipid and *E. coli* polar lipid bilayer. The anchoring of ZipA follows after the formation and characterization of the SLB.

We have used a soluble form of ZipA, sZipA, in which the N-terminus is replaced by a six histidine tail (His-tag). This His-tag will be used to orient sZipA to the bilayer by incorporating a percentage of DOGS-NTA to the lipid mixture, which has a special head group able to bind two histidines in the presence of nickel.

Figures 37a and 37b show the resonant frequency change and dissipation for sZipA bound to EPC and *E. coli* polar lipid bilayers respectively.

sZipA is injected into the QCM chamber at $0.6\,\mu$M for 3 minutes, followed by a 15 minutes rinse with buffer leading to a stable signal. When washing with a high concentration of imidazole (200 mM) displaces the histidine bound to the NTA and sZipA is removed from the lipid bilayer.

This concentration and incubation time ensures an irreversibly bound sZipA monolayer. The reversibility of the signal due to the imidazole injection indicates that sZipA anchoring to the lipid bilayer is made

through its amino terminal domain to the DOGS-NTA lipid present in the bilayer.

At lower NTA concentration, a stable but partial sZipA coverage was observed; whereas for NTA content above 10% full coverage was achieved (data not shown).

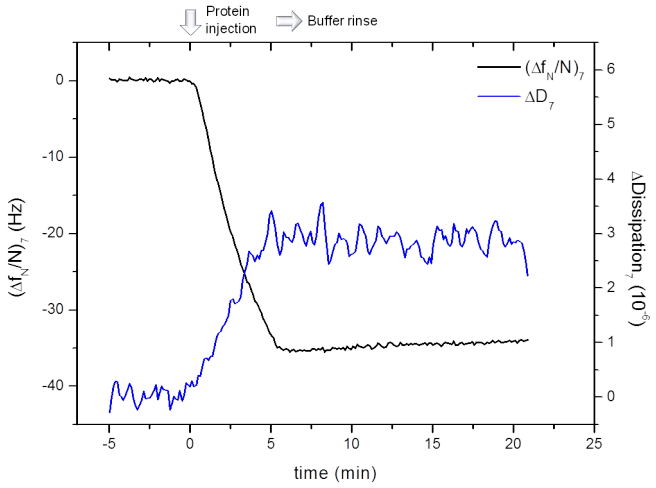

(a) sZipA bound to an EPC lipid bilayer.

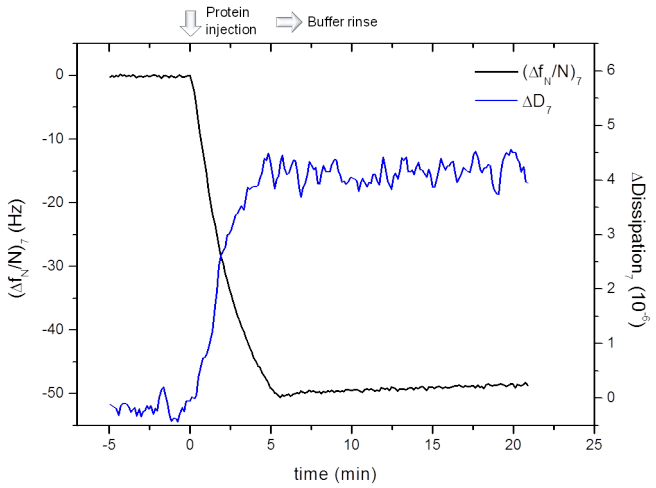

(b) sZipA bound to an *E. coli* polar lipid bilayer.

Figure 37: Simultaneous measurement of frequency change (solid black line) and dissipation (solid blue line) for sZipA bound to (a) an EPC and to (b) an *E. coli* polar lipid bilayer respectively.

For the adsorption of sZipA to an EPC bilayer, the change in resonant frequency is $-36.3 \pm 2.3\,\mathrm{Hz}$ and a dissipation $< 3.5 \times 10^{-6}$. Whereas, for the binding of sZipA to an EcPl bilayer the resonance

frequency shifts are $-44.9 \pm 6.3\,\mathrm{Hz}$ and dissipation $< 4 \times 10^{-6}$. The averaged frequency values correspond to a mass per unit area of $19.6 \pm 2.3\,\mathrm{pmol/cm^2}$ for EPC bilayers and $24.3 \pm 3.4\,\mathrm{pmol/cm^2}$ for EcPl bilayers; giving an average diameter available per molecule on the surface of $\sim 3.3\,\mathrm{nm}$ and $\sim 3\,\mathrm{nm}$ respectively.

There is a slight difference in the dissipations of sZipA bound to the different lipid bilayers. The small increase in the dissipation observed on *E. coli* lipids might indicate that the sZipA protein layer is less compact in spite the smaller area available per molecule. It is possible to accommodate a larger number of sZipAs per area if some of them are more stretched, i.e., by changing the conformation of sZipA P/Q unstructured domain due to the lipid composition of the bilayer [Mateos-Gil et al., 2012a, López-Montero et al., 2013a].

We therefore conclude that we have a sZipA protein monolayer; and that sZipA is bound to the bilayer through the histidine tail present in its amino terminal domain.

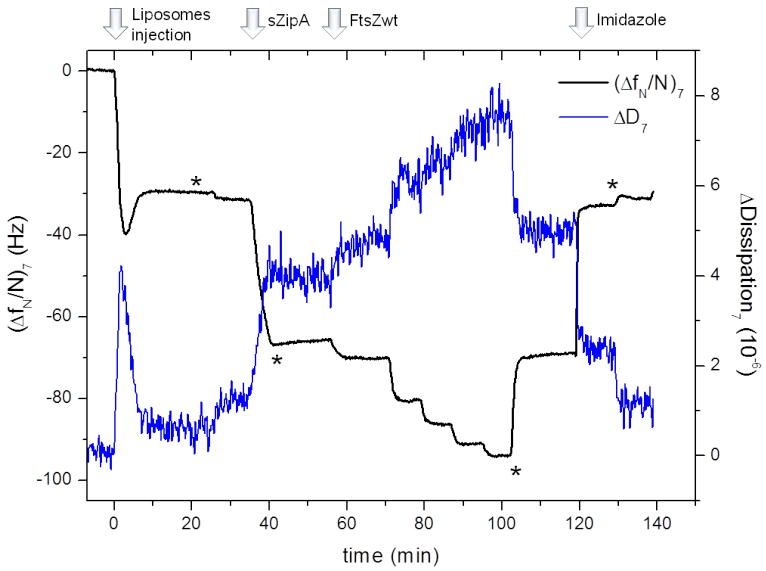

Figure 38: QCM-D monitoring on SiO_2 substrate. Simultaneous measurement of frequency (solid black line) and dissipation (solid blue line) responses for an SLB formation, sZipA adsorption, FtsZwt titration binding. Arrows indicate the successive liposomes, proteins and imidazole injections; and the stars indicate the corresponding buffer rinses.

FtsZ binding to the anchored sZipA will complete our reconstituted system. Figure 38 shows a typical QCM-D experiment monitoring performed for this thesis, and it shows the successive liposomes, proteins and imidazole injections and corresponding rinses.

Data acquisition starts with the signal registered in the presence of buffer followed by the injection of a liposomes solution that leads to a rapid absorption and formation of an SLB. sZipA is then anchored to the bilayer previous to FtsZ binding. A final rinse with imidazole removes sZipA from the bilayer leaving the bare membrane. There is no binding observed of FtsZ to the bilayer in the absence of sZipA (data not shown).

7.1.2 *FtsZ - ZipA binding and unbinding*

FtsZ protein, wild type and lateral mutants, were bound to a saturated monolayer of sZipA previously anchored to a lipid bilayer. The samples were injected following a titration experiment by gradually increasing FtsZ concentration. The chamber was rinsed with buffer after the maximum protein concentration loading was complete.

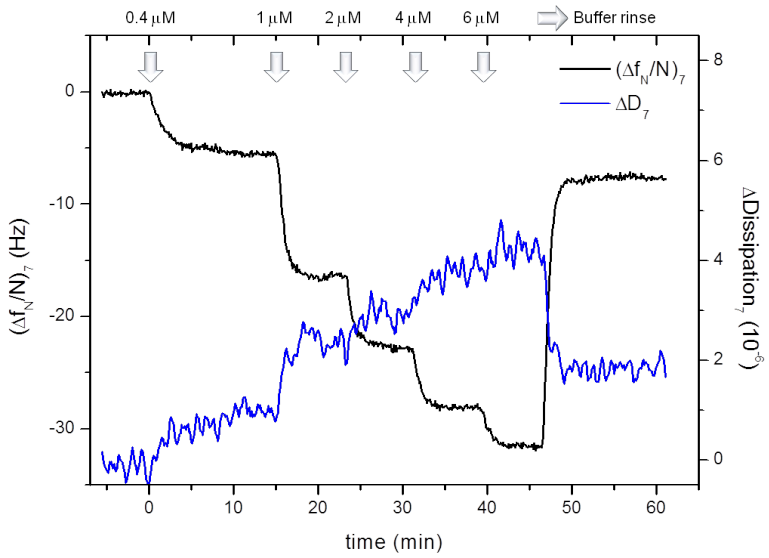

Figure 39: Resonant frequency shift (solid black line) and dissipation (solid blue line) measurement for FtsZwt-GDP on EPC bilayer.

FtsZwt binding in the presence of GDP. Figure 39 shows a FtsZwt-sZipA complex formation on a neutral lipid bilayer in the presence of GDP. After the buffer measurement was stabilized, FtsZwt was injected at increasing protein concentration from 0.4 μM to 6 μM.

The change in resonant frequency and dissipation account for the increasing protein binding to the sensor surface. The protein is rinsed from the chamber with buffer after its complete adsorption. The observed increase in the frequency change shows the desorption of a certain amount of protein.

The values measured for the adsorption of FtsZwt to sZipA on EPC and EcPl lipids bilayers correspond to an adsorbed mass per unit area of $16 \pm 2\,\mathrm{pmol/cm^2}$ and $21 \pm 2\,\mathrm{pmol/cm^2}$ respectively (giving $\sim 3.6\,\mathrm{nm}$ and $\sim 3.3\,\mathrm{nm}$ diameter available per FtsZ on the surface respectively).

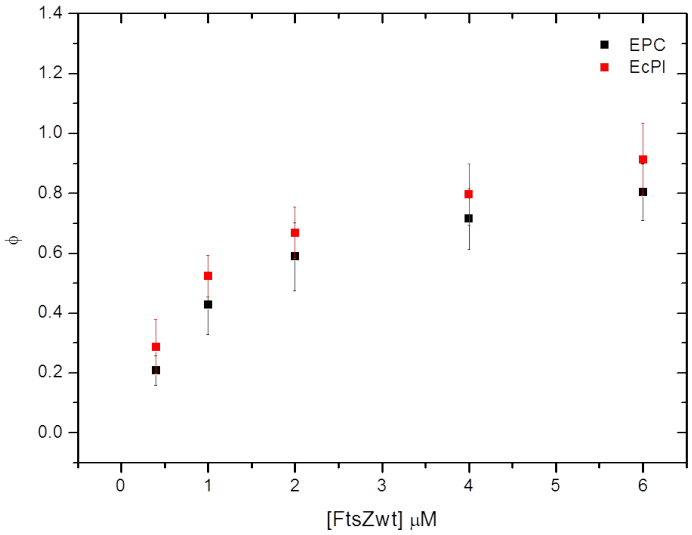

Figure 40: Fractional saturation ϕ as function of FtsZwt-GDP concentration, bound to sZipA on EPC and EcPl lipid bilayer.

	EPC	EcPl
n	(1.1±0.1)	(0.9±0.2)
ϕ_{max}	(0.93±0.05)	(1.1±0.1)
$C_{1/2}$ (μM)	(1.2±0.2)	(1.1±0.4)

Table 1: Non-linear least squares fit to the Hill equation of the binding isotherms for FtsZwt-GDP to sZipA on EPC and *E. coli* polar lipids. The fitted parameters are n (Hill cooperative coefficient), ϕ_{max} and $C_{1/2}$.

Figure 40 shows the fractional saturation ϕ (Chapter 6.4.2) as a function of FtsZwt concentration, when the protein is injected in the

presence of GDP on both lipid bilayers: EPC and EcPl. ϕ represents the fraction of receptor (sZipA) forming a complex with the ligand (FtsZ) on the surface.

Quantification for the FtsZwt-sZipA complex formation is shown on Table 1. The experimental data were fit to the empirical Hill equation (Equation 24, Chapter 6.4.2).

The binding of FtsZwt to sZipA is independent on the charge of the bilayer. The fit yielded a Hill coefficient n is approximately 1 for data corresponding to both lipid bilayers, and FtsZwt-sZipA complex formation with GDP on a lipid bilayer follows a single site binding model; i.e., data can be fit by a Langmuir isotherm (Equation 23, Chapter 6.4.1) where $C_{1/2} = K_d$, the dissociation constant.

FtsZ lateral mutants binding in the presence of GDP. To compare FtsZ lateral mutants binding to FtsZwt we carried out the corresponding binding isotherms under the same conditions of lipid bilayers and nucleotide.

Figure 41 shows the binding isotherms for FtsZ lateral mutants - sZipA complex formation in the presence of GDP for the different bilayers: EPC and EcPl.

A mutation in the lateral side of FtsZ that replaces a positive charge with a neutral aa (FtsZR85Q) favors the binding to sZipA on EPC lipids, enhancing their interaction at larger protein concentration. On the contrary, replacing a negative charged aa by a neutral one (FtsZE83Q) hinders the binding to sZipA on the same lipid bilayer (Figure 41a). The average of the measured values for the mass loaded to the sensor per unit area are $15 \pm 1\,\mathrm{pmol/cm^2}$ and $27 \pm 1\,\mathrm{pmol/cm^2}$ for FtsZE83Q and FtsZR85Q respectively, giving an available diameter per protein on the surface of $\sim 3.7\,\mathrm{nm}$ and $\sim 3\,\mathrm{nm}$.

Both FtsZ lateral mutants display the same binding behavior on *E. coli* polar lipids as on neutral EPC lipids (Figure 41b): a positive to neutral aa mutation favors the binding while a negative to neutral aa mutation does not. Although both FtsZ lateral mutants change the binding to sZipA on lipid bilayers, they approach FtsZ wild type binding behavior when *E. coli* polar lipids are present. The measured loading of the surface yielded a mass uptake per unit area of $20 \pm 1\,\mathrm{pmol/cm^2}$ and $33 \pm 2\,\mathrm{pmol/cm^2}$ for FtsZE83Q and FtsZR85Q respectively, corresponding values of an available diameter per FtsZ on the surface of $\sim 3.2\,\mathrm{nm}$ and $\sim 2.8\,\mathrm{nm}$.

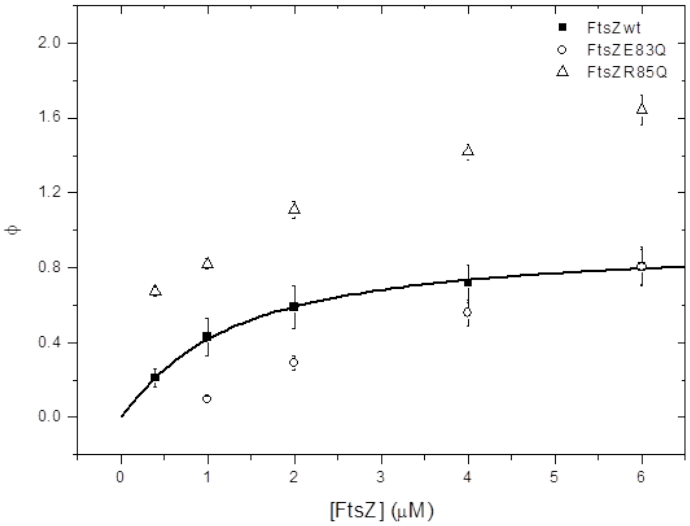

(a) FtsZ-sZipA complex formation on EPC lipid bilayer.

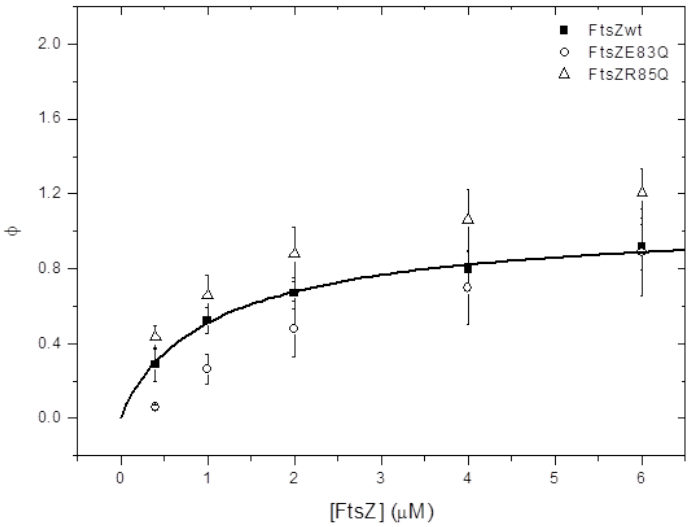

(b) FtsZ-sZipA complex formation on EcPl lipid bilayer.

Figure 41: Fractional saturation ϕ as a function of FtsZ concentration for FtsZE83Q (open circles) and FtsZR85Q (open triangles) bound to sZipA on EPC and EcPl lipid bilayer with GDP. Data for FtsZwt binding are plotted in black for the sake of comparison.

		FtsZE83Q	FtsZR85Q
EPC	n	(1.8±0.3)	------
	ϕ_{max}	(1.1±0.3)	------
	$C_{1/2}$ (μM)	(3.5±1.2)	------
EcPl	n	(1.7±0.2)	(0.64±0.07)
	ϕ_{max}	(0.95±0.12)	(1.9±0.3)
	$C_{1/2}$ (μM)	(1.9±0.4)	(2.7±1.2)

Table 2: Non-linear least squares fit to the Hill equation of the binding isotherms for FtsZ lateral mutants to sZipA on EPC and EcPl lipids with GDP. The fitted parameters are n (Hill cooperative coefficient), ϕ_{max} and $C_{1/2}$.

From Table 2, FtsZE83Q binds cooperatively to sZipA on both EPC and EcPl bilayers (Hill coefficient $n > 1$), and FtsZR85Q binds non cooperatively to sZipA on EcPl lipids ($n < 1$). However, it is not possible to fit FtsZR85Q data to Hill equation on EPC lipid bilayer.

In vitro experiments show there is no polymerization of FtsZ-GDP in solution but FtsZ-GTP polymerizes when the protein reaches a critical concentration (as mentioned on Chapter 2.2). We wanted to evaluate how the binding of FtsZ to sZipA changes when incubating the polymerized protein. For these experiments we have used GMPCPP nucleotide injecting the protein at increasing concentrations spanning from not polymerized to polymerized FtsZ. GMPCPP is a slowly hydrolyzable GTP analogue that also promotes polymerization giving more stable polymers that allow obtaining more reliable experimental results. The experiments take at least 10 minutes per FtsZ concentration to reach equilibrium adsorption in a titration experiment, and FtsZ filaments are more stable within experimental time if bound in the presence of GMPCPP.

Light scattering experiments indicate there is no polymerization of all three FtsZ proteins (wild type and lateral mutants) at concentrations $\leq 0.4\,\mu$M in the presence of GTP or GMPCPP (data not shown).

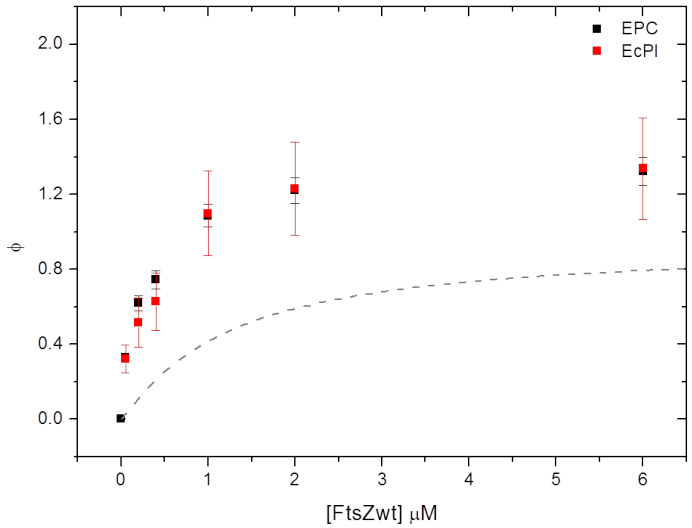

Figure 42: Fractional saturation ϕ as function of FtsZwt concentration, bound to sZipA with GMPCPP on EPC and *E. coli* polar lipids bilayer. Data from FtsZwt-sZipA complex on EPC lipids with GDP are plotted in a dashed gray line as reference.

FtsZwt binding in the presence of GMPCPP. The lipid composition of the bilayer does not significantly affect the fractional saturation ϕ, neither with GMPCPP (Figure 42) nor GDP (Figure 40). However, there is a larger fraction of surface receptors occupied in the presence of GMPCPP than GDP (dashed gray line in Figure 42).

Table 3 shows the experimental binding data fit for FtsZwt - sZipA in the presence of GMPCPP on EPC and EcPl lipids. The binding of FtsZwt is non cooperative ($n < 1$) on both bilayer.

	EPC	EcPl
n	(0.6±0.1)	(0.5±0.2)
ϕ_{max}	(1.6±0.2)	(2.0±0.9)
$C_{1/2}$ (μM)	(0.4±0.2)	(1.3±2.2)

Table 3: Non-linear least squares fit to the Hill equation of the binding isotherms for FtsZwt-GMPCPP to sZipA on EPC and *E. coli* polar lipids. The fitted parameters are n (Hill cooperative coefficient), ϕ_{max} and $C_{1/2}$.

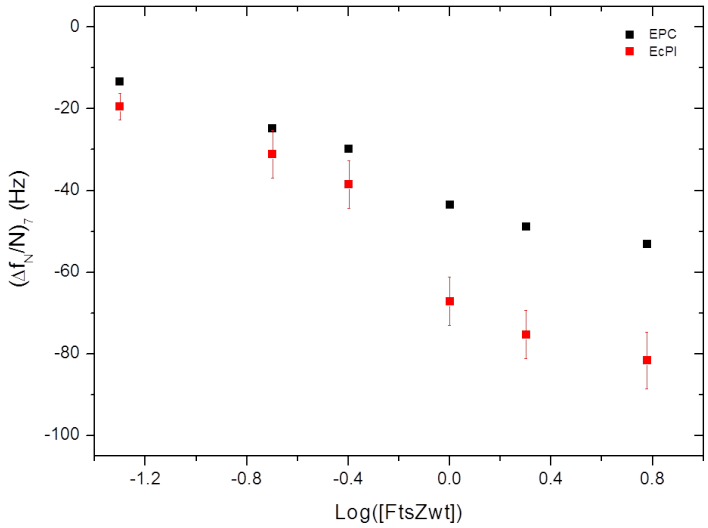

Figure 43: Resonant frequency change $(\Delta f_N/N)_7$ *vs.* $Log([FtsZ])$ for FtsZwt-GMPCPP bound to sZipA on EPC and *E. coli* polar lipids bilayers.

Figure 43 is a semilogarithmic plot of the resonant frequency change $(\Delta f_N/N)_7$ against $Log([FtsZ])$. This semilog plot representation allows showing data covering different orders of magnitude in FtsZ concentration. There are two binding regimes concentration dependent: below and above critical polymerization concentration (1 μM, $Log([FtsZ]) = 0$). The binding behavior is comparable in the two lipid bilayers below the critical FtsZwt concentration, but a significant change is observed at higher concentrations. On *E. coli* lipids the amount of bound FtsZwt is enhanced most significantly above the critical polymerization concentration. The mass adsorbed at $[FtsZ] = 0.4\,\mu$M (below the FtsZ critical concentration) corresponds to a mass per unit area of $13.4 \pm 0.4\,\mathrm{pmol/cm^2}$ for EPC lipids and $17 \pm 3\,\mathrm{pmol/cm^2}$ for EcPl lipids; whereas the values measured at maximum FtsZ concentration above critical correspond to $23.8 \pm 0.1\,\mathrm{pmol/cm^2}$ and $37 \pm 3\,\mathrm{pmol/cm^2}$ on each bilayer respectively. These values gives a diameter available per protein of $\sim 3\,$nm and $\sim 2.3\,$nm at maximum FtsZwt concentration on EPC and EcPl lipid respectively.

Dissipation measurements show also a two zone behavior when binding FtsZwt to sZipA in the presence of GMPCPP for EPC and EcPl lipids (Figure 44). Above critical concentration of 1 μM, dissipation data indicate the adsorbed layer becomes less rigid. On *E. coli* polar lipid bilayer the dissipation at maximum polymer concentration

of 6 μM increases about six times its value compared to dissipation for FtsZwt bound at the same concentration with GDP (gray dashed line in Figure 44). On EPC lipids this dissipation increase is about three times.

Figure 44 also shows that dissipation data below FtsZwt-GMPCPP critical concentration are comparable to those measured in the presence of GDP, indicating the adsorbed layer has a similar rigidity as the one bound in the absence of polymers.

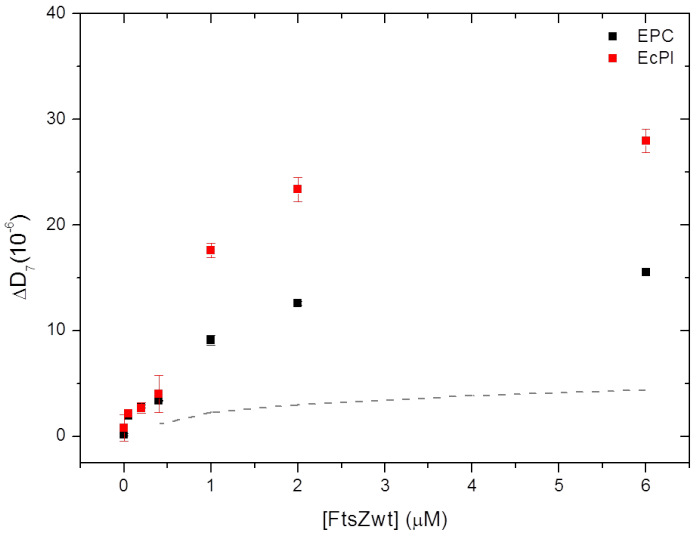

Figure 44: Dissipation measurement ΔD_7 (10^{-6}) as a function of FtsZwt-GMPCPP concentration, bound to sZipA on EPC and *E. coli* polar lipids bilayer. Data for FtsZwt-sZipA binding on EPC lipids with GDP are plotted in a dashed gray line as reference.

At the FtsZ wild type concentration where polymers are expected to form, we observe an significant increase in mass and dissipation. We can interpret these results as having polymers on the surface (increase in mass adsorbed) and that these polymer layer are more loosely bound (increase in dissipation).

FtsZ lateral mutants binding in the presence of GMPCPP. Figure 45 shows the binding isotherms of FtsZ lateral mutants compared to FtsZwt under the same conditions of nucleotide and lipid bilayer. The binding of FtsZ lateral mutants with GMPCPP is independent of the lipid bilayer: the fraction of receptors occupied is smaller than FtsZwt on either bilayer. This fraction approaches the value for FtsZwt as the concentration of FtsZ lateral mutant increases.

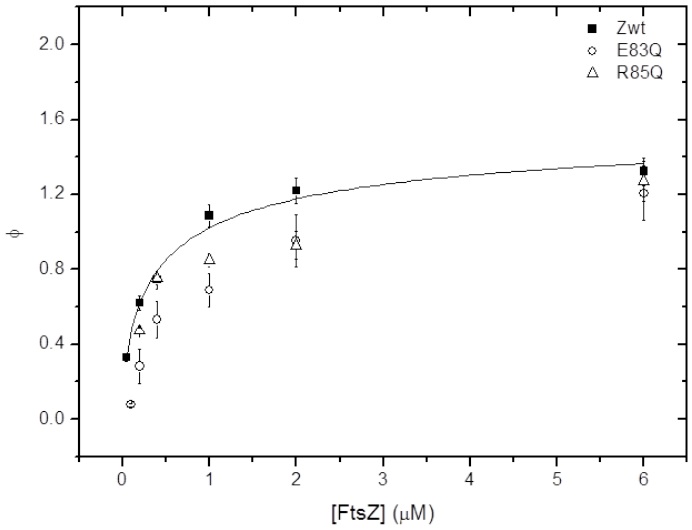

(a) FtsZ-sZipA complex formation on EPC lipid bilayer.

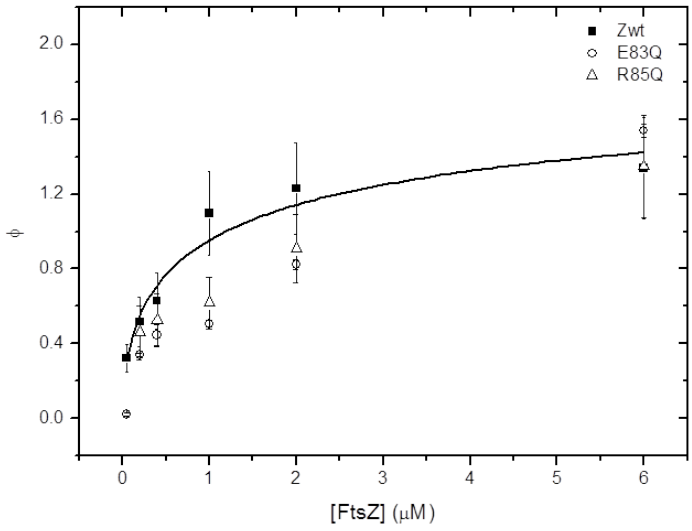

(b) FtsZ-sZipA complex formation on EcPl lipid bilayer.

Figure 45: Fractional saturation ϕ as a function of FtsZ concentration for FtsZE83Q (open circles) and FtsZR85Q (open triangles) bound to sZipA on EPC and EcPl lipid bilayer with GMPCPP. Data for FtsZwt binding are plotted in black for the sake of comparison.

Figure 46 shows a comparison of the resonant frequency changes $(\Delta f_N/N)_7$ as a function of $Log([FtsZ])$ for both FtsZ lateral mutants bound to sZipA with GMPCPP on the two lipid bilayers tested. The binding on neutral EPC bilayer is not significantly different among

the three FtsZ proteins (Figure 46a), but on EcPl lipid bilayer the different behavior of FtsZ lateral mutants is enhanced.

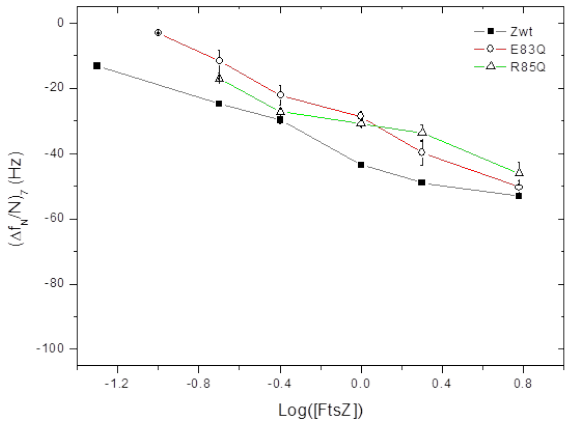

(a) Binding of FtsZ-GMPCPP to sZipA on EPC lipid bilayer.

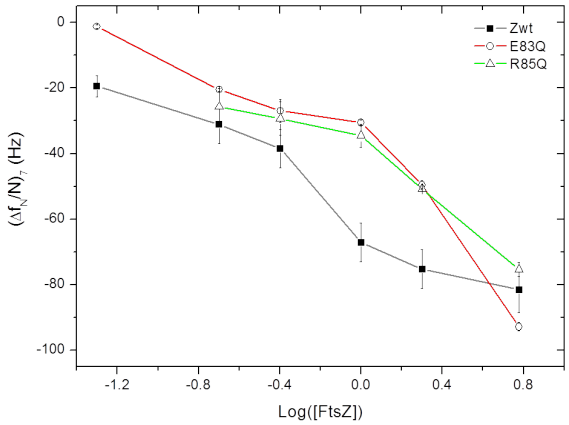

(b) Binding of FtsZ-GMPCPP to sZipA on *E. coli* polar lipids bilayer.

Figure 46: Resonant frequency change $(\Delta f_N/N)_7$ *vs.* $Log([FtsZ])$ for FtsZ lateral mutants bound to sZipA with GMPCPP on a) EPC and b) *E. coli* polar lipids bilayer. Data from FtsZwt-sZipA complex are plotted in black as comparison.

The quantification analysis of the binding isotherms for FtsZ-sZipA complex formation is summarized in Table 4, where experimental data were fit with the empirical Hill equation (Chapter 6.4.2). In light green are highlighted the fitting values for FtsZE83Q-GMPCPP bound to sZipA on EPC lipids, these experimental data fit the empirical Hill equation for protein concentrations below 1 μM. Data for

		GDP			GMPCPP		
		FtsZwt	FtsZE83Q	FtsZR85Q	FtsZwt	FtsZE83Q	FtsZR85Q
EPC	n	(1.1±0.1)	(1.8±0.3)	------	(0.6±0.1)	(0.96±0.26)	------
	ϕ_{max}	(0.93±0.05)	(1.1±0.3)	------	(1.6±0.2)	(1.4±0.3)	------
	$C_{1/2}$ (μM)	(1.2±0.2)	(3.5±1.2)	------	(0.4±0.2)	(0.85±0.41)	------
EcPl	n	(0.9±0.2)	(1.7±0.2)	(0.64±0.07)	(0.5±0.2)	(2.8±0.2)	------
	ϕ_{max}	(1.1±0.1)	(0.95±0.12)	(1.9±0.3)	(2.0±0.9)	(0.51±0.01)	------
	$C_{1/2}$ (μM)	(1.1±0.4)	(1.9±0.4)	(2.7±1.2)	(1.3±2.2)	(0.155±0.003)	------

Table 4: Non-linear least squares fit to the Hill equation of the isotherm binding for FtsZ (wild type and lateral mutants) to sZipA under the different conditions of nucleotide and bilayer composition. The fitted parameters are n (Hill cooperative coefficient), ϕ_{max} and $C_{1/2}$.

the binding of FtsZR85Q to sZipA on both bilayers with GMPCPP as well as on EPC with GDP do not fit the empirical Hill equation.

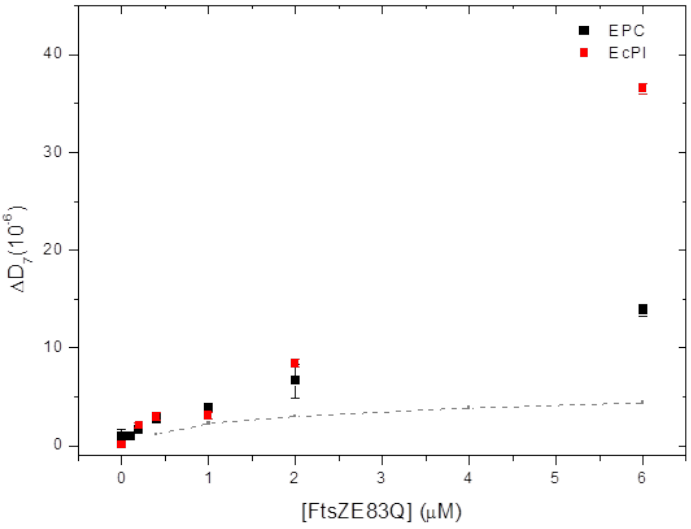

(a) FtsZE83Q-GMPCPP bound to sZipA on EPC and EcPl lipid bilayer.

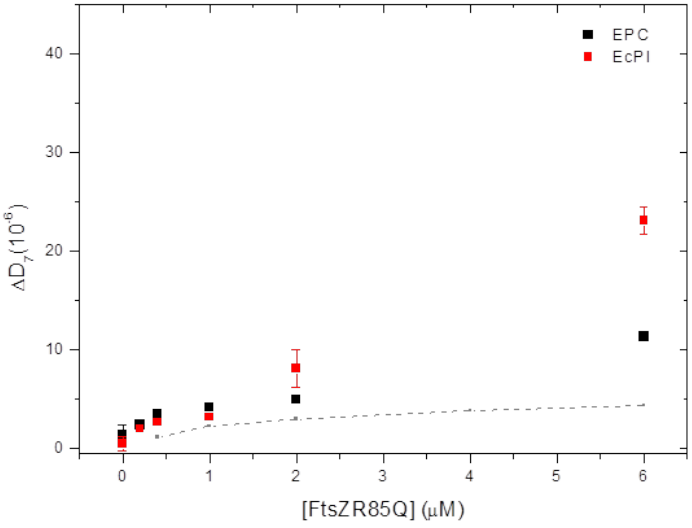

(b) FtsZR85Q-GMPCPP bound to sZipA on EPC and EcPl lipid bilayer.

Figure 47: Dissipation measurement ΔD_7 (10^{-6}) as function of FtsZ concentration, for (a) FtsZE83Q and (b) FtsZR85Q binding to sZipA with GMPCPP on EPC and *E. coli* polar lipids bilayer. Data from FtsZwt-sZipA binding on EPC lipids with GDP are plotted in a dashed gray line as reference.

The rigidity of a protein layer adsorbed to the sensor surface is associated to the dissipation measured. Figure 47 shows dissipation measurements for FtsZ wild type and lateral mutants bound to sZipA under different conditions of lipid bilayers and nucleotide. One way to analyze the experimental data is to take the acoustic ratio $(\Delta D/\Delta f)$ which is related to the intrinsic viscosity of the protein layer (as mentioned on Chapter 6.3).

Figure 48 shows the acoustic ratio for FtsZwt and lateral mutants individually: black and dark gray squares are taken with GDP on both bilayers type as comparison. The rigidity of the bound FtsZ-GDP layer is independent of protein type (wild type and lateral mutants), mass adsorbed and lipid bilayer composition.

If FtsZ proteins are bound to sZipA with GMPCPP, two regimes are distinct dependent on the protein concentration. For FtsZwt (Figure 48a) there is a critical concentration of 0.5 μM below which the layer is as rigid as in the GDP form. Above that critical value the adsorbed layer becomes less rigid independently of the lipid bilayer composition. This increase in the acoustic ratio might reflect the polymerization of FtsZwt on the surface.

Differences arise when comparing the acoustic ratio for the FtsZ lateral mutants with respect to FtsZwt (Figures 48b and 48c). The value at which the behavior changes for the FtsZ lateral mutant lies between 1 μM and 2 μM, instead of 0.5 μM observed for FtsZwt. *E. coli* polar lipids start inducing changes in the adsorbed protein layer rigidities at the maximum concentration: FtsZE83Q layer is less rigid whereas FtsZR85Q layer is more rigid than FtsZwt.

The differences observed with GMPCPP on the polymer regime could be due to the lack of polymerization, or due to a different polymer formation for the FtsZ lateral mutants layer.

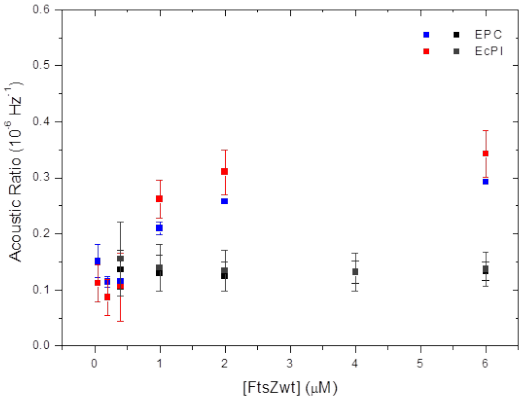

(a) FtsZwt bound to sZipA

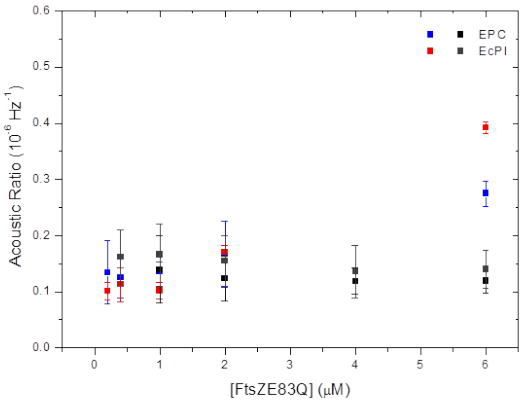

(b) FtsZE83Q bound to sZipA

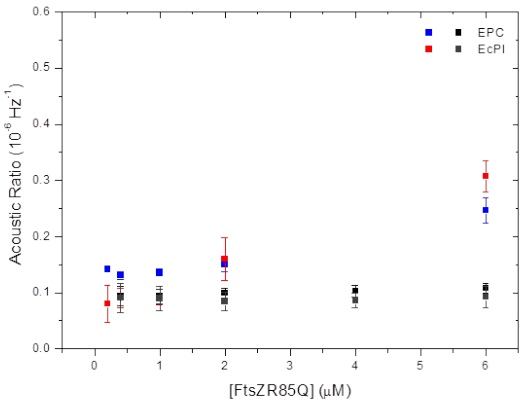

(c) FtsZR85Q bound to sZipA

Figure 48: Acoustic ratio $\Delta D/\Delta f$ as a function of FtsZ concentration at all experimental conditions of nucleotide and bilayer. For all FtsZ proteins (wild type and lateral mutants) black and dark gray squares are taken with GDP, and blue and red squares are taken with GMPCPP on EPC and EcPl lipid bilayer respectively.

FtsZ wild type and lateral mutants unbinding. Once the FtsZ titration binding experiment is completed, the protein is rinsed from the chamber. Frequency change measurements allow calculating the percentage of protein that remains bound to sZipA on the surface with respect to the maximum protein adsorbed.

Table 5 show the reversibility of the binding and the percentage of FtsZ that remains bound to sZipA after the buffer rinse is completed.

Reversibility is dependent on lipid composition for FtsZwt-sZipA complex formation with GDP (Table 5): most of FtsZwt remains bound to sZipA on EPC lipid bilayer (↑); while a minimum of FtsZwt remains bound to sZipA when EcPl lipids are present (↓). Changing the nucleotide to GMPCPP makes the binding completely reversible regardless lipid composition.

FtsZ lateral mutants binding to sZipA with GDP is almost irreversible independently of the lipid composition. Reversibility of FtsZE83Q - sZipA binding with GMPCPP is equal to FtsZwt-GMPCPP. On the contrary, reversibility of FtsZR85Q lateral mutant binding is more uncertain: EPC lipids promotes half the experiment to be completely reversible (♢), while *E. coli* polar lipids makes most of the experiments reversible (∗).

	GDP			GMPCPP		
	FtsZwt	FtsZE83Q	FtsZR85Q	FtsZwt	FtsZE83Q	FtsZR85Q
EPC	No 30-70% ↑	No 90%	No 100%	Yes 0%	Yes 0%	Yes/No ♢
EcPl	No 10-30% ↓	No 95%	No 100%	Yes 0%	Yes 0%	Yes *

Table 5: Reversibility of the binding and percentage of FtsZ (wild type and lateral mutant) that remains bound to sZipA under all experimental conditions of nucleotide and lipid bilayer composition. ↑ indicates that most of FtsZwt-GDP remains bound to sZipA, while ↓ that at least the 30% of the protein remains bound to the surface. For FtsZR85Q-GMPCPP ♢ indicates that half the experiment are completely reversible and ∗ that most of the binding experiments are reversible.

Therefore, the differences for the binding, rigidity and the unbinding of the FtsZ lateral mutants compared to FtsZwt under the different *in vitro* conditions of lipid composition and nucleotide type tested on this thesis might be one of the factors to explain their impaired *in vivo* behavior as will be discussed later.

7.2 ATOMIC FORCE MICROSCOPY

AFM is a high-resolution surface microscopy technique that allows scanning biological samples under physiological conditions (as described in Chapter 6.2.1). This technique will give us the topography of the structures and their reorganization on the substrate.

We studied FtsZ behavior on surfaces of increasing complexities: on mica, on mica with sZipA and on lipid bilayers with sZipA.

All images for FtsZ wild type on mica and on the two lipid bilayers studied (DOPC and *E. coli* polar lipids) were taken with permission from Pablo Mateos-Gil PhD thesis [Mateos-Gil, 2013] for the sake of comparison.

7.2.1 *FtsZ polymerization on mica*

We first study FtsZ lateral mutants polymerization on bare mica and compare their behavior to FtsZwt. The three samples were prepared as described in Chapter 6.2.2 and scanned on buffer with GTP.

Figure 49 shows that the three FtsZ proteins are able to polymerize on mica with GTP. The profile corresponds to the green line on the AFM image. Individual filaments are observed to be $3-4\,\text{nm}$ height and hundreds of nm long. Straight and curved filament aggregates are formed.

AFM also allows following the dynamics of the structures adsorbed to the surface. In the presence of GTP, FtsZ polymers are able to reorganize on the surface. Figure 50 shows snapshots for the time evolution of these polymers for the three FtsZ proteins studied. As time evolves some protein is desorbed from the surface promoting the formation of other condensates like rolls. FtsZE83Q filaments on mica are dynamic and appears to desorb more slowly than FtsZwt. FtsZR85Q polymers also reorganize but are fragile as they break easily when scanning.

FtsZ polymers from the three proteins on mica are almost indistinguishable, there are slight differences that are noticeable when comparing them at the same time. Therefore, the reduced GTPase activity in solution of the FtsZ lateral mutants seems to be irrelevant for their surface polymer reorganization.

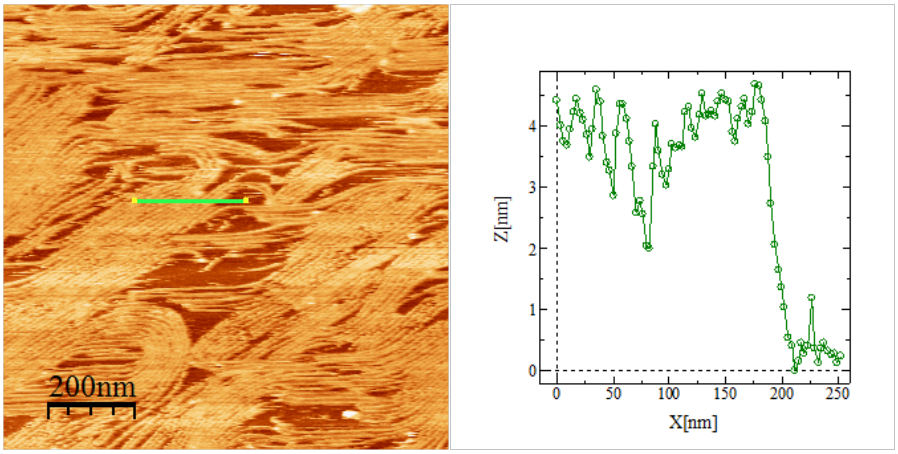

(a) FtsZwt

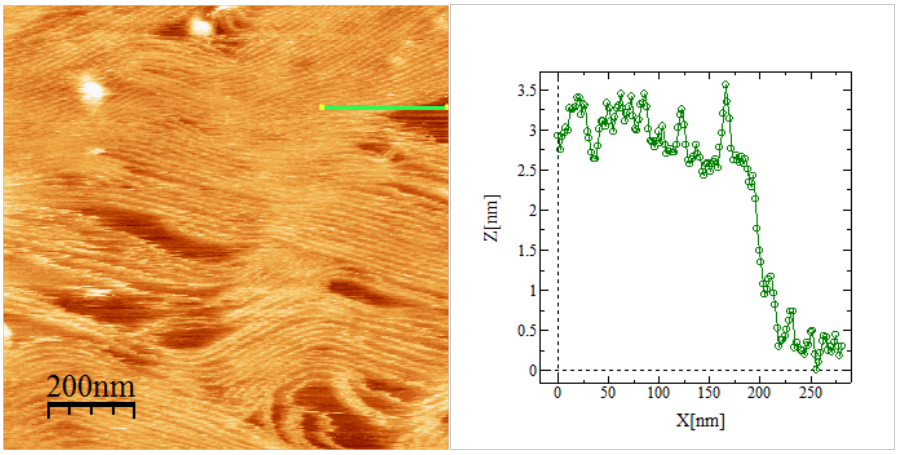

(b) FtsZE83Q

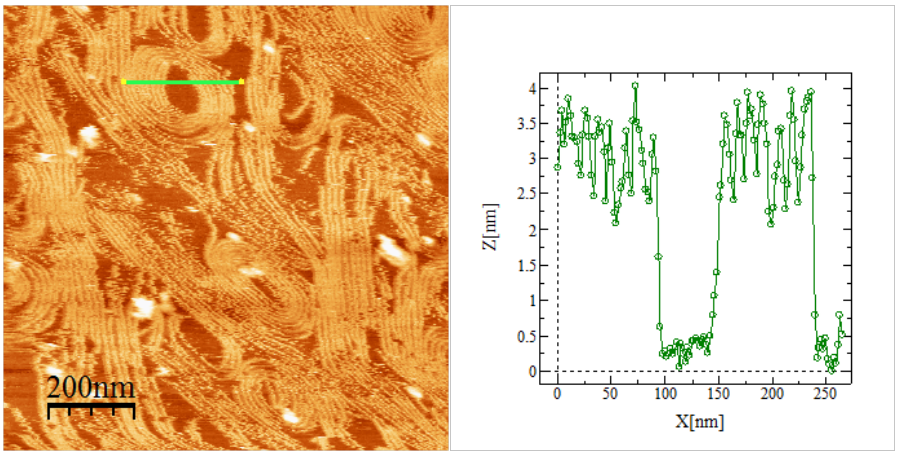

(c) FtsZR85Q

Figure 49: AFM images for the three FtsZ polymers on mica with GTP. To the right, a profile of their heights corresponding to the green line on the AFM image. The scanning area of the images is 1 μm $\times$ 1 μm.

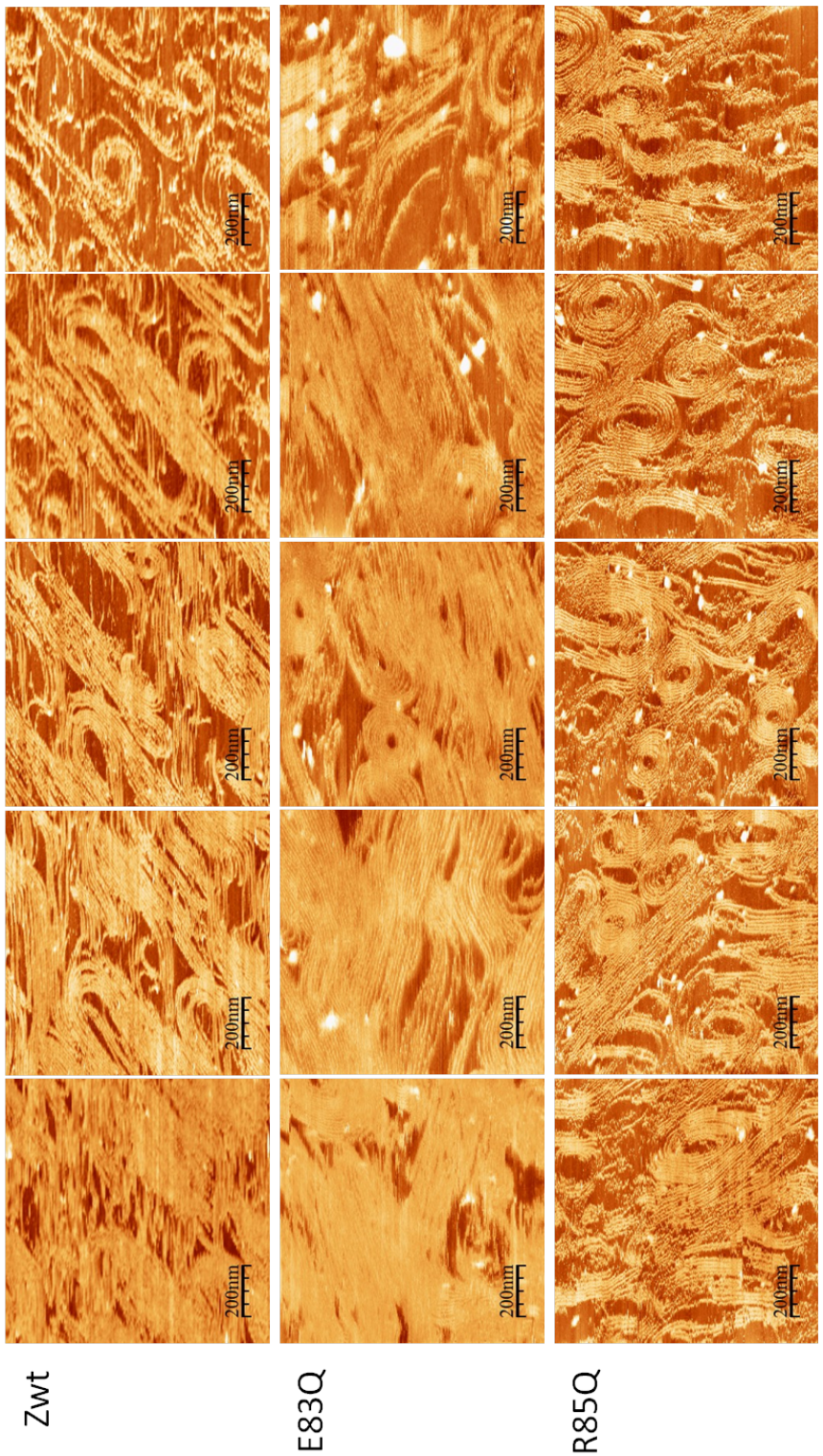

Figure 50: AFM snapshots of FtsZ polymers dynamics on mica with GTP. Scanning area of all images is $1\,\mu\mathrm{m} \times 1\,\mu\mathrm{m}$.

7.2.2 *FtsZ - sZipA interaction on mica*

We next explored how the FtsZ lateral mutants polymerization is affected or not by the presence of sZipA. The samples were prepared as described on Chapter 6.2.2 and scanned in the presence of GTP.

Figure 51 shows that FtsZ wild type and lateral mutants are still able to polymerize on mica in the presence of sZipA.

The profile plots indicate the heights of the FtsZ polymers are not affected by the addition of a second protein, they are still one protein height and sZipA might be placed beside the polymers.

Figure 52 shows how these FtsZ polymers reorganize on the surface as snapshots. FtsZ wild type filaments undergo several conformations during the experimental timescale: at $t = 0$ they are tightly packed and individual polymers are indistinguishable. As time evolves, some rolls start to appear (see $t = 3\,\mathrm{h}$ snapshot), and eventually they start to straighten and condense in large straight aggregates. The height of the final condensates is still 4 nm.

FtsZE83Q polymers also reorganize: at $t = 3\,\mathrm{h}$ some polymers start to straighten and individual filaments are distinguishable, but they finally condensate in the form of tight rolls instead of long and straight bundles as FtsZwt does.

FtsZR85Q filaments are dynamic but evolve more slowly: at $t = 3\,\mathrm{h}$ some curved filaments start being discernible and a few rolls are observed. At the end of the scanning time the condensates are similar as those for FtsZE83Q, but the rolls are less tight and it is possible to distinguish individual filaments within them.

The presence of sZipA affects the way FtsZwt reorganize on the surface, inducing the formation of long and straight condensates.

Although both FtsZ lateral mutants start to reorganize at some point into straight filaments, their final condensates are in the form of rolls instead of straight bundles formed by FtsZwt.

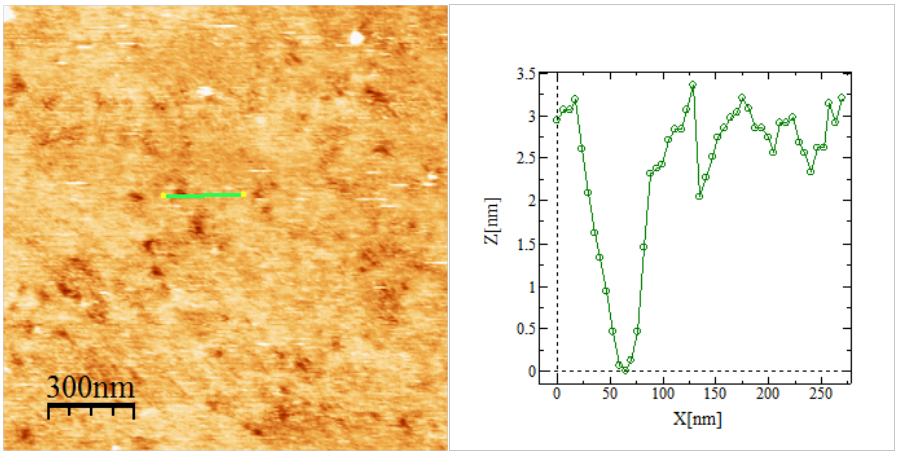

(a) FtsZwt with sZipA

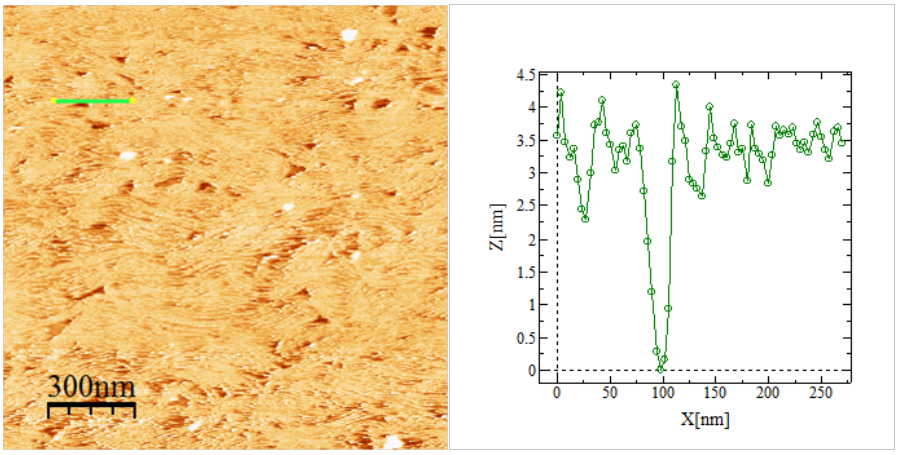

(b) FtsZE83Q with sZipA

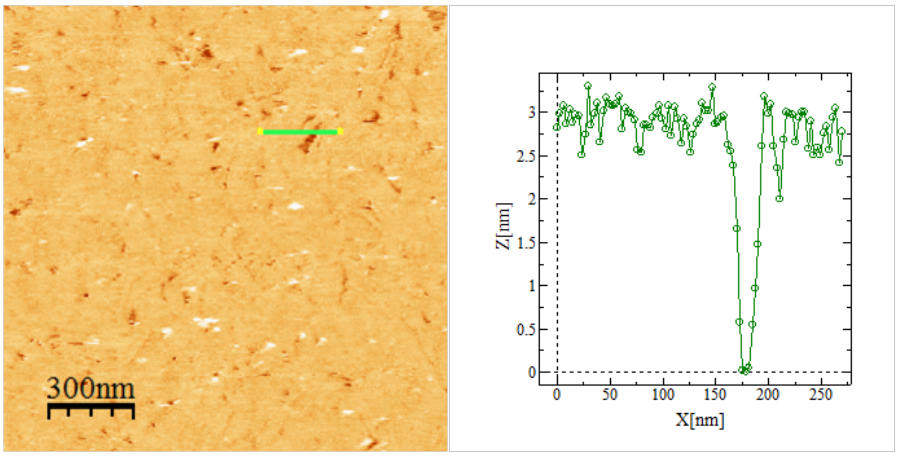

(c) FtsZR85Q with sZipA

Figure 51: AFM images for FtsZ wild type and lateral mutants polymers on mica with sZipA and GTP. To the right, a profile of their heights corresponding to the green line on the AFM image. The scanning area of the images is 1.5 μ m $\times$ 1.5 μ m.

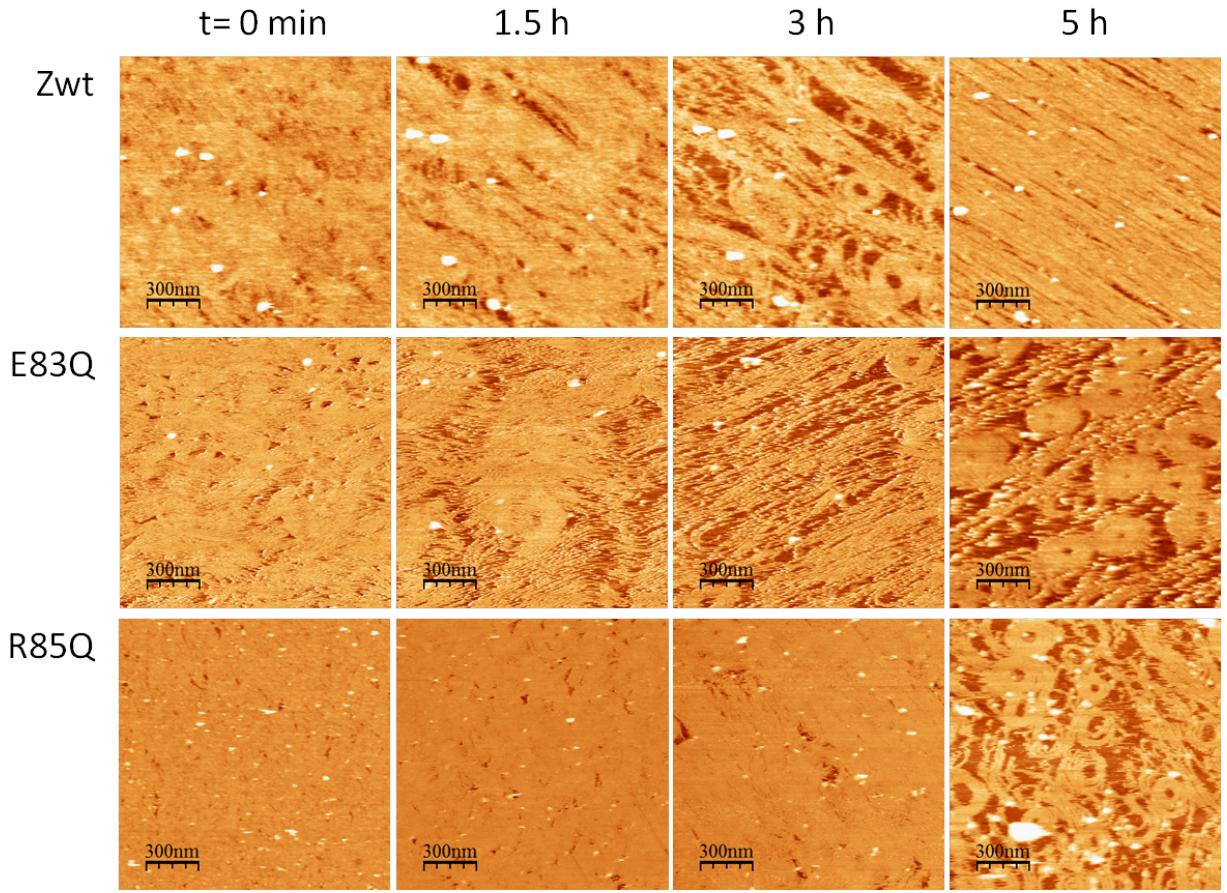

Figure 52: AFM snapshots of FtsZ polymers dynamics on mica with sZipA and GTP. Scanning area of all images is 1.5 μ m $\times$ 1.5 μ m.

7.2.3 *FtsZ - ZipA interaction on a lipid bilayer*

The reconstituted system with the highest complexity studied on this thesis will be complete by adding a supported lipid bilayer. We have used neutral (DOPC) and negatively charged (*E. coli* polar) lipid bilayers, as in QCM experiments, to anchor first sZipA and then bind both FtsZ lateral mutants to it. We want to evaluate how the polymerization of FtsZ mutants is affected by the different lipid composition of the bilayers.

Mateos-Gil *et al.* [Mateos-Gil et al., 2012a] have characterized the formation of FtsZ wild type bundles bound to sZipA on DOPC and EcPl bilayers by AFM under the same conditions we used on this thesis.

We start our characterization for the binding of FtsZ lateral mutants to sZipA anchored on neutral DOPC lipids preparing the samples as described in Chapter 6.2.2.

FtsZ, wild type and lateral mutants, are able to polymerize on neutral DOPC lipids in the presence of GTP as shown on Figure 53. The formed structures are about $3.5 - 5\,\text{nm}$ height above the bilayer and individual filaments are observed.

Figure 54 shows a series of snapshots for the dynamics of these polymers. FtsZwt polymers reorganize on the surface and form high order structures. Those final condensates are about 8 nm in height from the bilayer.

On the contrary, FtsZ lateral mutants are not capable of forming high order filament condensates. FtsZE83Q polymers show a small reorganization on the surface as time evolves. These condensates are mostly composed of tight rolls. FtsZR85Q single filaments start to be distinguishable as the protein desorbs from the surface. As time progress, this particular FtsZ mutant finally condensates into rolls. The final condensates for both FtsZ lateral mutants are 4.5 nm in height, i.e., a single layer of protein and 1 nm more than in mica. Another feature observed is that FtsZ lateral mutants bind to sZipA as islands of protein, this characteristic is shared by both proteins but it is completely different compared to FtsZwt.

Figure 55 shows the polymerization and reorganization of FtsZ on *E. coli* polar lipids. At $t = 0$ there are no FtsZ polymers on the surface for the wild type and lateral mutants proteins. As time progress, FtsZwt starts to polymerize and reorganize until a highly connected and dynamic network is formed. These polymers extend from the surface about 20 nm in height.

Contrary to the native protein, FtsZ lateral mutants display a different behavior, they do not polymerize on EcPl lipids. FtsZE83Q at $t = 3\,\text{h}$ starts to resemble the first stage of FtsZwt reorganization but it does not evolve further. As for FtsZR85Q instead, its final structures are not filamentous aggregates.

We therefore conclude that either lateral aa mutation on FtsZ affects the interaction between polymers and their interaction with sZipA when anchored to a supported lipid bilayer.

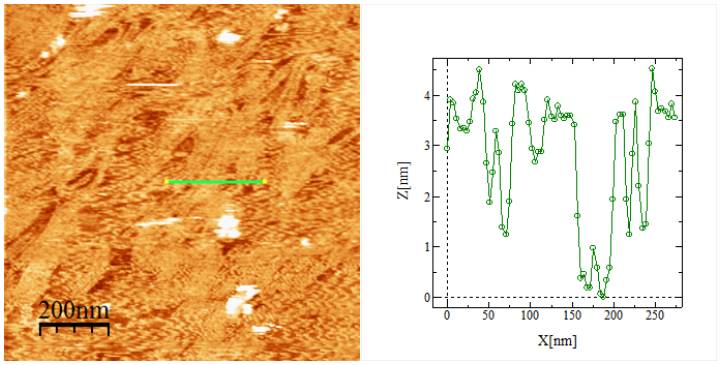

(a) FtsZwt-GTP bound to sZipA. Scanned area of 1 μ m $\times$ 1 μ m.

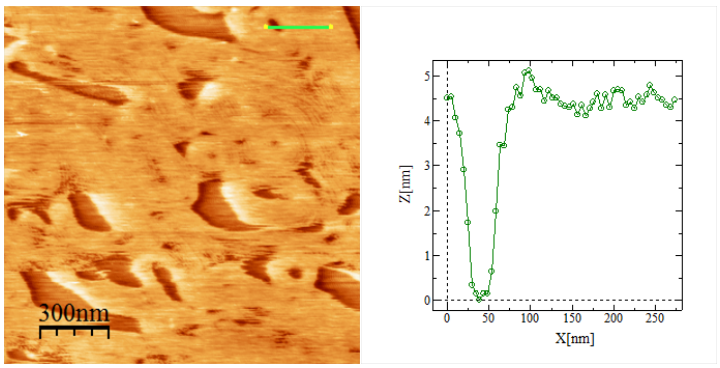

(b) FtsZE83Q-GTP bound to sZipA. Scanned area of 1.5 μ m $\times$ 1.5 μ m.

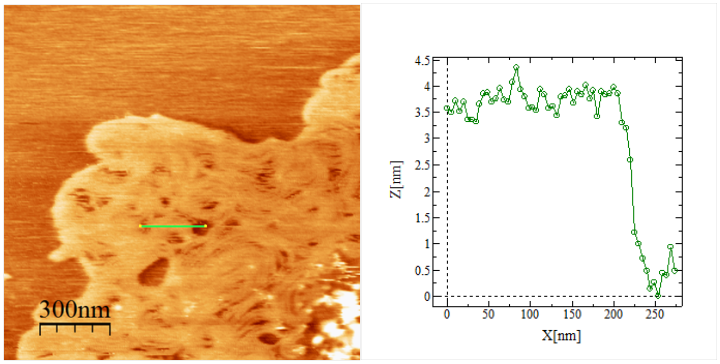

(c) FtsZR85Q-GTP bound to sZipA. Scanned area of 1.5 μ m $\times$ 1.5 μ m.

Figure 53: AFM images of FtsZ polymers bound to sZipA on neutral DOPC lipids. To the right, a profile of their heights corresponding to the green line on the AFM image.

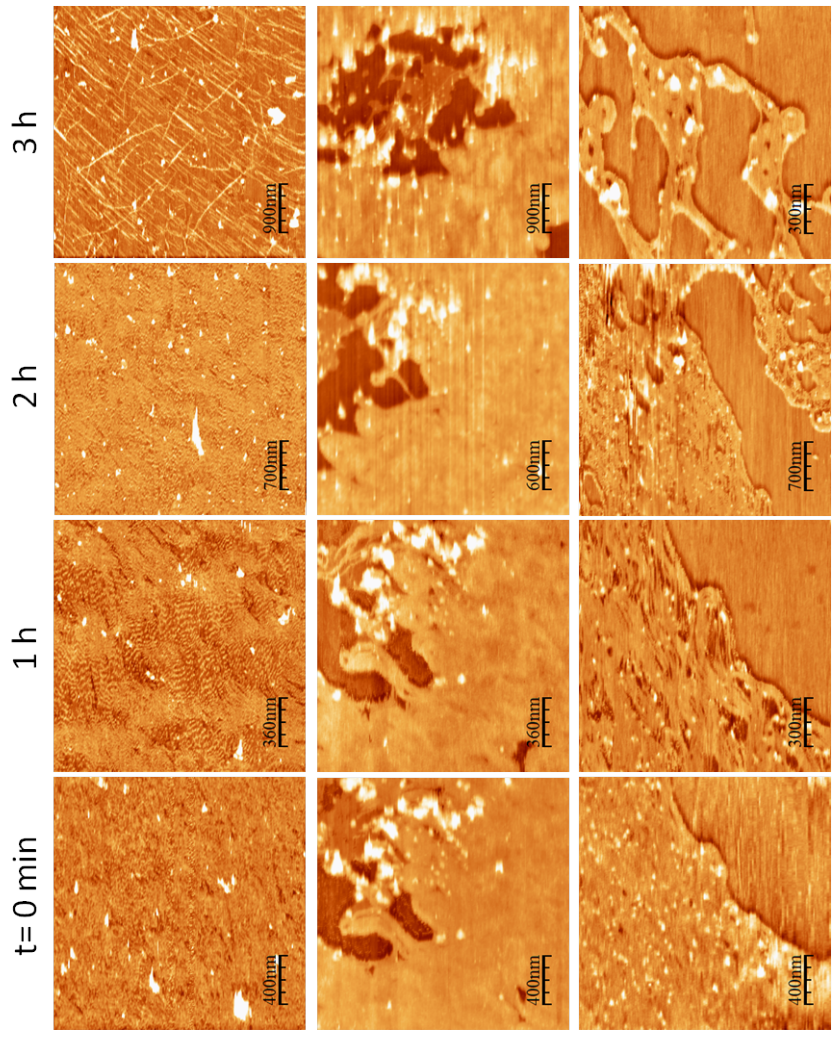

Figure 54: AFM snapshots of FtsZ polymers dynamics on a neutral DOPC bilayer with sZipA and GTP.

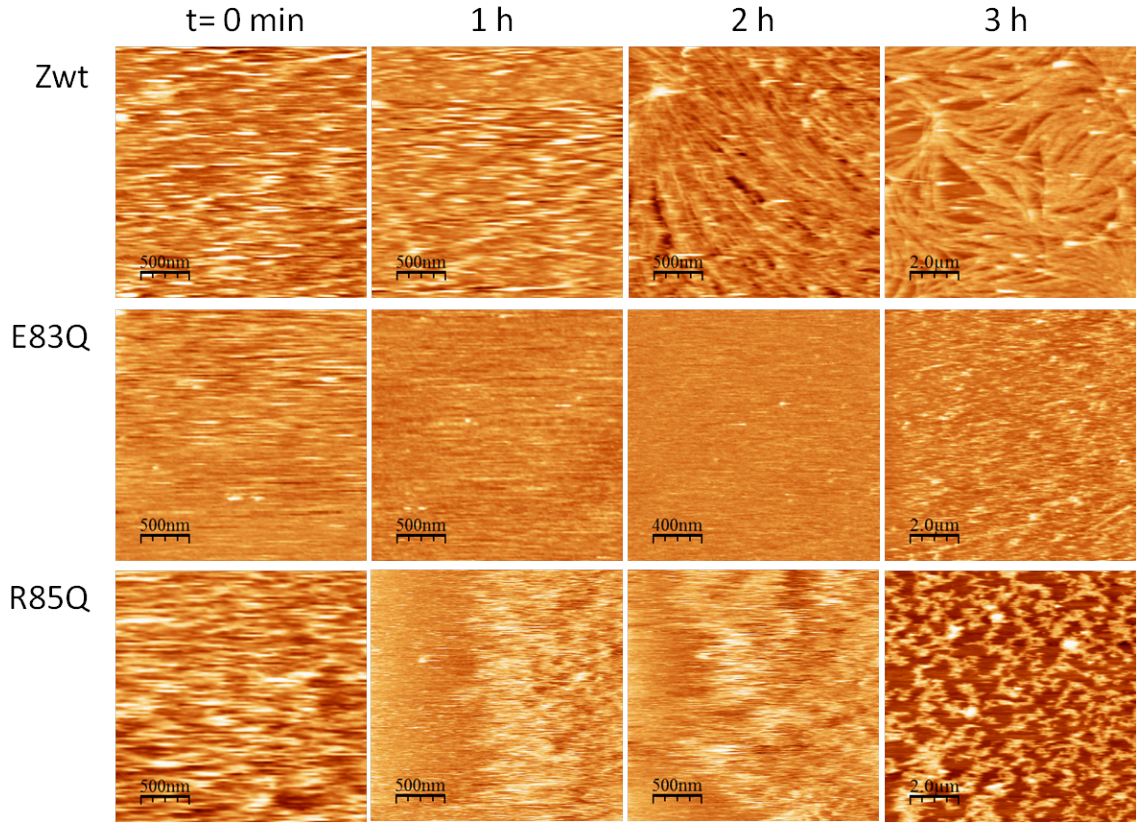

Figure 55: AFM snapshots for the time evolution of FtsZ structures with sZipA and GTP on *E. coli* polar lipids.

8 DISCUSSION

The aim of this thesis was to provide a biophysical characterization of two single-site mutations directed to the lateral side of FtsZ with the use of AFM and QCM techniques. A comparison with native FtsZ was made trying to elucidate which differences *in vitro* could be relevant for these two FtsZ mutants functionality *in vivo*. Our results show that the differences in behavior of both FtsZ lateral mutants with respect to the native protein become apparent when we increase the complexity of our reconstituted system.

ABOUT FTSZ POLYMERIZATION ON MICA

We first studied the effect of these two single-site FtsZ mutations on polymerization on mica.

FtsZE83Q and FtsZR85Q mutants have been characterized by Shin *et al.* [Shin et al., 2013] by biochemical and Electron microscopy techniques. Their *in vitro* results show that both mutations changed the FtsZ GTPase activity, and that the mutations affected the longitudinal interactions and their ability to form bundles. FtsZE83Q polymerizes into long and curved filaments, while FtsZR85Q polymers are short and straight as observed by EM on negatively stained samples.

Our results show a distinct behavior of the polymerization induced by the planar surface with respect to EM previous results. AFM experiments have shown that both FtsZ lateral mutants are able to polymerize on mica in the presence of GTP. The filaments formed are long, single stranded and curved of several hundredths of nm in length. Adsorption of the filaments to the surface stabilizes them. So, contrary to what Shin *et al.* conclude, we observe that these lateral mutations on FtsZ allow the longitudinal interaction when the proteins are oriented on a surface.

With respect to the dynamic behavior of the polymers, we observed that FtsZR85Q depolymerizes as FtsZwt whereas FtsZE83Q does it more slowly. Hence, we conclude that an impaired GTPase activity for both FtsZ lateral mutants does not affect polymerization and reorganization on mica.

ABOUT FTSZ-SZIPA INTERACTION ON MICA

It was shown that the presence of ZipA stabilizes FtsZ protofilaments and induces bundling in solution and on surfaces [Hale et al., 2000, Kuchibhatla et al., 2011, Mateos-Gil et al., 2012a].

Our AFM experiments show that both FtsZ lateral mutants polymerize and reorganize on mica in the presence of sZipA and GTP. However, instead of evolving into straight bundles like the wild type FtsZ, they evolve into tightly packed round bundles. FtsZE83Q displays an intermediate stage of aggregation in which stretched and straight filaments are observed, but the filaments keep evolving until they condensate into tight rolls. As for FtsZR85Q filaments, they evolve directly into rolls.

We conclude that the presence of sZipA allows the polymerization of both FtsZ lateral mutants on mica but prevents the formation of straight bundles favoring instead circular condensates.

ABOUT FTSZ-SZIPA INTERACTION ON LIPID BILAYERS

A lipid surface allow studying the binding of FtsZ to the membrane through sZipA. This way it is possible to look at the effect of the lipid composition on the FtsZ-sZipA complex formation and structure of the filaments.

FtsZ wild type. QCM experiments on planar bilayers show an specific binding of FtsZwt to sZipA in the presence of GDP [Mateos-Gil et al., 2012a]. We observed that this binding follows a single site binding model and that the affinity for the formation of FtsZwt-sZipA complex with GDP is is in the microcolar range, comparable to in solution results [Martos et al., 2010, Hernández-Rocamora et al., 2012b], and this affinity is independent on the lipid composition.

Once FtsZwt is bound to sZipA, the addition of the hydrolyzable nucleotide GTP induces spontaneous FtsZwt polymerization on PC lipids, as observed by AFM [Mateos-Gil et al., 2012a]. The bundles formed by FtsZ wild type on neutral PC lipids are standing $\sim 8\,\text{nm}$ away from the bilayer. On the contrary, on *E. coli* polar lipids the polymerization of FtsZ native takes place after a certain lag time and the filaments are suspended 20 nm above the lipid bilayer [Mateos-Gil et al., 2012a]. The authors suggested that sZipA affects in a different manner on FtsZ polymers depending on the lipid composition of the bilayer, and that the presence of charged lipids is essential to increase the flexibility of the sZipA nonstructured domain. The new QCM study presented in this thesis supports their interpretation. When binding FtsZwt-GMPCPP to sZipA anchored to an *E. coli* polar lipid bilayer, we observe an increase in mass, corresponding to the formation of polymers, and also an associated increase in acoustic ratio larger than the one observed on neutral PC lipids. This indicates that the protein layer adsorbed is more loosely bound on *E. coli* than on PC lipids, as expected for filaments suspended 20 nm away from the surface.

Therefore, our results together with previous studies [Mateos-Gil et al., 2012a, López-Montero et al., 2013a] suggest the presence of

negatively charged lipids induce changes on the unstructured P/Q domain of sZipA, which in turn might be responsible for the lag time observed for FtsZwt polymerization, their ulterior reorganization and bundling.

The straight bundles formed by FtsZwt on neutral PC lipid bilayers, where the sZipA protein layer is more rigid can be explained by González de Prado Salas *et al.* model [González de Prado Salas et al., 2014]. They propose that the way the filaments are anchored to a surface can determine the shape of the aggregates. That is, straight FtsZ filaments can form when they are firmly attached to the surface and the orientation leaves the prefential curvature of the filaments facing upward, with the FtsZ N-terminus to C-terminus plane perpendicular to the surface. The FtsZwt curved bundles formed on EcPl lipid bilayers can also be explained by this model by decreasing the anchoring strength, i. e., a more loose protein layer, and/or changing the orientation of the FtsZwt N-terminus to C-terminus plane with respect to the surface.

FtsZ lateral mutants. FtsZ lateral mutants, in the presence of GDP, bind differently to sZipA than FtsZ wild type on a neutral PC lipid bilayer. However, when anchoring sZipA to an *E. coli* polar lipid bilayer, the binding behavior of both FtsZ lateral mutants approaches the one observed for the native FtsZ.

QCM experiments show that in the presence of GMPCPP the polymers formed by the FtsZ lateral mutants are different than the ones formed by FtsZ wild type: a smaller acoustic ratio indicates the protein layer is more rigid at the protein concentration when polymers are expected to form.

AFM experiments show the same effect. Both FtsZ lateral mutants polymerize on neutral PC lipid bilayers immediately after addition of GTP but the protein layer is more compact than FtsZ wild type, as single filaments are difficult to observe. These polymers are able to reorganize on the surface but the final bundles are in the form of rolls instead of the straight bundles formed by FtsZ wild type.

The aggregates in the form of tight rolls formed by the FtsZ lateral mutants on neutral PC lipids could also be explained by González de Prado Salas *et al.* model [González de Prado Salas et al., 2014]: a stronger anchoring given by a higher rigidity of the protein layer and a change in the orientation of the FtsZ N-terminus to C-terminus plane respect to the surface.

On *E. coli* polar lipid bilayers the polymerization behavior of the FtsZ lateral mutants is different. Although QCM binding results are similar to those where neutral PC lipids are present, negatively charged lipids prevent FtsZ lateral mutants polymerization within experimental AFM time employed on this thesis (up to 5 hours of continuous scanning). At the end of scanning time, FtsZE83Q reaches an intermediate stage in reorganization comparable to the initial stage

in reorganization for FtsZwt. On the contrary, for FtsZR85Q we observed protein aggregates with no structure.

Therefore, we conclude that both FtsZ lateral mutations affect the interaction among polymers and with sZipA when anchored to a lipid bilayer.

Thus far, AFM and QCM studies provided information about the formation and structure of filaments on a surface. However, since QCM allows real time measurements of surface loading and unloading, we also explored the extent to which FtsZ-sZipA binding was reversible. We found that FtsZ wild type binding to sZipA was completely reversible only with GMPCPP. For FtsZwt-GDP, unexpectedly, we found that a fraction of the protein is irreversibly bound to sZipA. This amount of FtsZ-GDP that irreversible binds to sZipA could be due to the presence of additional interactions between FtsZ-FtsZ, FtsZ-sZipA or FtsZ-lipids that could stabilize the protein layer.

FtsZ lateral mutants show a different behavior. In the presence of GDP, both FtsZ lateral mutants bind 100% irreversibly to sZipA regardless the lipid composition, indicating a higher stabilization of the protein layer. However, GMPCPP nucleotide makes the unbinding for FtsZR85Q uncertain: on some experiments a fraction of the protein remains irreversibly bound to sZipA regardless lipid composition, suggesting this mutant interacts differently with sZipA.

FtsZ lateral mutants are not able to reach the same high order bundles as FtsZ wild type. The lateral region of the FtsZ monomers altered by the mutations affects the binding to sZipA and the interaction between filaments that prevents them from reorganizing. FtsZE83Q similar intermediate stage of bundling as FtsZwt in addition to the same reversibility observed in our *in vitro* experiments might explain the small cell viability observed *in vivo* [Shin et al., 2013]. Nevertheless, FtsZR85Q observed differences respect to FtsZwt regarding binding, polymerization and reversibility *in vitro* might explain why this particular mutation does not support cell division *in vivo* [Shin et al., 2013]. Hence, the complete reversibility on *E. coli* polar lipid bilayer along with filament reorganization observed for the native FtsZ might be relevant for its biological function.

While the Z-ring is present in the bacterium, FtsZ polymers might undergo different stages: from binding to ZipA, bundling, remodelling to unbinding. The fact that the binding of native FtsZ polymers on *E. coli* lipids is completely reversible might contribute to a rapid remodelling of the structures induced by a change in the bacterium membranes or *vice versa.*

We conclude that reorganization of the FtsZ filaments and reversibility of the binding to sZipA, anchored to an *E. coli* polar lipid bilayer, are important characteristics *in vitro* associated to FtsZ function *in vivo*.

Part IV

CONCLUSION

9 CONCLUSION

Following, I present the conclusions of this thesis.

- The behavior of FtsZ lateral mutants on surfaces is different as the behavior on solution described for the same proteins:
  - Lateral mutants monomers interact longitudinally forming filaments on surface.
  - In spite of their impaired GTPase activity detected in solution both mutant proteins polymerize and reorganize on mica.
  - Contrary to what is observed for the native protein, the aggregates formed by both lateral mutants in the presence of sZipA are circular instead of straight bundles.

- Both FtsZ lateral mutants behavior is different to the native protein when bound to ZipA anchored to a supported lipid bilayer:
  - They alter the amount of protein bound to ZipA, the affinity and reversibility of the binding.
  - On neutral lipids, circular condensates are promoted instead of the straight bundles observed for the native FtsZ.
  - *E. coli* polar lipids bilayer prevents polymers to form, and affects the intrinsic viscoelasticity of the protein layer, indicating a different conformation and rigidity of the anchoring to the surface compared to the native protein.

- The lateral region of the FtsZ monomers altered by the mutations affects the interaction between filaments and prevents them from organizing. We propose that this aspect, along with the reverisbility of the binding to ZipA, as relevant for the formation of a contractile ring.

Part V

CONCLUSIONES

10 CONCLUSIONES

A continuación presento las conclusiones de esta tesis.

- El comportamiento en superficies es diferente del descrito en solución para los mismos mutantes laterales de FtsZ:
  - Los monómeros de éstos mutantes interactúan longitudinalmente en superficie formando filamentos.
  - A pesar de su baja actividad GTPasa observada en solución no impide la polimerización y la reorganización en mica de ambos mutantes.
  - ZipA induce la formación de condensados circulares en lugar de los agregados rectos que se forman con la proteina nativa.

- Ambos mutantes laterales de FtsZ muestran un comportamiento diferente a la proteína nativa en su unión a sZipA anclada a una bicapa lipídica plana:
  - Alteran la cantidad de proteína unida, la afinidad a ZipA y la reversibilidad de la unión.
  - En lípidos neutros se forman condensados en forma de rollos, a diferencia de los agregados rectos observados para FtsZ nativa.
  - La bicapa de lípidos polares de *E. coli* previene la formación de polímeros, y afecta las propiedades viscoelásticas intrínsecas de la capa de proteína, indicando que la conformación y rigidéz del anclaje a la superficie son distintos a los observados en la proteína nativa.

- La región lateral de los monómeros alterada por las mutaciones afecta la interacción entre los filamentos e impide que se reorganicen. Proponemos que éste aspecto, junto con la reversibilidad de la unión a ZipA, son relevantes para la formación de un anillo contráctil.

Parte VI

APPENDIX

A

SLB FORMATION ON AU SUBSTRATES

On this appendix we want to show the methodological contribution of this thesis: forming a supported *E. coli* polar lipid bilayer on a QCM *Au*-coated substrate.

Since a reported QCM characterization for the formation of an SLB composed by negatively charged lipids is lacking in the literature, this new approach will allow us to characterize the binding of FtsZ to sZipA anchored to an *E. coli* polar lipids bilayer by Quartz crystal microbalance (QCM).

A.1 SUBSTRATE CHEMICAL MODIFICATION

A supported lipid bilayer formation on untreated gold surfaces does not take place spontaneously as on SiO_2 surfaces [Wang et al., 2010]. However, Gutiérrez-Sánchez *et al.* [Gutiérrez-Sánchez et al., 2011] have formed successfully a negatively charged *E. coli* lipid bilayer on gold substrates functionalized with a 4-Aminothiophenol (4-ATP) Self-Assembled Monolayer (SAM). We used the same construction for QCM experiments but the surface became inactive within minutes making our results difficult to reproduce. We used instead a similar approach by treating the QCM gold coated sensor with a different thiol: 3-mercaptopropionic acid. This particular thiol was chosen in order to reproduce the negative surface charge distribution on gold as is on freshly cleaved mica, in which *E. coli* polar lipid vesicles spontaneously spread forming a bilayer in the presence of a divalent cation, i. e., $CaCl_2$.

Au-coated QCM substrates were cleaned with piranha solution (3 : 1, H_2SO_4 98 % : H_2O_2 30 %), rinsed extensively with Milli-Q water and dried under a nitrogen stream. Then a 3-mercaptopropionic acid SAM was formed by immersing *Au* substrates in a 0,2 mM 3-mercaptopropionic acid solution in deionized water/ethanol (1 : 1) for 18 h at room temperature. The substrates were rinsed with Milli-Q water and dried with N_2 prior to assembly of the QCM chamber.

Within the pH range used on this thesis, the 3-mercaptopropionic acid SAM will be negatively charged. The isoelectric point for the propionic acid is 4.87 and are extensively used to produce hydrophilic SAMs.

We then proceeded to characterize the SLB formed on a gold modified QCM substrates by Quartz Crystal Microbalance (QCM), Atomic force microscopy (AFM) and Fluorescence recovery after photobleaching (FRAP) measurements.

A.2 SLB FORMATION BY QCM-D

E. coli polar lipid liposomes were prepared as described on Chapter 6.1.1. The liposomes were injected at 0,1 mg/mL in the presence of different $CaCl_2$ concentration ($NiCl_2$ was also tested but generated a low reproducibility, data not shown). Simultaneous resonant frequency and dissipation measurements (Figure 56) indicate that an SLB might be formed, if a concentration of 2 mM $CaCl_2$ is present in the buffer. This Ca^{2+} concentration seems to be the suitable concentration needed to bridge the interaction between the charged lipid head group and the negatively charged substrate [Richter et al., 2003]. At different cation concentrations the resonant frequency shift in addition to dissipation measurements show that vesicles fusion does not occur.

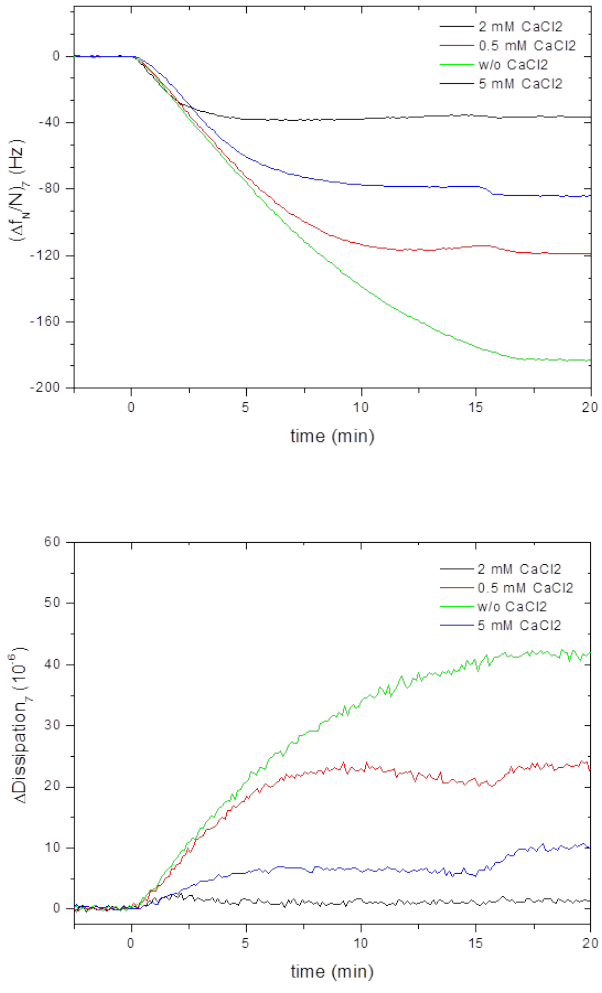

Figura 56: Resonant frequency shift and dissipation measurements for EcPl liposomes at different $CaCl_2$ concentration on Au substrate modified chemically with a 3-mercaptopropionic acid SAM.

Our QCM measurements show the resonance frequency change for the *E. coli* polar lipid bilayer is $-36{,}5 \pm 2{,}0\,\text{Hz}$, which corresponds to a loaded mass per unit area of $660 \pm 36\,ng/\text{cm}^2$ using Sauerbrey model (Equation 9, Chapter 6.3), and a dissipation $< 1{,}25 \times 10^{-6}$. These values are higher than the reported values for EPC bilayers formed on SiO_2 [Keller and Kasemo, 1998] and the differences can be due to the lipid composition (*E. coli* lipids have a larger molecular weight than EPC lipids in addition to the a percentage of DOGS-NTA lipid), ionic strength of the buffer solution, and hydration degree of the supported bilayer [Cho et al., 2010].

We tested the homogeneity of the SLB by anchoring sZipA protein to it. This protein has a 6-Histidine tail which shows an specific binding to the DOGS-NTA lipid present in the lipid composition, and this binding site can be competed with the addition of imidazole. We have shown that sZipA binding to the lipid bilayer is reversible after addition of imidazole, and there is no unspecific binding of sZipA to the substrate (see Chapter 7.1.1).

A.3 SLB CHARACTERIZATION BY AFM

The bilayer was further characterized by AFM. Prior to imaging the substrate was cleaned with piranha solution (3 : 1, H_2SO_4 98 % : H_2O_2 30 %), rinsed extensively with Milli-Q water and dried with N_2. Figure 57 shows an AFM topographic image of the bare *Au*-coated QCM substrate.

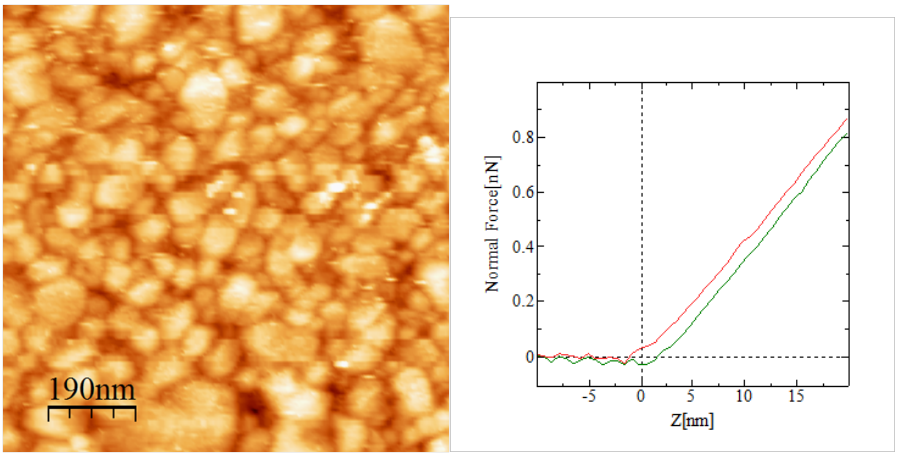

Figura 57: AFM image for bare *Au*-coated QCM substrate. Indentation curve indicates a rigid substrate.

After the *Au*-coated QCM substrate was chemically modified with a 3-mercaptopropionic acid SAM, we proceed to incubate liposomes

at 0,2 mg/mL with and with-out $CaCl_2$ for 1 h at room temperature. Previously to imaging, the samples were extensively rinsed with buffer.

Figure 58 show a topographic image for liposomes incubated without $CaCl_2$. We observe a fragmented lipid layer with a height corresponding to a bilayer. This non-completely fused bilayer was fragile and a continuous scanning easily exposed the substrate, as observed in the zoomed image.

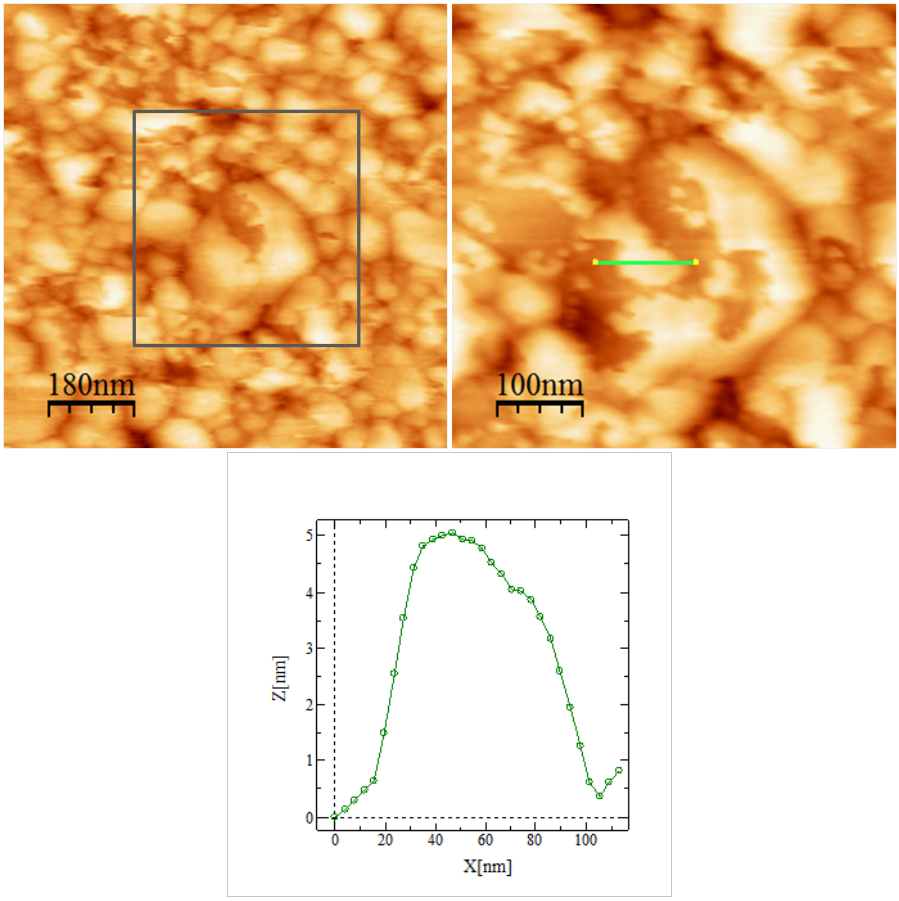

Figura 58: AFM images for EcPl liposomes incubated without $CaCl_2$ on *Au*-coated QCM substrate chemically modified with a 3-mercaptopropionic acid SAM. Profile shows the height of the bilayer across the green line on the AFM image.

If *E. coli* polar lipid liposomes were incubated with 2 mM $CaCl_2$ a complete bilayer was formed. Figure 59 show a topographic image of the fused bilayer. The gray square indicates the location zoomed area, and the profile of the heights is measured across the green line. The indentation curve also in Figure 59 shows the rupture of the bilayer on the approaching curve displayed in green (compare indentation curve for the bare *Au* substrate on Figure 57).

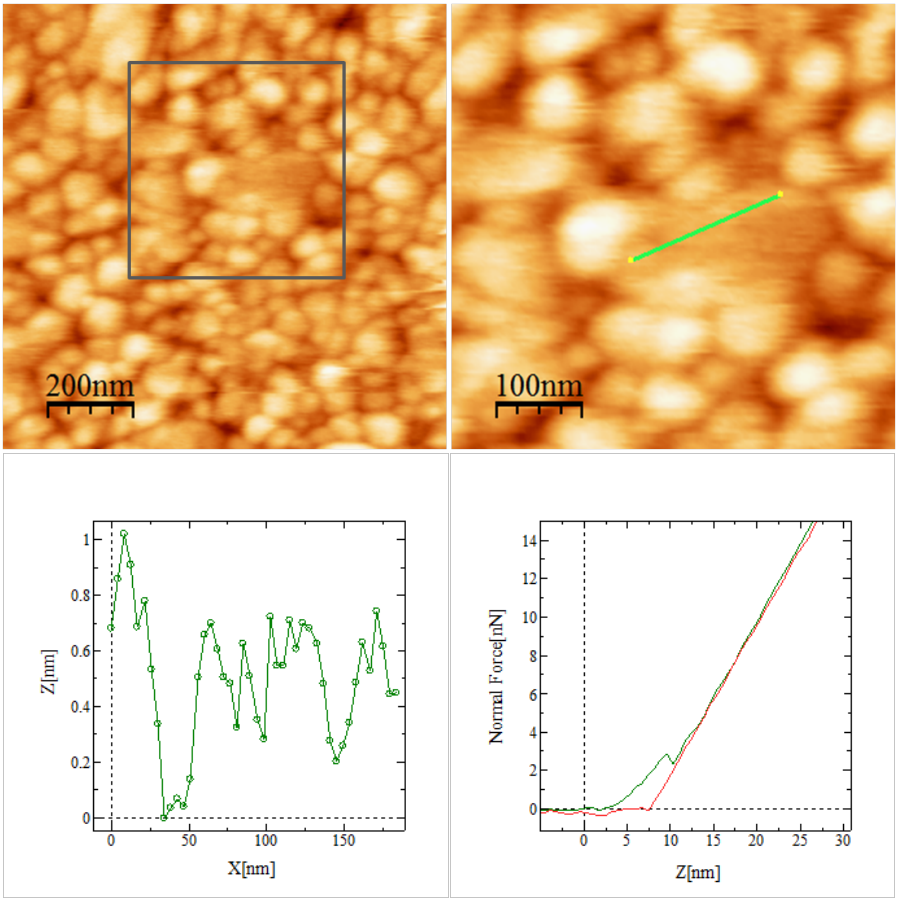

Figura 59: AFM image for EcPl liposomes incubated with $CaCl_2$ on Au substrate modified chemically with a 3-mercaptopropionic acid SAM. Profile of the bilayer surface across the green line on the AFM image. Indentation curve displays rupture of the bilayer.

Surface roughness analysis also shows the presence of a bilayer. The bilayer smooths the surface: the average height for liposomes incubated with $CaCl_2$ is 6 nm whereas for bare Au is 8 nm.

A.4 SLB CHARACTERIZATION BY FRAP

We made a final characterization for the mobility of the phospholipids by measuring the diffusion coefficient for the *E. coli* lipid bilayer. Lipid vesicles were prepared as described on Chapter 6.1.1, with a lipid mixture containing a 1 % molar ratio DiI C18 lipid fluorescence tracer. Supported lipid bilayers were formed on functionalized Au coated QCM substrate incubating the liposomes at 0,2 $^{mg}/_{mL}$ with and without $CaCl_2$ for 1 h at room temperature, and on mica with $CaCl_2$ as reference.

Plot on Figure 60 shows FRAP data from *E. coli* lipid bilayers. Fluorescence recovers after 15 minutes from the end of the photobleaching

to a 75 % for gold substrate treated with 3-mercaptopropionic acid and to a 90 % on mica, both in the presence of $CaCl_2$. When liposomes are incubated without $CaCl_2$, the fluorescence intensity recovers up to a 25 % only.

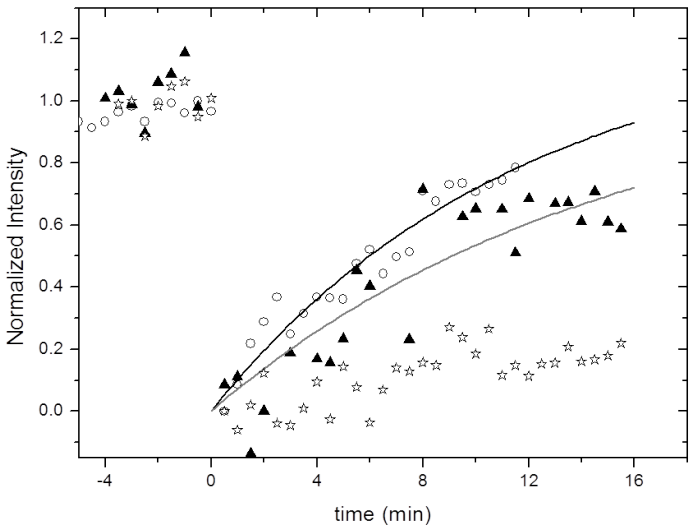

Figura 60: FRAP data for *E. coli* lipid bilayer on *Au* substrate modified with a 3-mercaptopropionic acid SAM. Liposomes were incubated with and without $CaCl_2$ (black triangles and open stars respectively). Mica measurements are for reference (open circles).

The diffusion coefficient for the phospholipids gave a mean value of $1{,}0 \pm 0{,}2\,\mu m^2 s^{-1}$ and $0{,}8 \pm 0{,}2\,\mu m^2 s^{-1}$ for *E. coli* bilayer on mica and on functionalized *Au* respectively. These values are of the same order of magnitude as for other reported fluid lipid bilayers [Adalsteinsson and Yu, 2000, Nishibori et al., 2005, Weng et al., 2006, Dodd et al., 2008, Gutiérrez-Sánchez et al., 2011].

A.5 SUMMARY

We have successfully formed an *E. coli* polar lipid bilayer on an *Au*-coated QCM substrate functionalized with a 3-mercaptopropionic acid SAM. Our QCM experiments indicate the *E. coli* polar lipid bilayer obtained gives the expected values for mass adsorbed and dissipation, and that this bilayer is uniformly distributed if 2 mM $CaCl_2$ is present in the buffer. Through AFM measurements we have shown the bilayer is uniform and it smooths the surface giving as a result a lower average height for the formed structures as for bare *Au*. And finally,

FRAP experiments indicate the phospholipids forming the bilayer are mobile with the expected diffusion coefficient.

BIBLIOGRAPHY

T. Adalsteinsson and H. Yu. Lipid lateral diffusion in multi-bilayers, and in monolayers at the air/water and heptane/water interfaces. *Langmuir*, 16(24):9410–9413, 2000.

D. W. Adams and J. Errington. Bacterial cell division: assembly, maintenance and disassembly of the Z-ring. *Nat. Rev. Microbiol.*, 7(9): 642–653, Sep. 2009.

S. G. Addinall, E. Bi, and J. Lutkenhaus. FtsZ ring formation in fts mutants. *J. Bacteriol.*, 178(13):3877–3884, July 1996.

S. G. Addinall, C. Cao, and J J. Lutkenhaus. Temperature shift experiments with an ftsZ84(Ts) strain reveal rapid dynamics of FtsZ localization and indicate that the Z ring is required throughout septation and cannot reoccupy division sites once constriction has initiated. *J. Bacteriol.*, 179(13):4277–4284, July 1997.

S. G. Addinall, E. Small, D. Whitaker, S. Sturrock, W. D. Donachie, and M. M. Khattar. New temperature-sensitive alleles of FtsZ in Escherichia coli. *J. Bacteriol.*, 187(1):358–365, Jan. 2005.

J. F. Allard and E. N. Cytrynbaum. Force generation by a dynamic Z-ring in Escherichia coli cell division. *Proceedings of the National Academy of Sciences*, 106(1):145–150, Jan. 2009.

B. Becker and M. A. Cooper. A survey of the 2006-2009 Quartz Crystal Microbalance biosensor literature. *J. Mol. Recognit.*, 24(5):754–787, Sep. 2011.

T. K. Beuria, J. H. Shah, M. K. Santra, V. Kumar, and D. Panda. Effects of pH and ionic strength on the assembly and bundling of FtsZ protofilaments: A possible role of electrostatic interactions in the bundling of protofilaments. *Int. J. Biol. Macromol.*, 40(1):30–39, Dec. 2006.

C. Binnig, C. F. Quate, and Ch. Gerber. Atomic force microscope. *Phys. Rev. Lett.*, 56:930–933, Mar. 1986.

J. Buss, C. Coltharp, T. Huang, C. Pohlmeyer, S. Wang, C. Hatem, and J. Xiao. In vivo organization of the FtsZ-ring by ZapA and ZapB revealed by quantitative super-resolution microscopy. *Mol. Microbiol.*, 89(6):1099–1120, 2013.

H. J. Butt, B. Cappella, and M. Kappl. Force measurements with the atomic force microscope: Technique, interpretation and applications. *Surface Science Reports*, 59:1–152, 2005.

M. Carrión-Vázquez, A. F. Oberhauser, S. B. Fowler, P. E. Marszalek, S. E. Broedel, J. Clarke, and J. M. Fernandez. Mechanical and chemical unfolding of a single protein: A comparison. *Proceedings of the National Academy of Sciences*, 96(7):3694–3699, 1999.

F. Cava, E. Kuru, Y. V. Brun, and M. A. de Pedro. Modes of cell wall growth differentiation in rod-shaped bacteria. *Curr. Opin. Microbiol.*, 16:1–7, 2013.

R. Chang. *Physical Chemistry for the Biosciences*. University Science Books, 2005.

Y. Chen and H. P. Erickson. Rapid in vitro assembly dynamics and subunit turnover of FtsZ demonstrated by fluorescence resonance energy transfer. *J. Biol. Chem.*, 280(23):22549–54, June 2005.

Y. Chen and H. P. Erickson. Conformational changes of FtsZ reported by tryptophan mutants. *Biochemistry*, 50(21):4675–4684, Apr. 2011.

Y. Chen, K. Bjornson, S. D. Redick, and H. P. Erickson. A rapid fluorescence assay for FtsZ assembly indicates cooperative assembly with a dimer nucleus. *Biophys. J.*, 88(1):505–514, Jan. 2005.

N. J. Cho, C. W. Frank, B. Kasemo, and F. Höök. Quartz Crystal Microbalance with Dissipation monitoring of supported lipid bilayers on various substrates. *Nature Protocols*, 5(6):1096–1104, 2010.

H. Clausen-Schaumann, M. Seitz, R. Krautbauer, and H. E. Gaub. Force spectroscopy with single bio-molecules. *Current Opinion in Chemical Biology*, 4(5):524–530, 2000.

K. A. Connors. *BINDING CONSTANTS. The Measurement of Molecular Complex Stability*. John Wiley & Sons, Inc., 1987.

M. A. Cooper and V. T. Singleton. A survey of the 2001 to 2005 Quartz Crystal Microbalance biosensor literature: applications of acoustic physics to the analysis of biomolecular interactions. *J. Mol. Recognit.*, 20(3):154–184, May 2007.

E. N. Cytrynbaum, D. L. Yongnan, J. F. Allard, and H. Mehrabian. Estimating the bending modulus of a FtsZ bacterial-division protein filament. *Phys. Rev. E*, 85:011902, 2012.

J. F. Díaz, A. Kralicek, J. Mingorance, J. M. Palacios, M. Vicente, and J. M. Andreu. Activation of cell division protein FtsZ: CONTROL OF SWITCH LOOP T3 CONFORMATION BY THE NUCLEOTIDE γ-PHOSPHATE. *J. Biol. Chem.*, 276(20):17307–17315, May 2001.

P. A. J. de Boer. Advances in understanding *E. coli* cell fission. *Curr. Opin. Microbiol.*, 13:730–737, 2010.

P. J. de Pablo, J. Colchero, J. Gómez-Herrero, and A. M. A. M. Baró. Jumping mode scanning force microscopy. *Appl. Phys. Lett.*, 73(22): 3300–3302, 1998.

T. den Blaauwen. Prokaryotic cell division: flexible and diverse. *Curr. Opin. Microbiol.*, 16:1–7, 2013.

C. E. Dodd, B. R. G. Johnson, L. J. C. Jeuken, T. D. H. Bugg, R. J. Bushby, and S. D. Evans. Native E. coli inner membrane incorporation in solid-supported lipid bilayer membranes. *Biointerphases*, 3 (2):FA59–FA67, June 2008.

A. J. F. Egan and V. Waldemar. The physiology of bacterial cell division. *Ann. N. Y. Acad. Sci.*, 1277:8–28, 2013.

A. Engel and D. J. Muller. Observing single biomolecules at work with the atomic force microscope. *Nat. Struct. Mol. Biol.*, 7(9):715–718, Sep. 2000.

H. P. Erickson. The FtsZ protofilament and attachment of ZipA-structural constraints on the FtsZ power stroke. *Curr. Opin. Cell Biol.*, 13(1):55–60, Feb. 2001.

H. P. Erickson, D. W. Taylor, K. A. Taylor, and D. Bramhill. Bacterial cell division protein FtsZ assembles into protofilament sheets and minirings, structural homologs of tubulin polymers. *Proc. Natl. Acad. Sci. U. S. A.*, 93(1):519–523, Jan. 1996.

H. P. Erickson, D. E. Anderson, and M. Osawa. FtsZ in bacterial cytokinesis: cytoskeleton and force generator all in one. *Microbiol. Mol. Biol. Rev.*, 74:504–28, 2010.

J. Errington, R. A. Daniel, and D. J. Scheffers. Cytokinesis in bacteria. *Microbiol. Mol. Biol. Rev.*, 67:52–65, 2003.

G. N. M. Ferreira, A-C da Silva, and B. Tomé. Acoustic wave biosensors: physical models and biological applications of Quartz Crystal Microbalance. *Trends Biotechnol.*, 27(12):689–697, Dec. 2009.

G. Fu, T. Huang, J. Buss, C. Coltharp, Z. Hensel, and J. Xiao. In vivo structure of the *E. coli* FtsZ-ring revealed by photoactivated localization microscopy (PALM). *PLoS One*, 5(9):e12682, Sep. 2010.

J. M. González, M. Jiménez, M. Vélez, J. Mingorance, J. M. Andreu, M. Vicente, and G. Rivas. Essential cell division protein FtsZ assembles into one monomer-thick ribbons under conditions resembling the crowded intracellular environment. *J. Biol. Chem.*, 278(39): 37664–37671, Sep. 2003.

J. M. González, M. Vélez, M. Jiménez, C. Alfonso, P. Schuck, J. Mingorance, M. Vicente, A. P. Minton, and G. Rivas. Cooperative behavior

of Escherichia coli cell-division protein FtsZ assembly involves the preferential cyclization of long single-stranded fibrils. *Proc. Natl. Acad. Sci. U. S. A.*, 102(6):1895–1900, Feb. 2005.

P. González de Prado Salas, I. Hörger, F. Martín-García, J. Mendieta, A. Alonso, M. Encinar, P. Gómez-Puertas, M. Vélez, and P. Tarazona. Torsion and curvature of ftsz filaments. *Soft Matter*, 10(12): 1977–1986, Feb. 2014.

C. Gutiérrez-Sánchez, D. Olea, M. Marques, V. M. Fernández, I. A C. Pereira, M. Vélez, and A. L. De Lacey. Oriented immobilization of a membrane-bound hydrogenase onto an electrode for direct electron transfer. *Langmuir*, 27(10):6449–6457, May 2011.

C. A. Hale and P. A. J. de Boer. Direct binding of FtsZ to ZipA, an essential component of the septal ring structure that mediates cell division in *E. coli*. *Cell*, 88(2):175–185, Jan. 1997.

C. A. Hale and P. A. J. de Boer. Recruitment of ZipA to the septal ring of Escherichia coli is dependent on FtsZ and independent of FtsA. *J. Bacteriol.*, 181(1):167–176, Jan. 1999.

C. A. Hale, A. C. Rhee, and P. A. J. de Boer. ZipA-induced bundling of FtsZ polymers mediated by an interaction between C-terminal domains. *J. Bacteriol.*, 182(18):5153–5166, Sep. 2000.

D. T. Haynie. *Biological Thermodynamics*. Cambridge University Press, 2001.

C. A. Helm, J. N. Israelachvili, and P. M. McGuiggan. Molecular mechanisms and forces involved in the adhesion and fusion of amphiphilic bilayers. *Science*, 246(4932):919–922, Nov. 1989.

V. M. Hernández-Rocamora, C. García-Montañés, G. Rivas, and O. Llorca. Reconstitution of the Escherichia coli cell division ZipA-FtsZ complexes in nanodiscs as revealed by electron microscopy. *J. Struct. Biol.*, 180(3):531–538, Dec. 2012a.

V. M. Hernández-Rocamora, B. Reija, C. García, P. Natale, C. Alfonso, A. P. Minton, S. Zorrilla, G. Rivas, and M. Vicente. Dynamic interaction of the Escherichia coli cell division ZipA and FtsZ proteins evidenced in nanodiscs. *J. Biol. Chem.*, 287(36):30097–30104, Aug. 2012b.

P. Hinterdorfer and Y. F. Dufrene. Detection and localization of single molecular recognition events using atomic force microscopy. *Nat. Methods*, 3(5):347–355, May 2006.

A. J. Hoff, R. Lipowsky, and E. Sackmann. *Structure and Dynamics of Membranes: I. From Cells to Vesicles / II. Generic and Specific Interactions (Handbook of Biological Physics) (Vol 1)*. North Holland, 1995.

I. Hörger, E. Velasco, J. Mingorance, G. Rivas, P. Tarazona, and M. Vélez. Langevin computer simulations of bacterial protein filaments and the force-generating mechanism during cell division. *Phys. Rev. E: Stat., Nonlinear, Soft Matter Phys.*, 77:011902, 2008a.

I. Hörger, E. Velasco, G. Rivas, M. Vélez, and P. Tarazona. FtsZ bacterial cytoskeletal polymers on curved surfaces: The importance of lateral interactions. *Biophysical Journal: Biophysical Letters*, 94(11): L81–L83, June 2008b.

J. Hsin, A. Gopinathan, and K. C. Huang. Nucleotide-dependent conformations of FtsZ dimers and force generation observed through molecular dynamics simulations. *Proceedings of the National Academy of Sciences*, 109(24):9432–9437, June 2012.

C. H. Huang. Studies on phosphatidylcholine vesicles. formation and physical characteristics. *Biochemistry (Mosc)*, 8(1):344–352, Jan. 1969.

J. N. Israelachvili. *Intermolecular and surface forces: revised third edition*. Academic press, 2011.

R. Jaiswal, R. Y. Patel, J. Asthana, B. Jindal, P. V. Balaji, and D. Panda. E93R substitution of Escherichia coli FtsZ induces bundling of protofilaments, reduces GTPase activity, and impairs bacterial cytokinesis. *J. Biol. Chem.*, 285(41):31796–31805, Oct. 2010.

A. Janshoff, H-J Galla, and C. Steinem. Piezoelectric mass-sensing devices as biosensors-an alternative to optical biosensors? *Angewandte Chemie International Edition*, 39(22):4004–4032, Nov. 2000.

R. L. Hamilton Jr., J. Goerke, L. S. Guo, M. C. Williams, and R. J. Havel. Unilamellar liposomes made with the french pressure cell: a simple preparative and semiquantitative technique. *J. Lipid Res.*, 21(8):981–992, Nov. 1980.

K. K. Kanazawa and J. G. Gordon. The oscillation frequency of a quartz resonator in contact with liquid. *Anal. Chim. Acta*, 175(0): 99–105, 1985.

C. A. Keller and B. Kasemo. Surface specific kinetics of lipid vesicle adsorption measured with a Quartz Crystal Microbalance. *Biophys J*, 75(3):1397–1402, Sep. 1998.

N. Kodera, T. Kinoshita, T. Ito, and T. Ando. High-resolution imaging of myosin motor in action by a high-speed atomic force microscope. In *Molecular and Cellular Aspects of Muscle Contraction*, volume 538 of *Advances in Experimental Medicine and Biology*, pages 119–127. Springer US, 2003.

C. M. Koppelman, M. E. G. Aarsman, J. Postmus, E. Pas, A. O. Muijsers, D. J. Scheffers, N. Nanninga, and T. den Blaauwen. R174 of Escherichia coli FtsZ is involved in membrane interaction and protofilament bundling, and is essential for cell division. *Molecular Microbiology*, 51(3):645–657, Feb. 2004.

A. Kuchibhatla, A. Bhattacharya, and D. Panda. ZipA binds to FtsZ with high affinity and enhances the stability of FtsZ protofilaments. *PLoS ONE*, 6(12):e28262, Dec. 2011.

G. Lan, A. Dajkovic, D. Wirtz, and S. X. Sun. Polymerization and bundling kinetics of FtsZ filaments. *Biophys. J.*, 95(8):4045–4056, Oct. 2008.

G. Lan, B. R. Daniels, T. M. Dobrowsky, D. Wirtz, and S. X. Sun. Condensation of FtsZ filaments can drive bacterial cell division. *Proceedings of the National Academy of Sciences*, 106(1):121–126, Jan. 2009.

Y. Li, J. Hsin, L. Zhao, Y. Cheng, W. Shang, K. C. Huang, H. W. Wang, and S. Ye. FtsZ protofilaments use a hinge-opening mechanism for constrictive force generation. *Science*, 341:392–5, 2013.

M. Loose, E. Fischer-Friedrich, J. Ries, K. Kruse, and P. Schwille. Spatial regulators for bacterial cell division self-organize into surface waves in vitro. *Science*, 320:789–792, 2008.

I. López-Montero, P. Mateos-Gil, M. Sferrazza, P. L. Navajas, G. Rivas, M. Vélez, and F. Monroy. Active membrane viscoelasticity by the bacterial FtsZ-division protein. *Langmuir*, 28(10):4744–4753, Mar. 2012.

I. López-Montero, P. López-Navajas, J. Mingorance, G. Rivas, M. Vélez, M. Vicente, and F. Monroy. Intrinsic disorder of the bacterial cell division protein ZipA: coil-to-brush conformational transition. *FASEB Journal*, 27(8):3363–75, Aug. 2013a.

I. López-Montero, P. López-Navajas, J. Mingorance, M. Vélez, M. Vicente, and F. Monroy. Membrane reconstitution of FtsZ-ZipA complex inside giant spherical vesicles made of *E. coli* lipids: large membrane dilation and analysis of membrane plasticity. *Biochim. Biophys. Acta*, 1828(2):687–698, Feb. 2013b.

C. Lu, J. Stricker, and H. P. Erickson. FtsZ from Escherichia coli, Azotobacter vinelandii, and Thermotoga maritima–quantitation, GTP hydrolysis, and assembly. *Cell Motil. Cytoskeleton*, 40(1):71–86, 1998.

C. Lu, M. Reedy, and H. P. Erickson. Straight and curved conformations of FtsZ are regulated by GTP hydrolysis. *J. Bacteriol.*, 182: 164–70, 2000.

C. Lu, J. Stricker, and H. P. Erickson. Site-specific mutations of FtsZ–effects on GTPase and in vitro assembly. *BMC Microbiology*, 1(7), May 2001.

J. Löwe and L.A. Amos. Crystal structure of the bacterial cell-division protein FtsZ. *Nature*, 391(6663):203–6, Jan. 1998.

J. Löwe and L.A. Amos. Tubulin-like protofilaments in Ca2+-induced FtsZ sheets. *EMBO J.*, 18(9):2364–2371, 1999.

W. Margolin. Sculpting the bacterial cell. *Curr. Biol.*, 19:812–822, 2009.

S. J. Martin, V. E. Granstaff, and G. C. Frye. Characterization of a Quartz Crystal Microbalance with simultaneous mass and liquid loading. *Anal. Chem.*, 63(20):2272–2281, 1991.

A. Martos, C. Alfonso, P. López-Navajas, R. Ahijado-Guzmán, J. Mingorance, A. P. Minton, and G. Rivas. Characterization of self-association and heteroassociation of bacterial cell division proteins FtsZ and ZipA in solution by composition gradient-static light scattering. *Biochemistry*, 49(51):10780–10787, Dec. 2010.

W. P. Mason and T. B. Bateman. Relation between third-order elastic moduli and the thermal attenuation of ultrasonic waves in nonconducting and metallic crystals. *The Journal of the Acoustical Society of America*, 40(4):852–862, 1966.

P. Mateos-Gil. *Structure and dynamics of filaments formed by bacterial cell division protein FtsZ on flat surfaces.* Phd thesis, Universidad Autónoma de Madrid, 2013.

P. Mateos-Gil, I. F. Márquez, P. López-Navajas, M. Jiménez, M. Vicente, J. Mingorance, G. Rivas, and M. Vélez. FtsZ polymers bound to lipid bilayers through ZipA form dynamic two dimensional networks. *Biochimica Et Biophysica Acta-biomembranes*, 1818:806–813, 2012a.

P. Mateos-Gil, A. Paez, I. Hörger, G. Rivas, M. Vicente, P. Tarazona, and M. Vélez. Depolymerization dynamics of individual filaments of bacterial cytoskeletal protein FtsZ. *Proc. Natl. Acad. Sci. U. S. A.*, 109(21):8133–8138, May 2012b.

K. Matsumoto, J. Kusaka, A. Nishibori, and H. Hara. Lipid domains in bacterial membranes. *Mol. Microbiol.*, 61(5):1110–1117, Sep. 2006.

J. Mendieta, A. I. Rico, E. López-Viñas, M. Vicente, J. Mingorance, and P. Gómez-Puertas. Structural and functional model for ionic (K+/Na+) and pH dependence of GTPase activity and polymerization of FtsZ, the prokaryotic ortholog of tubulin. *J. Mol. Biol.*, 390 (1):17–25, July 2009.

J. Mingorance, S. Rueda, P. Gómez-Puertas, A. Valencia, and M. Vicente. Escherichia coli FtsZ polymers contain mostly GTP and have a high nucleotide turnover. *Mol. Microbiol.*, 41(1):83–91, July 2001.

J. Mingorance, M. Tadros, M. Vicente, J. M. González, G. Rivas, and M. Vélez. Visualization of single Escherichia coli FtsZ filament dynamics with Atomic Force Microscopy. *J. Biol. Chem.*, 280:20909–20914, 2005.

J. Mingorance, G. Rivas, M. Velez, P. Gómez-Puertas, and M. Vicente. Strong FtsZ is with the force: mechanisms to constrict bacteria. *Trends in Microbiology*, 18(8):348–56, Aug. 2010.

D. J. Müller and A. Engel. Conformations, flexibility, and interactions observed on individual membrane proteins by atomic force microscopy. *Methods Cell Biol.*, 68:257–299, 2002.

D. J. Müller, H. Janovjak, T. Lehto, L. Kuerschner, and K. Anderson. Observing structure, function and assembly of single proteins by AFM. *Prog. Biophys. Mol. Biol.*, 79:1–43, 2002.

L. G. Monahan, A. Robinson, and E. J. Harry. Lateral FtsZ association and the assembly of the cytokinetic Z ring in bacteria. *Mol. Microbiol.*, 74(4):1004–1017, Nov. 2009.

F. Moreno-Herrero, J. Colchero, J. Gómez-Herrero, and A. M. Baró. Atomic force microscopy contact, tapping, and jumping modes for imaging biological samples in liquids. *Phys. Rev. E*, 69:031915, Mar. 2004.

L. Mosyak, Y. Zhang, E. Glasfeld, S. Haneyand M. Stahl, J. Seehra, and W. S. Somers. The bacterial cell-division protein ZipA and its interaction with an FtsZ fragment revealed by X-ray crystallography. *EMBO J*, 19(13):3179–3191, July 2000.

O. G. Mouritsen. *Life - As a Matter of Fat*. Springer, 2004.

A. Mukherjee and J. Lutkenhaus. Guanine nucleotide-dependent assembly of FtsZ into filaments. *Journal of Bacteriology*, 176:2754–2758, May 1994.

A. Mukherjee and J. Lutkenhaus. Dynamic assembly of FtsZ regulated by GTP hydrolysis. *EMBO J.*, 17(2):462–469, Jan. 1998.

A. Mukherjee and J. Lutkenhaus. Analysis of FtsZ assembly by light scattering and determination of the role of divalent metal cations. *J. Bacteriol.*, 181:823–832, 1999.

P. Natale, M. Pazos, and M. Vicente. The Escherichia coli divisome: born to divide. *Environ. Microbiol.*, 15:3169–3182, 2013.

A. Nishibori, J. Kusaka, H. Hara, M. Umeda, and K. Matsumoto. Phosphatidylethanolamine domains and localization of phospholipid synthases in bacillus subtilis membranes. *J. Bacteriol.*, 187(6): 2163–2174, Mar. 2005.

T. Nomura and M. Okuhara. Frequency shifts of piezoelectric quartz crystals immersed in organic liquids. *Anal. Chim. Acta*, 142(0):281–284, Oct. 1982.

T. Ohashi, C. A. Hale, P. A. J. de Boer, and H. P. Erickson. Structural evidence that the P/Q domain of ZipA is an unstructured, flexible tether between the membrane and the C-terminal FtsZ-binding domain. *Journal of Bacteriology*, 184(15):4313–4315, Aug. 2002.

M. A. Oliva, S. C. Cordell, and J. Lowe. Structural insights into FtsZ protofilament formation. *Nat. Struct. Mol. Biol.*, 11(12):1243–1250, Dec. 2004.

M. Osawa and H. P. Erickson. Inside-out Z rings - constriction with and without GTP hydrolysis. *Mol. Microbiol.*, 81(2):571–579, July 2011.

M. Osawa, D. E. Anderson, and H. P. Erickson. Reconstitution of contractile FtsZ rings in liposomes. *Science*, 320:792–794, 2008.

M. Osawa, D. E. Anderson, and H. P. Erickson. Curved FtsZ protofilaments generate bending forces on liposome membranes. *EMBO J.*, 28(22):3476–3484, Nov. 2009.

K. W. Osteryoung and J. Nunnari. The division of endosymbiotic organelles. *Science*, 302:1698–1704, 2003.

A. Páez, P. Mateos-Gil, I. Hörger, J. Mingorance, G. Rivas, M. Vicente, M. Vélez, and P. Tarazona. Simple modeling of FtsZ polymers on flat and curved surfaces: correlation with experimental in vitro observations. *PMC Biophysics*, 2, 2009a.

A. Páez, P. Tarazona, P. Mateos-Gil, and M. Vélez. Self-organization of curved living polymers: FtsZ protein filaments. *Soft Matter*, 5: 2625–2637, 2009b.

P. Phoenix and G. R. Drapeau. Cell division control in Escherichia coli K-12: some properties of the ftsZ84 mutation and suppression of this mutation by the product of a newly identified gene. *J. Bacteriol.*, 170(9):4338–4342, June 1988.

O. Piro, G. Carmon, M. Feingold, and I. Fishov. Three-dimensional structure of the Z-ring as a random network of FtsZ filaments. *Environ. Microbiol.*, 2013.

D. Popp and R. C. Robinson. Bacterial cytoskeleton suprastructures and their physical origin. *Communicative & Integrative Biology*, 3(5): 451–453, Sep./Oct. 2010.

D. Popp, M. Iwasa, A. Narita, H. P. Erickson, and Y. Maéda. FtsZ condensates: an in vitro electron microscopy study. *Biopolymers*, 91 (5):340–350, May 2009.

C. R. Raetz and W. Dowhan. Biosynthesis and function of phospholipids in Escherichia coli. *J. Biol. Chem.*, 265(3):1235–1238, Jan. 1990.

J. D. Rawn. *Biochemistry*. Harper & Row, 1983.

R. Richter, A. Mukhopadhyay, and A. Brisson. Pathways of lipid vesicle deposition on solid surfaces: A combined QCM-D and AFM study. *Biophys. J.*, 85(5):3035–3047, Nov. 2003.

R. P. Richter and A. Brisson. QCM-D on mica for parallel QCM-D-AFM studies. *Langmuir*, 20(11):4609–4613, 2004.

R. P. Richter, R.d Bérat, and A. R. Brisson. Formation of solid-supported lipid bilayers: an integrated view. *Langmuir*, 22(8):3497–3505, Apr. 2006.

A. I. Rico, M. Krupka, and M. Vicente. In the beginning, Escherichia coli assembled the proto-ring: an initial phase of division. *J. Biol. Chem.*, 288:20830–6, 2013.

M. Rief, M. Gautel, F. Oesterhelt, J. M. Fernández, and H. E. Gaub. Reversible unfolding of individual titin immunoglobulin domains by AFM. *Science*, 276(5315):1109–1112, 1997.

G. Rivas, A. López, J. Mingorance, M. J. Ferrandiz, S. Zorrilla, A. P. Minton, M. Vicente, and J. M. Andreu. Magnesium-induced linear self-association of the FtsZ bacterial cell division protein monomer. the primary steps for FtsZ assembly. *J. Biol. Chem.*, 275:11740–9, 2000.

L. Romberg, M. Simon, and H. P. Erickson. Polymerization of FtsZ, a bacterial homolog of tubulin. Is assembly cooperative? *J. Biol. Chem.*, 276(15):11743–11753, Apr. 2001.

S. Rueda, M. Vicente, and J. Mingorance. Concentration and assembly of the division ring proteins FtsZ, FtsA, and ZipA during the Escherichia coli cell cycle. *J. Bacteriol.*, 185:3344–51, 2003.

E. Sackmann. Supported membranes: scientific and practical applications. *Science*, 271(5245):43–48, Jan 1996.

G. Sauerbrey. Verwendung von schwingquarzen zur wagung dunner schichten und zur mikrowagung. *Zeitschrift Fur Physik*, 155(2):206–222, 1959.

J. Y. Shin, W. Vollmer, R. Lagos, and O. Monasterio. Glutamate 83 and arginine 85 of helix H3 bend are key residues for FtsZ polymerization, GTPase activity and cellular viability of Escherichia coli: lateral mutations affect FtsZ polymerization and *E. coli* viability. *BMC Microbiology*, 13(26), 2013.

F. Si, K. Busiek, W. Margolin, and S. X. Sun. Organization of FtsZ filaments in the bacterial division ring measured from polarized fluorescence microscopy. *Biophys. J.*, 105:1976–86, 2013.

K. Skoog and D. O. Daley. The Escherichia coli cell division protein ZipA forms homodimers prior to association with FtsZ. *Biochemistry*, 51(7):1407–1415, Jan. 2012.

T. M. Sossong, M. R. Brigham-Burke, P. Hensley, and K. H. Pearce. Self-activation of guanosine triphosphatase activity by oligomerization of the bacterial cell division protein FtsZ. *Biochemistry*, 38(45): 14843–14850, Nov. 1999.

D. M. Soumpasis. Theoretical analysis of fluorescence photobleaching recovery experiments. *Biophys. J.*, 41(1):95–97, Jan. 1983.

R. E. Speight and M. A. Cooper. A survey of the 2010 Quartz Crystal Microbalance literature. *J. Mol. Recognit.*, 25(9):451–473, Sep. 2012.

M. Tadros, J. M. González, G. Rivas, M. Vicente, and J. Mingorance. Activation of the Escherichia coli cell division protein FtsZ by a low-affinity interaction with monovalent cations. *FEBS Lett.*, 580: 4941–4946, 2006.

A. D. TerBush, Y. Yoshida, and K. W. Osteryoung. FtsZ in chloroplast division: structure, function and evolution. *Curr. Opin. Cell Biol.*, 25: 461–470, 2013.

M. Thompson and G. L. Hayward. Mass response of the thickness-shear mode acoustic wave sensor in liquids as a central misleading dogma. In *Frequency Control Symposium, 1997. Proceedings of the 1997 IEEE International*, pages 114–119, 1997.

A. Tsortos, G. Papadakis, and E. Gizeli. Shear acoustic wave biosensor for detecting DNA intrinsic viscosity and conformation: a study with QCM-D. *Biosens. Bioelectron.*, 24(4):842–847, Dec. 2008a.

A. Tsortos, G. Papadakis, K. Mitsakakis, K. A. Melzak, and E. Gizeli. Quantitative determination of size and shape of surface-bound DNA using an acoustic wave sensor. *Biophys J*, 94(7):2706–2715, Apr. 2008b.

D. J. Turner, I. Portman, T. R. Dafforn, A. Rodger, D. I. Roper, C. J. Smith, and M. S. Turner. The mechanics of FtsZ fibers. *Biophys. J.*, 102(4):731–738, Feb. 2012.

A. Typas, M. Banzhaf, C. A. Gross, and W. Vollmer. From the regulation of peptidoglycan synthesis to bacterial growth and morphology. *Nat. Rev. Micro.*, 10(2):123–136, Feb. 2012.

A. Valbuena, A. M. Vera, J. Oroz, M. Menéndez, and M. Carrión-Vázquez. Mechanical properties of β-catenin revealed by single-molecule experiments. *Biophysical Journal*, 103(8):1744 –1752, 2012.

M. Vicente and A. I. Rico. The order of the ring: assembly of Escherichia coli cell division components. *Mol. Microbiol.*, 61:5–8, 2006.

X. Wang, M. M. Shindel, S-W Wang, and R. Ragan. A facile approach for assembling lipid bilayer membranes on template-stripped gold. *Langmuir*, 26(23):18239–18245, Dec. 2010.

K. C. Weng, J. L. Kanter, W. H. Robinson, and C. W. Frank. Fluid supported lipid bilayers containing monosialoganglioside GM1: a QCM-D and FRAP study. *Colloids Surf B Biointerfaces*, 50(1):76–84, June 2006.

M. C. Woodle and D. Papahadjopoulos. Liposome preparation and size characterization. *Methods Enzymol.*, 171:193–217, 1989.

K. D. Young. Bacterial shape: two-dimensional questions and possibilities. *Annu. Rev. Microbiol.*, 64:223–240, 2010.

X. C. Yu and W. Margolin. Deletion of the min operon results in increased thermosensitivity of an ftsZ84 mutant and abnormal FtsZ ring assembly, placement, and disassembly. *J. Bacteriol.*, 182(21): 6203–6213, Nov. 2000.

B

CURRICULUM VITAE

DATOS PERSONALES

- Nombre Completo: Ileana Fernanda MÁRQUEZ
- Fecha de Nacimiento: 28 de Septiembre de 1972
- Nacionalidad: Argentina
- E-mail: [illegible]

ESTUDIOS

- Licenciado en Física (2000). Facultad de Ciencias Exactas y Naturales de la Universidad Nacional de La Pampa (FCEN - UNLPam), Argentina. Promedio 8.3/10 (2.54/4).
- Candidato a Doctorado en la Universidad Nacional de la Plata (UNLP). Instituto de Física de Fluidos y Sistemas Biológicos (IFLySIB). La Plata, Bs. As., Argentina.
- Máster en Física (2006) en Michigan State University (MSU). Departamento de Física y Astronomía, BPS Building, MSU, East Lansing, MI, USA, 48824.
- Máster en Biofísica (2008) en la Universidad Autónoma de Madrid. Instituto Nicolás Cabrera, Facultad de Ciencias C-XVI 4a. planta, Universidad Autónoma de Madrid, Cantoblanco, Madrid, 28049.

EXPERIENCIA EN ENSEÑANZA

- Ayudante alumno no graduado. Desde el 01/01/1995 hasta el 30/04/2000. FCEN - UNLPam. Curso en ecuaciones diferenciales: Física Matemática I. Responsabilidades: Preparación y enseñanza de trabajos prácticos (solución de problemas, implementación con Mathematica®).
- Ayudante graduado. Desde 01/01/2004 hasta 31/12/2006. Departamento de Física y Astronomía, MSU, USA. Curso de laboratorio de física para alumnos no graduados: PHY 251- PHY 252. Responsabilidades: Preparación y enseñanza de experimentos de laboratorio en Física, corrección y evaluación de informes, y evaluación del rendimiento académico de los alumnos.

EXPERIENCIA LABORAL

- Desde 02/2008 – 05/2009. Instituto Nicolás Cabrera, Facultad de Ciencias C-XVI 4a. planta, Universidad Autónoma de Madrid. Responsabilidades: Estudio de membranas lipídicas sometidas a la técnica de "softlithography" obteniéndose de esta manera patrones a escala micrométrica. Dichos patrones son caracterizados mediante técnicas biofísicas tales como microscopio de fuerzas atómicas (AFM) y microscopio de fluorescencia.

- Desde 04/05/2009. Contrato Laboral en la categoría de Titulado Superior de Actividades Técnicas y Profesionales (contrato 5) cuyas tareas se realizaron en el Instituto de Catálisis y Petroleoquímica, C/ Marie Curie 2, Cantoblanco, Madrid, E-28049. Responsabilidades: Incorporación y caracterización del conector soluble del bacteriófago ϕ29 en membranas lipídicas, Caracterización de las preparaciones mediante técnicas biofísicas y bioquímicas tales como microscopía de fuerzas atómicas, microbalanza de cuarzo y microscopía de fluorescencia; y su capacidad de formar poros activos sensibles a la presencia de ATP.

- Desde 29/04/2010 – 04/11/2013: Contrato Laboral en la categoría de Titulado Superior de Actividades Técnicas y Profesionales en el marco del proyecto "Exploiting Gram-negative cell division targets in the test tube to obtain anti-microbial compounds", cuyas tareas se realizaron en el Instituto de Catálisis y Petroleoquímica, C/ Marie Curie 2, Cantoblanco, Madrid, E-28049. Responsabilidades: Realizar una caracterización bioquímica y estructural mediante microscopía de fuerzas atómicas y microscopía de fluorescencia de la proteína FtsZ y de su interacción con la proteína ZipA.

BECAS RECIBIDAS Y AYUDANTÍAS

- Facultad de Ciencias Exactas y Naturales de la Universidad Nacional de La Pampa (FCEN-UNLPam), Argentina . Ayudante alumno de investigación no graduado. *Estudio Viscosimétrico de la acción de la radiación Gamma en la estructura del DNA*. Desde 01/01/1996 hasta 31/12/1997. Director: Dr. J. A. Bertolotto.

- Agencia Española de Cooperación Internacional (AECI). Ayudante alumno no graduado en *Métodos Matemáticos de la Física II* en la Universidad de Valladolid. España. Desde 24/01/1997 hasta 05/03/1997. Director: Dr. L. M. Nieto Calzada.

- Beca doctoral de la Agencia Nacional de Promoción Científica y Tecnológica en *Percolación continua y transiciones de fase*. Ar-

gentina. Desde 01/08/2000 hasta 01/04/2002. Director: Dr. F. Vericat.

- Beca doctoral del Consejo Nacional de Investigación Científica y Tecnológica en *Percolación continua y transiciones de fase*. Argentina. Desde 01/04/2002 hasta 01/02/2003. Director: Dr. F. Vericat.

- Investigador Visitante en el laboratorio del Dr. E. Lomba. Instituto de Química y Física Rocasolano (IQFR), Madrid, España. Septiembre de 2002.

- Ayudante graduado de enseñanza en el Departamento de Física y Astronomía, MSU, East Lansing, MI, USA. Desde 01/01/2004 hasta Mayo de 2005. Cursos: PHY 251 - 252. Directores: Drs. H. Weerts, B. Golding, K. Tollefson.

- Ayudante graduado de investigación en el National Superconducting Cyclotron Laboratory (NSCL), MSU, East Lansing, MI, USA. Desde Mayo de 2005 hasta Julio de 2006. Director: Dr. A. Brown.

- Ayudante graduado de enseñanza en el Departamento de Física y Astronomía, MSU, East Lansing, MI, USA. Desde Agosto a Diciembre de 2006. Curso: PHY 251. Director: Dr. K. Tollefson.

- Investigador Visitante en el laboratorio de la Dra. Katherine Oestryoung, Plant Biology Department, Michigan State University (MSU), East Lansing, MI, USA. Desde 31/10/2009 hasta 15/11/2009.

PUBLICACIONES

- Márquez I., et al. The effect of lateral interactions: a biophysical characterization of E. coli FtsZ lateral mutants. (en preparación)

- Márquez I., et al. Preparation of charged lipid bilayers on gold. (en preparación)

- Mateos-Gil P, Márquez I., López-Navajas P, Jiménez M, Vicente M, Mingorance J, Rivas G, Vélez M. FtsZ polymers bound to lipid bilayers through ZipA form dynamic two dimensional networks. *Biochim Biophys Acta*. 2012. Mar.; **1818**(3):806-13.

- Moleiro LH, López-Montero I, Márquez I., Moreno S, Vélez M, Carrascosa JL, Monroy F. Efficient Orthogonal Integration of the Bacteriophage ϕ29 DNA-Portal Connector Protein in Engineered Lipid Bilayers. *ACS Synth Biol*. 2012. Sep.; **1**(9):414-24.

- L. A. Pugnaloni, I. F. Márquez and F. Vericat. Continuum percolation in simple fluids: energetic connectivity criteria. *Physica A: Statistical Mechanics and its Applications*. 2003. **321**:398-410.

- I. F. Márquez, J. Negro and L. M. Nieto. Factorization method in singular Hamiltonians. *J. Phys. A: Math. Gen*. 1998. **31**:4115-4125.

COMUNICACIONES EN REUNIONES CIENTÍFICAS

- I. F. Márquez, L. A. Pugnaloni and F. Vericat. "Percolación en el fluido de Lennard-Jones". 86ª Reunión Anual de la Asociación de Física de Argentina (AFA). Septiembre 2001. Rosario, Santa Fe, Argentina.

- I. F. Márquez, L. A. Pugnaloni and F. Vericat. "Criterio energético para la identificación de clusters en sistemas continuos". 87ª Reunión Anual de la Asociación de Física de Argentina (AFA). 2002. Córdoba, Argentina.

- L. H. Moleiro, I. F. Márquez, R. Miranda, S. Moreno, I. López-Montero, J. L. Carrascosa, M. Vélez and F. Monroy, "Towards a gene-delivering engine: Integration of viral (ϕ29) portal proteins in lipids membranes." 7th European Biophysics Congress (EBSA). 11-15 de Julio de 2009. Genova, Italy.

- I. F. Márquez, L. H. Moleiro, R. Miranda, S. Moreno, F. Monroy, J. L. Carrascosa and M. Vélez. "Inserting bacteriophage ϕ29 connector into planar lipid bilayers: creating an artificial active DNA pore." NANO2009 - Perspectives in Nanoscience and Nanotechnology. 28-30 de Septiembre de 2009. Donostia – San Sebastián, España.

- I. F. Márquez, O. Monasterio and M. Vélez. "AFM characterization of FtsZ mutants: the effect of lateral interactions". AFM BioMed Conference, 12-15 May, 2010, Red Island, Croatia.

- I. F. Márquez, O. Monasterio and M. Vélez. "The funcional relevance of lateral interaction in FtsZ polymers: an AFM study of FtsZ lateral mutants". Biophysical Society 55th Annual Meeting. 5-9 March, 2011, Baltimore, Maryland, USA.

ASISTENCIA A REUNIONES CIENTÍFICAS

- 9ª Reunión Nacional de Enseñanza de la Física (APFA). 18-22 de Septiembre de 1995. Salta, Argentina.

- 86ª Reunión Anual de la Asociación de Física de Argentina (AFA). 18-21 de Septiembre de 2001. Rosario, Santa Fe, Argentina.

- Conferencia sobre Proteínas de Membrana Virales. 12-14 de Diciembre de 2008. Heilderberg, Alemania.
- NANO2009 - Perspectives in Nanoscience and Nanotechnology. 28-30 de Septiembre de 2009. Donostia – San Sebastián, España.
- 3^a Conferencia AFM BioMed. 12-15 Mayo de 2010. Red Island, Croacia.
- 55 Reunión Anual de la Biophysical Society. 5-9 de Marzo de 2011, Baltimore, Maryland, USA.

MEMBRESÍAS CIENTÍFICAS

- Asociación de Profesores de Física de Argentina (APFA). Miembro activo desde 1995 hasta 2000, y representante provincial en La Pampa durante el periodo 1999-2000.
- Asociación de Física de Argentina (AFA). Miembro activo durante el periodo 2000-2003.
- Biophysical Society. Miembro activo durante el periodo 2011-2012.